Title
Microtopographical control of cell adhesion, organization, and proliferation in a cardiac tissue engineering scaffold

Author
Patel, Anuj Ashwin

Publication Date
2011

Peer reviewed|Thesis/dissertation

Microtopographical control of cell adhesion, organization, and proliferation in a cardiac tissue engineering scaffold

By

Anuj Ashwin Patel

A dissertation submitted in partial satisfaction of the

requirements for the degree of

Joint Doctor of Philosophy
with the University of California, San Francisco

in

Bioengineering

in the

Graduate Division

of the

University of California, Berkeley

Committee in charge:

Professor Sanjay Kumar, Chair
Professor Tejal Desai
Professor Liwei lin

Fall 2011

Abstract

Microtopographical control of cell adhesion, organization, and proliferation in a cardiac tissue engineering scaffold
by
Anuj Ashwin Patel
Doctor of Philosophy in Bioengineering
University of California, Berkeley
Professor Sanjay Kumar, Chair

Myocardial infarction, commonly known as a heart attack, is caused by the blockage of blood flow to heart, resulting in the death of cardiomyocytes, or heart muscle cells. Scar tissue formation occurs in the area of the damage due to the heart's inability to regenerate myocardial tissue. Therefore, regeneration of myocardial tissue through the use of synthetic scaffolds requires strategies to promote cardiomyocyte attachment while minimizing proliferation of the fibroblast cells that contribute to scar tissue. Previous studies have demonstrated that a synthetic platform consisting of an array of microscale polydimethylsiloxane (PDMS)-based pillars ("micropegs") can accomplish both of these goals, but the mechanism through which this occurs has remained a mystery.

In this work the interaction between microtopographical cues and both fibroblasts and cardiomyocytes is further explored. It is shown that a fibroblast that is attached to a micropeg is less likely to proliferate than ones on a flat surface, but this difference can be partially abrogated in the presence of drugs that inhibit cell contractility. The cells also show increased adhesion to the micropegs as opposed to flat surfaces, as demonstrated by measurements of the dynamics of deadhesion from the surface and changes in expression of specific mechanotransductive genes. Together, these data support a model in which microtopographical cues alter the local mechanical microenvironment of cells by modulating adhesion and adhesion-dependent mechanotransductive signaling, thereby leading to a reduction in proliferation capability.

The research focus then shifts to the use of microtopographical cues to control cardiomyocyte adhesion and organization. Cardiomyocytes cluster around and interact with the full length of the micropegs, exhibiting three-dimensional organization on a two-dimensional surface. By controlling the diameter and spatial arrangement of the micropegs, the degree of clustering can be regulated. The expression of functional markers N-cadherin and connexin 43 also exhibit a dependence on the spatial arrangement of the micropegs. The preference of cardiomyocytes for three-dimensional adhesion is further investigated in the final part of the thesis. By isolating cardiomyocytes in PDMS microwells, the cells are presented with the option of attaching to a vertical wall or a flat space. The cells demonstrate a preferential attachment to the side walls and corners of the microwell. Introduction of the myosin inhibitor blebbistatin reduces the percentage of cells attached to these side walls. Cells attached to a side wall also are less likely to proliferate, similar to the behavior of fibroblasts attached to micropegs. Taken together, these data indicate that incorporation of microtopographical features into cardiac tissue engineering scaffolds can be used to control the adhesion and organization of cardiomyocytes while simultaneously limiting the formation of scar tissue.

Table of Contents

Acknowledgments

First of all, I would like to thank my dissertation advisor, Professor Sanjay Kumar. Thank you for your constant guidance throughout the five years I spent in your lab. You have been an incredible advisor, and your support, wisdom, and patience have been invaluable in helping foster my growth throughout the years. I have been very fortunate to have had the opportunity to work with you and learn from you.

I would like to also thank the members of the Kumar Lab, past and present, for creating such a wonderful environment to work in. It is remarkable how incredibly helpful and easily approachable everyone has been. The closeness of our lab is a rare thing, and I would not have been able to survive this dissertation without you.

Thank you as well to Professor Tejal Desai and the Desai Lab at UCSF. Your knowledge and expertise greatly elevated the quality of this research, and your support was invaluable in moving the project forward. The opportunity to work with your lab allowed me to meet some wonderful people and interesting characters. In particular, the support and advice from Dr. Rahul Thakar made the collaboration particularly fruitful.

To my fellow students in the BioE program: the most memorable part of this graduate school experience has been the friendships I have made and the amazing people I have gotten the chance to meet in this program. You have made graduate school infinitely more enjoyable, whether it was at departmental retreats, soccer games, Cal football and basketball games, shenanigans in Berkeley and San Francisco, or in parody music videos. Thank you, and hopefully we will be able to continue these friendships no matter where we end up.

Last, but certainly not least, to my parents and my brother: thank you for your neverending support and love. Your pride in what I have been doing has been evident since day one, and your patience and understanding during what must have seemed like an endless amount of time in school kept me going every day. You have always pushed me to become a better student and a better person, and for that I cannot thank you enough.

Chapter 1 - Introduction

Myocardial infarction (MI) occurs when a blockage of blood flow to the heart results in the death of myocardial tissue. This damage to the heart causes several changes to the structure and proper function of the tissue which can lead to arrhythmias and eventual heart failure. In this section the changes to the cellular structure of the heart and strategies to repair it are explored.

Cardiac cell biology

Structure and function of healthy myocardium

The primary cells of the heart are cardiomyocytes, or heart muscle cells. These cells are cylindrical cells that control the beating of the myocardial tissue.[1] Cardiomyocytes are thought to be terminally differentiated and non-proliferative at birth. Another major cellular component is the fibroblast. These cells form the connective tissue of the heart and are responsible for creating the extracellular matrix (ECM) and controlling signaling between cells.[2] Unlike cardiomyocytes, fibroblasts within the heart continually proliferate after birth.[3-4]

The cardiac ECM provides structural support for the myocardial cells while also regulating cell signaling.[5] While the exact composition of this ECM varies with age and health, collagen is the primary ECM structural component.[6] The five major collagen types within the heart are types I, III, IV, V, and VI. Types I and III represent 90% of the total collagen in the ECM, while types IV and VI play a role in cell signaling and adhesion.[7] Several other matrix components play a key role in cellular adhesion and signaling. Laminin and fibronectin are two of these primary ECM proteins; they are primarily responsible for binding cardiomyocytes via integrin-based adhesion.[8-9]

The cytoskeletal network of cardiomyocytes functions both to process mechanical signals from the external microenvironment as well as generate the contractile force necessary for the cardiomyocytes to properly beat.[10] The ECM is linked to the cytoskeleton via integrins, which are heterodimeric receptors located at the cell surface. There are several α-integrin subunits expressed within cardiomyocytes, but the primary β subunit is β1-integrin.[11] These integrins connect to the actin cytoskeleton via proteins such as vinculin, talin, and α-actinin, proteins that are ubiquitous in cell types throughout the body.[10] Contraction and beating of the cardiomyocytes is controlled by a cytoskeletal structure known as the sarcomere, which is composed of actin filaments that slide along adjacent myosin filaments. Myofibrils within the cardiomyocyte are composed of a series of sarcomeres that work together to control contraction.[12]

The cytoskeleton also functions to regulate interactions at the cell-cell junction complexes. Adherens junctions, gap junctions, and desmosomes combine to form the intercalated disc, a structure that helps coordinate the development of functional tissue and allows for the propagation of signals necessary for coordinated beating of the myocardium.[13] N-cadherin within the adherens junction is responsible for the mechanical coupling from cell to cell. It anchors to the actin cytoskeleton and myofibrils and allow cells to remain connected while the heart expands and contracts.[14] Connexin 43 in the gap junction coordinates electrical coupling of the cells.[13] They connect the cytoplasm of adjacent cells and enable passive diffusion of ions.[15] Desmosomes provide structural support between cells via intermediate filaments.[13]

The structure and organization of cellular components of the heart are tightly regulated, and changes within them can severely impair proper function of the heart. Next, some of the changes that occur post-MI are explored.

Changes in cardiac structure and function post-MI

When cardiomyocytes undergo necrosis caused by blockage of blood flow to the heart, the cellular structure of the myocardium undergoes several significant changes, known as myocardial remodeling. Initially, cardiomyocytes undergo hypertrophy and a loss of organization, resulting in an increase in thickness of the cardiac wall.[16] As these cardiomyocytes begin to undergo necrosis and apoptosis, wall thinning and dilation occur. Changes in wall thickness can cause an inability to properly beat and support loads.

After death of the myocardial tissue, the resulting wound is repaired by the formation of scar tissue, composed primarily of fibroblasts. Fibroblasts within the heart begin to actively proliferate post-MI and begin to secrete large amounts of ECM protein in the infarct area.[17] While these fibroblasts initially serve to repair the damaged area, the overpopulation of fibroblasts can lead to significant changes in the propagation of signals from cell to cell, impairing the synchronous contraction of the heart and leading to arrhythmia and possible heart failure.[18]

Changes are also seen in the composition of the ECM supporting the myocardium. When fibroblasts overpopulate the area and begin depositing ECM, significant increases in the level of collagen are seen, leading to a stiffening of the cardiac tissue.[18] Increases have been reported across all the major types of collagen, but there are also changes in the proportions of the collagens.[19] One example occurs when there is an influx of cells involved in wound healing pathways, such as neutrophils and macrophages, in the damaged area. Macrophages are known to deposit collagen VI, which can lead to a change in the proportion of collagen VI.[20] There is also an increase in the levels of fibronectin and laminin post-MI. These increases serve many purposes, including the recruitment of wound healing cells and regulation of the function of matrix metalloproteinases.[21-22]

Strategies for regeneration of cardiac tissue

There are several strategies available for regeneration of cardiac tissue. One possibility is the direct transplantation cells into the damaged area. The major consideration here is to determine the source of cells for transplantation. Bone marrow stem cells have been widely employed to regenerate myocardium,[23-25] and while patients have shown improvement post implantation, the restored function is limited and sustainability is in doubt. In recent years, the idea that myocardium is completely incapable of self-regenerating has been challenged by the discovery of a population of cardiac stem cells within the heart.[26-29] These cells have shown greater potential to restore function of heart tissue, but there is still some debate over the effectiveness of these cells.

The use of tissue engineering scaffolds to either deliver cells to the damaged area or promote the recruitment of native cells is another area with great promise. These scaffolds generally combine biomaterials with growth factors to enhance cell adhesion. Several materials for these scaffolds have been investigated, each with its own advantages and disadvantages. Elastomeric materials such as 1,3 trimethylene carbonate, D,L-lactide polymers and their co-polymers have been explored because of the ability to match their mechanical properties to that of the heart,[30-31] but while improved cyclic loading has been observed, these materials have been abandoned for ones that more closely resemble the biochemical features, such as collagen or Matrigel. However, results with these gels have been inconsistent because they lack the mechanical properties to sustain proper function of the heart.[32-34] Further studies with natural

polymers such as alginate and chitosan have shown promise, but these materials lack the native cardiac ECM architecture.[35-36]

The use of decellularized matrices has gained traction in the tissue engineering field to deal with a lot of these disadvantages of other scaffolds. These substrates take native tissue and completely remove the cells, leaving just the native ECM in its natural architecture. A recent study by Ott, et al., applied this technique to the engineering of cardiac tissue.[37] By taking a decellularized ECM and reseeding it with cardiac cells. The recellularized heart construct was contracting, capable of pumping blood, and responsive to electrical stimulation within 8 days. The study showed that maintenance of the native ECM mechanical properties and architecture was key to engineering the functional heart tissue.

These scaffold studies have highlighted a very important aspect of the design of tissue engineering scaffolds. The ability to regenerate healthy, functional tissue is dependent not only on the biochemical nature of the ECM but also on controlling the mechanical properties of the scaffold, such as stiffness, architecture, and topography. In the next section, the use of how biophysical cues can be used to regulate cell behavior will be further explored.

Biophysical regulation of cell behavior

The use of biophysical cues in engineering scaffolds is emerging as valuable tool to guide cell function and behavior. For example, control of cell shape by modulating the spatial presentation of adhesive domains via microcontact printing, in which ECM proteins are imprinted on a surface in a controlled spatial arrangement, has been shown to regulate several cellular functions. Growth and apoptosis of cells has been shown to be regulated by cell shape and spreading area.[38] The lineage commitment of stem cells can also be controlled by similarly using microcontact printing to control cell shape.[39-40] In each of these studies, the researchers could control the behavior of the cells by simply controlling the shape or area of the ECM proteins that attach to them.

Elasticity of the substrate is another important mechanical parameter that can be used to govern cell behavior. Polyacrylamide has been used as a substrate in many studies because the elasticity is easily tuned by changing the ratio of crosslinking proteins. A study by Pelham and Wang in 1997 showed that fibroblasts seeded onto a highly flexible polyacrylamide surface showed reduced spreading, increased motility, and created irregular adhesion shapes.[41] Numerous subsequent studies have further explored the effects of substrate elasticity on adhesion and migration,[42] cellular contractility,[43] and lineage commitment and differentiation.[44-45]

While extensive research has been done to show the effects of these mechanical parameters on cell behavior, the effects of microtopography have been relatively underexplored. However, the patterning of microtopographical features into the underlying substrate has proven to be a very effective tool to control assembly and functionality of cells. For example, a number of studies have shown that by patterning microgrooves in a substrate of polydimethylsiloxane (PDMS), which is used because of the ease of molding features onto it, and allowing cells to adhered to the tops of the microgrooves, the adhesion, alignment, and proliferation of various cell types can be controlled.[46-47] Interestingly, when mesenchymal stem cells are patterned onto microgrooves and subjected to uniaxial, cyclical stretching forces, the cells preferentially differentiate into vascular lineages.[48]

In the next section cardiac tissue engineering is revisited, with a focus on how microtopographic cues can be used to guide cell behavior.

Topographical cues in encoded in cardiac tissue engineering scaffolds

Several studies have shown that microtopography can be used to guide the behavior of cells in a cardiac tissue engineering platform. In particular, experiments using microtopographically patterned PDMS substrates containing rows of microgrooves with vertical "micropegs" between each groove were used to study cardiomyocyte adhesion and organization.[49] They showed that cardiomyocytes seeded on the microgrooves exhibited a high degree of alignment on 5 μm wide grooves. The micropegs served as a point of attachment for the cardiomyocytes, as the cells on the grooves would end attachment on a micropeg. In a similar study with only microgrooves, cardiomyocytes exhibited higher expression of N-cadherin and connexin 43 on microgrooved surfaces.[50]

An interesting result of studies with micropegs and primary cardiac cultures was the decrease in the number of myofibroblasts in cultures on patterned surfaces. A study by Boateng, et al., in 2003 further explored the idea that microtopography could be used to decrease fibroblast proliferation.[51] They showed that fibroblasts grown on a silicone surface with 10 μm pegs exhibited a 50% decrease in cell growth after 5 days. They also demonstrated that the ability of cells to attach to the pegs was necessary for this control. Inhibition of stress fiber formation decreased attachment to the pegs, indicating a mechanism in which attachment to micropegs altered the contractility and adhesion of fibroblasts. This study was very important to the idea of limiting fibroblast proliferation, and consequently scar tissue formation, in a cardiac tissue engineering scaffold.

Outline of work

These studies of cardiac cells on micropatterned surfaces left some unanswered questions about the mechanisms through which microtopography can guide the behavior of fibroblasts and cardiomyocytes. The following work is a further investigation of the mechanisms of these interactions between cardiac cells and topographical cues within their microenvironment. PDMS scaffolds patterned with either "micropegs" or "microwells" are used to study how fibroblasts and cardiomyocytes respond to three-dimensional cues on a two-dimensional surface. Chapters 2 and 3 focus primarily on fibroblasts, as well as skeletal myoblasts as a comparative cell type. The effects of the presence of micropegs on proliferation of these cells is covered in Chapter 2, while Chapter 3 further explores the biophysical mechanisms of these interactions by studying the adhesion and migration of cells on patterned surfaces. Chapter 4 then turns its focus on how microtopography can be used to control the adhesion and organization of cardiomyocytes via control of the spatial arrangement and geometry of the micropegs. The interaction of cardiomyocytes with three-dimensional cues is further investigated in Chapter 5, where microwells are used to isolate individual cells and demonstrate the preference of cardiomyocytes to attach to three-dimensional surfaces.

References

1. K. K. Parker, D. E. Ingber, Extracellular matrix, mechanotransduction and structural hierarchies in heart tissue engineering, Philosophical transactions of the Royal Society of London. Series B, Biological sciences, 2007, 362, 1267-79.
2. P. Camelliti, T. K. Borg, P. Kohl, Structural and functional characterisation of cardiac

fibroblasts, Cardiovasc Res, 2005, 65, 40-51.
3. C. P. Adler, W. P. Ringlage, N. Bohm, DNA content and cell number in heart and liver of children. Comparable biochemical, cytophotometric and histological investigations, Pathology, research and practice, 1981, 172, 25-41.
4. I. Manabe, T. Shindo, R. Nagai, Gene expression in fibroblasts and fibrosis: involvement in cardiac hypertrophy, Circ Res, 2002, 91, 1103-13.
5. J. W. Holmes, T. K. Borg, J. W. Covell, Structure and mechanics of healing myocardial infarcts, Annual review of biomedical engineering 2005, 7, 223-53.
6. J. K. Bendall, C. Heymes, P. Ratajczak, J. L. Samuel, Extracellular matrix and cardiac remodelling, Archives des maladies du coeur et des vaisseaux, 2002, 95, 1226-9.
7. L. Espira, M. P. Czubryt, Emerging concepts in cardiac matrix biology, Canadian journal of physiology and pharmacology, 2009, 87, 996-1008.
8. N. Morishita, S. Kusachi, S. Yamasaki, J. Kondo, T. Tsuji, Sequential changes in laminin and type IV collagen in the infarct zone--immunohistochemical study in rat myocardial infarction, Japanese circulation journal, 1996, 60, 108-14.
9. E. S. White, F. E. Baralle, A. F. Muro, New insights into form and function of fibronectin splice variants, The Journal of pathology, 2008, 216. 1-14.
10. J. Y. Kresh, A. Chopra, Intercellular and extracellular mechanotransduction in cardiac myocytes, Pflugers Archiv: European journal of physiology, 2011, 462, 75-87.
11. N. Wang, J. P. Butler, D. E. Ingber, Mechanotransduction across the cell surface and through the cytoskeleton, Science, 1993, 260, 1124-7.
12. G. A. Dabiri, K. K. Turnacioglu, J. M. Sanger, J. W. Sanger, Myofibrillogenesis visualized in living embryonic cardiomyocytes, Proc Natl Acad Sci U S A, 1997, 94, 9493-8.
13. M. Noorman, M. A. van der Heyden, T. A. van Veen, M. G. Cox, R. N. Hauer, J. M. de Bakker, H. V. van Rijen, Cardiac cell-cell junctions in health and disease: Electrical versus mechanical coupling, J Mol Cell Cardiol, 2009, 47. 23-31.
14. M. C. Ferreira-Cornwell, Y. Luo, N. Narula, J. M. Lenox, M. Lieberman, G. L. Radice, Remodeling the intercalated disc leads to cardiomyopathy in mice misexpressing cadherins in the heart, J Cell Sci, 2002, 115, 1623-34.
15. C. Elfgang, R. Eckert, H. Lichtenberg-Frate, A. Butterweck, O. Traub, R. A. Klein, D. F. Hulser, K. Willecke, Specific permeability and selective formation of gap junction channels in connexin-transfected HeLa cells, The Journal of cell biology, 1995, 129, 805-17.
16. B. Swynghedauw, Molecular mechanisms of myocardial remodeling, Physiological reviews, 1999, 79, 215-62.
17. Y. Sun, K. T. Weber, Angiotensin converting enzyme and myofibroblasts during tissue repair in the rat heart, J Mol Cell Cardiol, 1996, 28, 851-8.
18. C. S. Long, R. D. Brown, The cardiac fibroblast, another therapeutic target for mending the broken heart? J Mol Cell Cardiol, 2002, 34, 1273-8.
19. M. Dobaczewski, M. Bujak, P. Zymek, G. Ren, M. L. Entman, N. G. Frangogiannis, Extracellular matrix remodeling in canine and mouse myocardial infarcts, Cell and tissue research, 2006, 324, 475-88.
20. M. Schnoor, P. Cullen, J. Lorkowski, K. Stolle, H. Robenek, D. Troyer, J. Rauterberg, S. Lorkowski, Production of type VI collagen by human macrophages: a new dimension in macrophage functional heterogeneity, Journal of immunology, 2008, 180, 5707-19.
21. T. L. Adair-Kirk, J. J. Atkinson, T. J. Broekelmann, M. Doi, K. Tryggvason, J. H. Miner, R. P. Mecham, R. M. Senior, A site on laminin alpha 5, AQARSAASKVKVSMKF, induces

inflammatory cell production of matrix metalloproteinase-9 and chemotaxis, Journal of immunology, 2003, 171, 398-406.
22. N. G. Frangogiannis, Targeting the inflammatory response in healing myocardial infarcts, Current medicinal chemistry, 2006, 13, 1877-93.
23. B. E. Strauer, M. Brehm, T. Zeus, M. Kostering, A. Hernandez, R. V. Sorg, G. Kogler, P. Wernet, Repair of infarcted myocardium by autologous intracoronary mononuclear bone marrow cell transplantation in humans, Circulation, 2002, 106, 1913-8.
24. H. F. Tse, Y. L. Kwong, J. K. Chan, G. Lo, C. L. Ho, C. P. Lau, Angiogenesis in ischaemic myocardium by intramyocardial autologous bone marrow mononuclear cell implantation, Lancet, 2003, 361, 47-9.
25. G. P. Meyer, K. C. Wollert, J. Lotz, J. Steffens, P. Lippolt, S. Fichtner, H. Hecker, A. Schaefer, L. Arseniev, B. Hertenstein, A. Ganser, H. Drexler, Intracoronary bone marrow cell transfer after myocardial infarction: eighteen months' follow-up data from the randomized, controlled BOOST (BOne marrOw transfer to enhance ST-elevation infarct regeneration) trial, Circulation, 2006, 113, 1287-94.
26. A. P. Beltrami, L. Barlucchi, D. Torella, M. Baker, F. Limana, S. Chimenti, H. Kasahara, M. Rota, E. Musso, K. Urbanek, A. Leri, J. Kajstura, B. Nadal-Ginard, P. Anversa, Adult cardiac stem cells are multipotent and support myocardial regeneration, Cell, 2003, 114, 763-76.
27. B. Nadal-Ginard, J. Kajstura, A. Leri, P. Anversa, Myocyte death, growth, and regeneration in cardiac hypertrophy and failure, Circ Res, 2003, 92, 139-50.
28. T. A. Deisher, Cardiac-derived stem cells, IDrugs : the investigational drugs journal, 2000, 3, 649-53.
29. H. Oh, S. B. Bradfute, T. D. Gallardo, T. Nakamura, V. Gaussin, Y. Mishina, J. Pocius, L. H. Michael, R. R. Behringer, D. J. Garry, M. L. Entman, M. D. Schneider, Cardiac progenitor cells from adult myocardium: homing, differentiation, and fusion after infarction, Proc Natl Acad Sci U S A, 2003, 100, 12313-8.
30. A.P. Pego, M.J. Van Luyn, L.A. Brouwer, P.B. van Wachem, A.A. Poot, D.W. Grijpma and J.J. Feijen, In vivo behaviour of poly1, 3-trimethylene carbonate and co-polymers of 1, 3-trimethylene carbonate with D, L-lactide or ε-caprolactone: Degradation and tissue response, J. Biomed. Res. A, 2003, 67, 1044-1054.
31. T.C. McDevitt, K.A. Woodhouse, S.D. Hauschka and C.E. Murry, Spatially organized layers of cardiomyocytes on biodegradable polyurethane films for myocardial repair, J. Biomater. Res. A, 2003, 66, 586-595.
32. P. Akhyari, P. W. Fedak, R. D. Weisel, T. Y. Lee, S. Verma, D. A. Mickle, R. K. Li, Mechanical stretch regimen enhances the formation of bioengineered autologous cardiac muscle grafts, Circulation, 2002, 106, I137-42.
33. Z. Xiang, R. Liao, M. S. Kelly, M. Spector, Collagen-GAG scaffolds grafted onto myocardial infarcts in a rat model: a delivery vehicle for mesenchymal stem cells, Tissue engineering, 2006, 12. 2467-78.
34. S. Zhong, W. E. Teo, X. Zhu, R. Beuerman, S. Ramakrishna, L. Y. Yung, Formation of collagen-glycosaminoglycan blended nanofibrous scaffolds and their biological properties, Biomacromolecules, 2005, 6, 2998-3004.
35. J. Leor, S. Aboulafia-Etzion, A. Dar, L. Shapiro, I. M. Barbash, A. Battler, Y. Granot, S. Cohen, Bioengineered cardiac grafts: A new approach to repair the infarcted myocardium?, Circulation, 2000, 102, III56–III61.
36. J. Leor, Cells, scaffolds, and molecules for myocardial tissue engineering, 2005, 105, 151-

163.
37. H. C. Ott, T. S. Matthiesen, S. K. Goh, L. D. Black, S. M. Kren, T. I. Netoff, D. A. Taylor, Perfusion-decellularized matrix: using nature's platform to engineer a bioartificial heart, Nat Med, 2008, 14, 213-21.
38. C. S. Chen, M. Mrksich, S. Huang, G. M. Whitesides, D. E. Ingber, Geometric control of cell life and death, Science, 1997, 276, 1425-8.
39. R. McBeath, D. M. Pirone, C. M. Nelson, K. Bhadriraju, C. S. Chen, Cell shape, cytoskeletal tension, and RhoA regulate stem cell lineage commitment, Dev Cell, 2004, 6, 483-95.
40. K. A. Kilian, B. Bugarija, B. T. Lahn, M. Mrksich, Geometric cues for directing the differentiation of mesenchymal stem cells, Proc Natl Acad Sci U S A, 2010, 107, 4872-7.
41. R. J. Pelham, Jr., Y. Wang, Cell locomotion and focal adhesions are regulated by substrate flexibility, Proc Natl Acad Sci U S A, 1997, 94, 13661-5.
42. T. A. Ulrich, E. M. de Juan Pardo, S. Kumar, The mechanical rigidity of the extracellular matrix regulates the structure, motility, and proliferation of glioma cells, Cancer Res, 2009, 69, 4167-74.
43. A. J. Engler, S. Sen, H. L. Sweeney, D. E. Discher, Matrix elasticity directs stem cell lineage specification, Cell, 2006, 126, 677-89.
44. K. Saha, A. J. Keung, E. F. Irwin, Y. Li, L. Little, D. V. Schaffer, K. E. Healy, Substrate modulus directs neural stem cell behavior, Biophys J, 2008, 95, 4426-38.
45. W. A. Lam, L. Cao, V. Umesh, A. J. Keung, S. Sen, S. Kumar, Extracellular matrix rigidity modulates neuroblastoma cell differentiation and N-myc expression, Mol Cancer, 2010, 9, 35.
46. Y. C. Wang, C. C. Ho, Micropatterning of proteins and mammalian cells on biomaterials, Faseb J, 2004, 18, 525-7.
47. R. B. Vernon, M. D. Gooden, S. L. Lara, T. N. Wight, Microgrooved fibrillar collagen membranes as scaffolds for cell support and alignment, Biomaterials, 2005, 26, 3131-40.
48. K. Kurpinski, J. Chu, C. Hashi, S. Li, Anisotropic mechanosensing by mesenchymal stem cells, Proc Natl Acad Sci U S A, 2006, 103, 16095-100.
49. D. Motlagh, T. J. Hartman, T. A. Desai, B. Russell, Microfabricated grooves recapitulate neonatal myocyte connexin43 and N-cadherin expression and localization, J Biomed Mater Res A 2003, 67, 148-57.
50. D. Motlagh, S. E. Senyo, T. A. Desai, B. Russell, Microtextured substrata alter gene expression, protein localization and the shape of cardiac myocytes, Biomaterials, 2003, 24, 2463-76.
51. S. Y. Boateng, T. J. Hartman, N. Ahluwalia, H. Vidula, T. A. Desai, B. Russell, Inhibition of fibroblast proliferation in cardiac myocyte cultures by surface microtopography, Am J Physiol Cell Physiol, 2003, 285, C171-82.

Chapter 2 - Contractility-Dependent Modulation of Cell Proliferation and Adhesion by Microscale Topographical Cues

Originally published by John Wiley and Sons:
http://onlinelibrary.wiley.com/doi/10.1002/smll.200701302/abstract

Abstract

Engineering of cellular assembly on biomaterial scaffolds by utilizing microscale topographical cues has emerged as a powerful strategy in cardiovascular tissue engineering and regenerative medicine. However, the mechanisms through which these cues are processed to yield changes in canonical cell behaviors remain unclear. Previously, we showed that when mixtures of cardiomyocytes and fibroblasts were cultured on polydimethylsiloxane surfaces studded with microscale pillars (micropegs), fibroblast proliferation was dramatically suppressed, which suggests that the micropegs could be exploited to minimize fibrosis and scar formation. Here, we demonstrate that this effect relies on altered adhesive and micromechanical interactions between individual cells and micropegs. First, we show that the proliferation of a cell physically attached to a micropeg is significantly lower than that of a cell cultured on a featureless region of the substrate. Micropeg adhesion is accompanied by a marked elongation in cell and nuclear shape. When fibroblast contractility is pharmacologically attenuated through low-dose inhibition of either Rho-associated kinase or myosin light chain kinase, the potency with which micropeg adhesion suppresses cell proliferation is significantly reduced. Together, our results support a model in which cell fate decisions may be directly manipulated within tissue engineering scaffolds by the inclusion of microtopographical structures that alter cellular mechanics.

Introduction

One of the central challenges of tissue engineering is the design of material scaffolds that offer microscale, cell-specific behavioral cues that vary in precise and predictable ways in space. By providing these cues, one may potentially pattern complex admixtures of cells into functional tissues and organs, as well as promote the physiological activity of one cell type while simultaneously suppressing that of another. Although this task is often accomplished in organismal development through the establishment of complex spatial and temporal gradients of soluble growth, death, and differentiation factors, this approach is not appropriate for tissue engineering and regenerative medicine applications, in which there is often little direct control over the local soluble milieu of the constituent cells. Instead, over the past two decades, the field has increasingly turned to the engineering of biophysical cues within the underlying material scaffold for this microscale, cell-specific instruction. Indeed, it has been demonstrated that cell growth, death, differentiation, and motility may all be controlled by culturing cells on two-dimensional extracellular matrix (ECM) scaffolds of defined geometry[1–6] and mechanical rigidity.[7–11] Integration of three-dimensional microstructures (microtopographies) into these scaffolds represents a third and comparatively understudied biophysical signal that can strongly influence cell behavior. For example, when vascular smooth muscle cells are cultured on polymeric scaffolds with micrometer-sized grooves, the cells align and elongate within the grooves and undergo concomitant changes in cell morphology and cytoskeletal

architecture.[12] Strikingly, when this experiment is repeated with mesenchymal stem cells and the scaffold is subjected to cyclic stretching forces, the cells preferentially differentiate into vascular lineages.[13]

This issue is particularly important in the context of myocardial tissue engineering, in which one must simultaneously create an environment that promotes productive cardiomyocyte function while at the same time limiting the function of cells that promote scar formation. With respect to the former goal, cardiomyocytes, or their cellular progenitors, must be provided with adhesive substrates that enable optimal attachment and alignment, since both of these are needed for coordinated, tissue-scale transmission of electrical signals and contractile forces.[14, 15] With respect to the latter issue, endothelial damage associated with either the underlying pathology or introduction of the implant can trigger rampant inflammation,[16, 17] ultimately culminating in fibroblast proliferation and activation and the formation of scar tissue.[18, 19] In both cases, knowledge of the cellular adhesive and mechanotransductive events that underlie cell–scaffold communication may provide an additional handle for the rational design of tissue engineering scaffolds. For example, it may be possible to incorporate drugs or inhibitory DNA/RNA molecules that reinforce the biophysical cues, much in the spirit of drug- and antisense DNA-eluting vascular stents.[20]

Previously, Russell, Desai, and co-workers developed a microscale tissue engineering scaffold where cells are cultured on microfabricated, polymeric surfaces that contain an array of micrometer-sized protrusions ("micropegs"). These micropegs facilitate cardiomyocyte adhesion and contractility generation; for example, cardiomyocytes cultured on micropeg surfaces readily form adhesions with the micropegs and develop significantly larger myofibrillar masses and more elongated morphologies than cardiomyocytes cultured on flat substrates.[21] When these experiments are repeated with cells capable of undergoing cell division, such as the fibroblasts that accompany the cardiomyocytes in cell isolation, surprising results begin to emerge. In particular, populations of fibroblasts cultured on micropeg surfaces proliferate less rapidly than those cultured on flat surfaces and express lower levels of markers associated with entry into the cell cycle, including cyclin D1.

Interestingly, fibroblast attachment to the micropegs may be attenuated by pharmacological inhibition of Rho-associated kinase (ROCK), which suggests a functional connection between adhesion, contractility, and cell proliferation mediated by the micropegs.[22] These studies have left several unanswered questions about the role of the micropegs in driving cell fate decisions. For example, since these emphasized whole populations of cells, it remains uncertain whether a specific cell attached to a micropeg is any more or less likely to proliferate than its counterpart on a flat portion of the substrate. An alternative possibility would be that cells attached to micropegs participate in cell–cell signaling events that curb proliferation throughout the culture. Moreover, while these studies suggest that micropeg attachment suppresses proliferation by altering the contractile phenotype of the cells, this mechanism has not been directly explored.

Thus, we sought to directly test whether microtopographical cues from the ECM are capable of influencing cell adhesion and proliferation through a mechanobiological mechanism. We cultured fibroblasts and skeletal myoblasts on polymeric micropeg scaffolds and determined if adhesion of a single cell to a single micropeg influenced the likelihood of cell proliferation. We then asked whether this effect depends on the ability of the cell to generate contractile forces through ROCK- and myosin light chain kinase (MLCK)-dependent pathways. Indeed, our studies reveal that micropeg adhesion strongly inhibits cell proliferation at the level of individual

cells and micropegs, and that this effect is decreased when the cells' ability to adhere and stress the micropegs is inhibited.

Results

Design of array

To study the effect of microtopography on cell behavior, we fabricated an array of microscale protrusions (micropegs) out of polydimethylsiloxane (PDMS)[23] (Figure 1A,B). The array dimensions were selected to enable some cells to interact with a single micropeg, some to interact with multiple micropegs, and others to lie entirely within the flat regions between the micropegs. Indeed, when the array was oxidized and passively coated with laminin, thereby rendering it suitable for cell adhesion, we observed all three modes of cell–micropeg interaction (Figure 1C). Scanning electron microscopy (SEM) imaging of the array revealed that the micropegs provide a three-dimensional surface for attachment, and that the cells are capable of interacting with the entire height of a 15-µm-tall peg (Figure 1D). This finding was confirmed by three-dimensional reconstructions of confocal sections (not shown); for example, cells presented with a 15-µm-tall peg "climb" the peg to heights ranging from <1 to >10 µm.

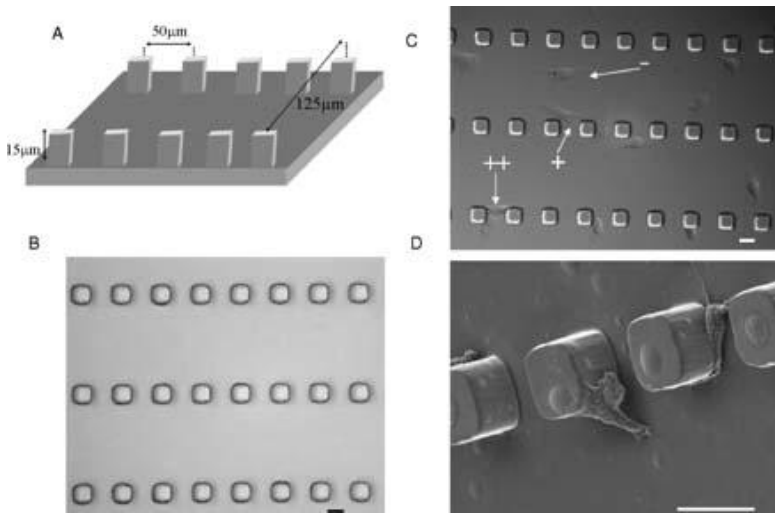

Figure 1. Micropeg arrays for cell adhesion. A) Schematic of the three-dimensional micropeg array. B) Phase-contrast image of the micropegs. C) Phase-contrast image of fibroblasts associated with the micropegs; "+" indicates a cell contacting a micropeg, "++" a cell touching two micropegs, and "–" a cell not contacting a micropeg. D) SEM image of NIH 3T3 fibroblasts interacting with 15-µm-tall micropegs. One cell tethers itself to the substrate and reaches for the top of the micropeg. On the adjacent micropeg, another cell attaches to the base of the micropeg. Scale bar: 25 µm.

Microposts alter cell proliferation

Previously, we had shown that neonatal rat ventricular fibroblast (NRVF) proliferation decreased when cultured on a micropeg array (10-µm-high pegs in a rectangular pattern with 30- and 100-µm center–center spacing between them).[22] To verify that this effect holds for a fibroblast cell line, we cultured NIH 3T3 fibroblasts on arrays of varying height and spacing. We hypothesized that the presence of the micropeg elicits phenotypic changes, whereas increasing the spacing of the array would lead to no discernible changes. After 24 hours of culture, the micropegs significantly decreased fibroblast proliferation (Figure 2). Micropeg height did not

play a role with respect to modulating the cells' proliferation. No significant difference existed between the proliferation of fibroblasts in contact with a 5-µm-tall peg versus a 15-µm-tall peg, which suggests that the effect was not enhanced by providing additional contact area for cell adhesion. As expected, increasing the micropeg array spacing to 500 µm, at which very few cells would be expected to contact micropegs, rendered proliferation indistinguishable from that of the nontextured substrate.

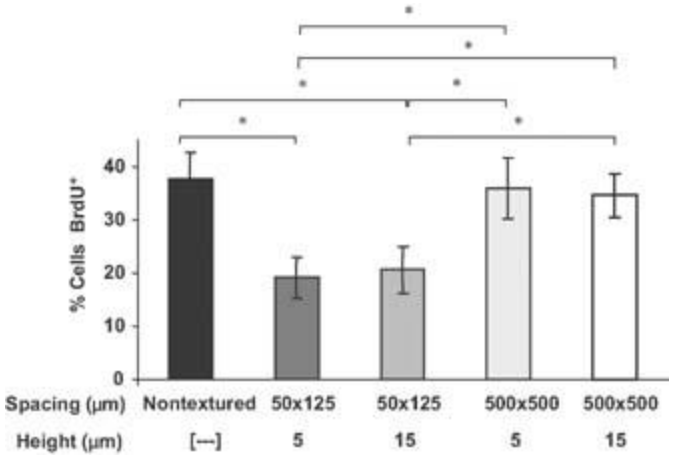

Figure 2. Micropegs affect fibroblast proliferation. Fibroblasts were seeded onto four micropeg arrays (50 × 125 × 5, 50 × 125 × 15, 500 × 500 × 5, 500 × 500 × 15 µm) and a nontextured control surface. Proliferation fell dramatically (* denotes $p < 0.001$) on substrates bearing 5- or 15-µm-tall micropegs spaced at a center-to-center distance of 50 × 125 µm (in each direction) compared to either nontextured control substrates or substrates in which the micropegs were spaced at a center-to-center distance of 500 × 500 µm. Results are representative of at least three independent experiments. BrdU = 5-bromo-2′-deoxyuridine.

To investigate whether the decrease in proliferation was tied to contact with a micropeg, we asked if a correlation existed between a single cell's adhesion to a micropeg and its propensity to proliferate (Figure 3). Cells in direct contact with a micropeg exhibited significantly lower proliferation than their counterparts with no contact to a micropeg or those cultured on a nontextured substrate. These results were also consistent for C2C12 mouse skeletal myoblasts, which indicates that this phenomenon is present in two cell types with different basal levels of contractility and rates of proliferation.

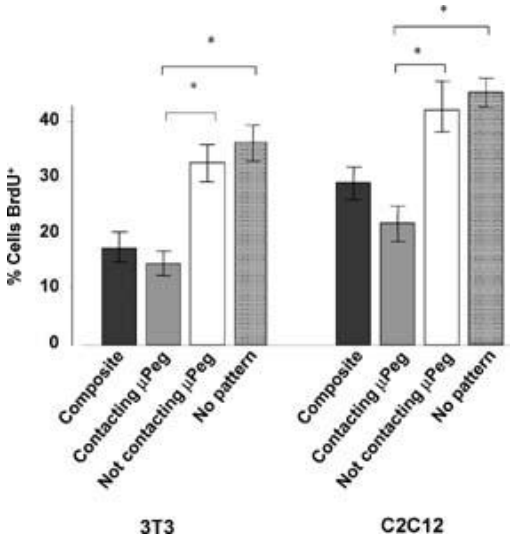

Figure 3. Proliferation effects are dependent upon cell–micropeg interactions. In both 3T3 fibroblasts and C2C12 skeletal myoblasts, proliferation decreased (* denotes $p < 0.01$) in cells making direct contact with a micropeg (µPeg), whereas cells not in contact with a micropeg exhibited proliferation rates similar to cells cultured on control, nontextured surfaces. The term "composite" refers to measurements taken on micropeg-textured surfaces, but without regard to whether a particular cell is or is not contacting a micropeg. It therefore includes contributions from both the "contacting µPeg" and "not contacting µPeg" categories.

Link of cell proliferation to cell and nuclear shape, cytoskeletal organization, and focal adhesion formation

Changes in proliferation are often accompanied by changes in cell and nuclear morphology, which in turn are indicators of changes in gene program and cellular contractility.[24, 25] In our system, cells in contact with a micropeg were more significantly elongated than cells not in contact with a micropeg or those cultured on a nontextured substrate. There were significant differences in the cell shape index (CSI) of the fibroblasts and skeletal myoblasts (Figure 4A). In both cases, cells in contact with a micropeg had a significantly lower CSI than those not in direct contact with a micropeg. Changes in the cell shape correlated with alteration in nuclear shape, as quantified by the nuclear shape index (NSI; Figure 4B). There was again a distinct divide between nuclear shape in cells in contact with a micropeg and in cells not in contact with a micropeg, regardless of cell type. We next examined whether micropegs were capable of supporting physiologically functional adhesion complexes. Fibroblasts formed vinculin-containing focal adhesions in close vicinity to the micropegs (Figure 4C–E).

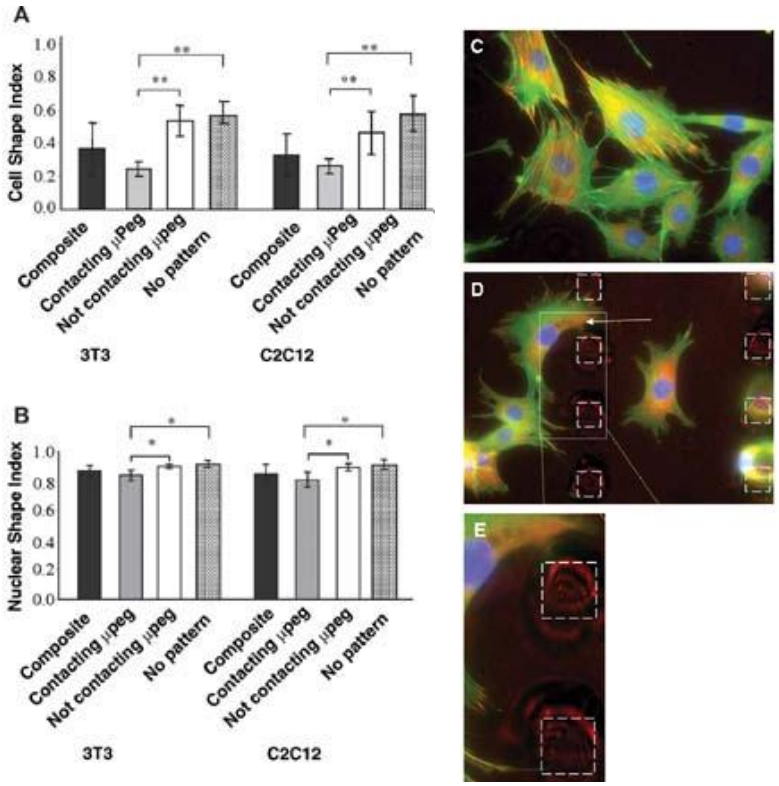

Figure 4. Cell and nuclear shape indices correlate with proliferation on micropegs. A) 3T3 and C2C12 cells in contact with a micropeg had lower CSIs, and therefore a more linear morphology than their counterparts not in contact with a micropeg B) Similarly, micropeg adhesion significantly influenced nuclear morphology, as the NSI fell when cells were in contact with a micropeg (* denotes $p < 0.05$ and ** denotes $p < 0.005$). C) 3T3 fibroblasts stained for nuclear DNA (blue), F-actin (green), and vinculin (red) are shown on a nontextured substrate. D) Fibroblasts cultured on textured substrates extended processes that form adhesions with the micropegs. E) A higher-magnification view of the vinculin staining around two micropegs. The white dashed squares are 25 × 25 μm and represent the positions of the micropegs.

Influence of micropegs is partially suppressed by inhibition of ROCK or MLCK

Based on the observed changes in cell shape and cytoskeletal organization induced by micropeg adhesion, we hypothesized that the attendant suppression of proliferation is tied to changes in cellular contractility. To test this directly, we pharmacologically inhibited two key cellular enzymes that regulate myosin-dependent contractility: ROCK and MLCK.[26–28] When fibroblasts were cultured in the presence of the ROCK inhibitor Y27632, the micropegs continued to suppress proliferation on cells in direct contact with micropegs to the same extent as the nondrug controls (Figure 5A). Similarly, micropeg adhesion suppressed proliferation for cells

cultured in the presence of the MLCK inhibitor ML7, despite the fact that overall proliferation increased slightly. When data from these experiments are represented ratiometrically, it becomes clear that inhibition of either ROCK or MLCK partially reverses the ability of the micropegs to suppress proliferation ($p < 0.05$ in both cases; Figure 5B). Importantly, and as expected, differences in proliferation between completely flat substrates ("no pattern") and flat regions of patterned substrates ("not contacting μPeg") were not statistically significant ($p > 0.05$) for any of the conditions studied.

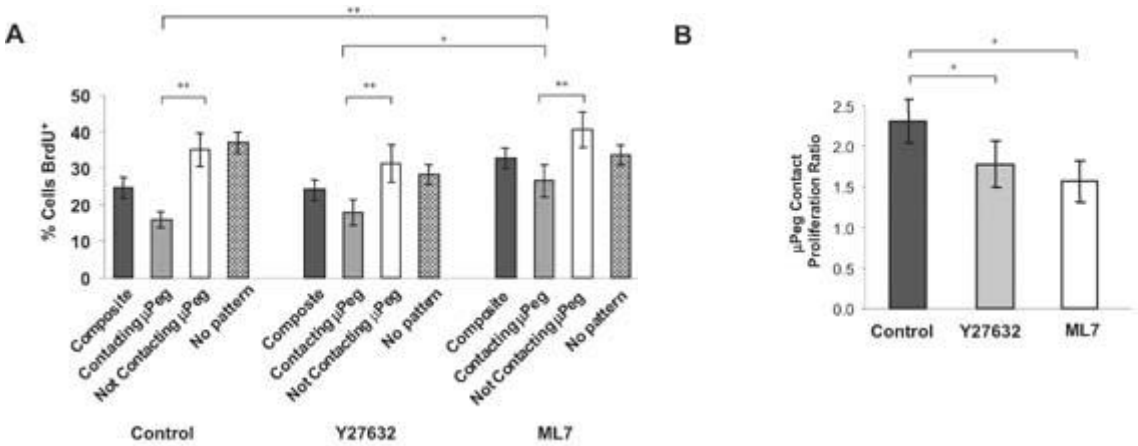

Figure 5. Contractile inhibitors suppress the function of micropegs. A) The addition of either Y27632 or ML7 to the culture reduces proliferation in cells attached to a micropeg. B) The μPeg contact proliferation ratio represents the ratio of the percentage of BrdU+ cells not touching a micropeg to the percentage of BrdU+cells in contact with a micropeg under each condition. The results represent three independent experiments, with each yielding three to four viewing fields (* denotes $p < 0.05$ and ** denotes $p < 0.005$).

Micropegs provide support and partially suppress contractile inhibitor function

To rule out the possibility that the contractility inhibitors could be exerting their effects by reducing cell adhesion to the micropegs, we quantified the number of micropegs engaged by each cell under each drug treatment (Figure 6A). Surprisingly, we found that inhibition of either ROCK or MLCK increased the likelihood of individual cells adhering to micropegs. Subsequent imaging revealed that contractility-inhibited cells cultured on nontextured substrates displayed a characteristic loss of stress fibers and reduced cell spreading (Figure 6B).

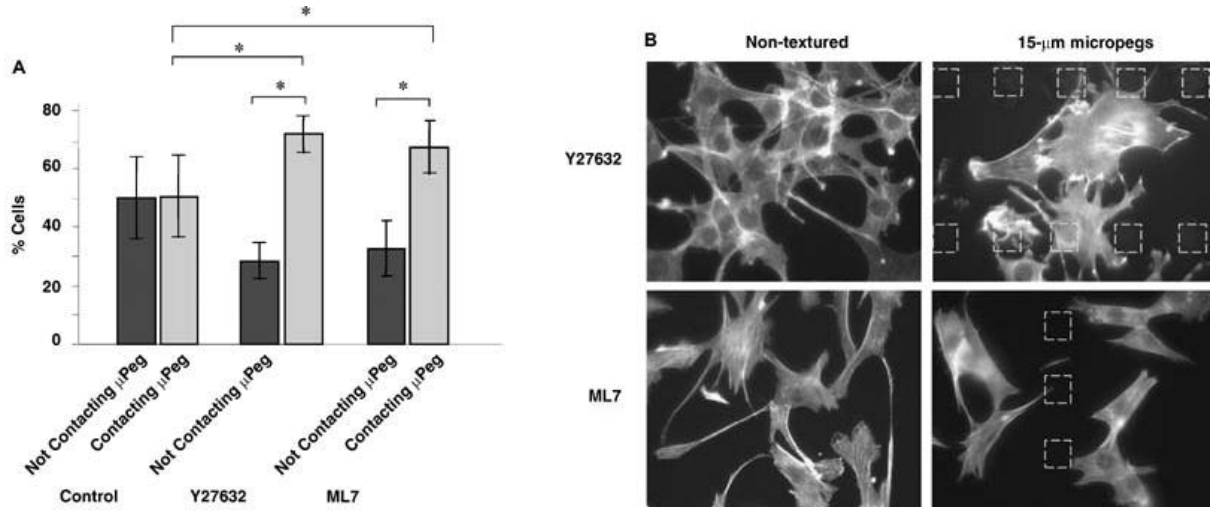

Figure 6. Fibroblasts increase adhesion to micropegs with administration of contractile inhibitors. A) The addition of Y27 and ML7 at 25 μm increases the tendency of 3T3 fibroblasts to adhere to micropegs (* denotes $p < 0.001$) Results are representative of five independent experiments yielding three to four viewing fields per experiment. B) Fluorescence imaging of F-actin reveals that inhibition of contractility produces characteristic changes in cell morphology and micropeg adhesion. The white dotted square is 25 × 25 μm and represents the position of the micropeg.

Discussion

We have shown that adhesion of cultured cells to microscale protrusions is sufficient to induce specific alterations in cell physiology that include cell and nuclear elongation, reorganization of cytoskeletal and adhesive structures, and, most strikingly, reduced cell proliferation. We have also shown that these effects depend on MLCK- and ROCK-dependent contractility, as pharmacological inhibition of these enzymes decreases the ability of the micropegs to induce these changes. This suggests a mechanism where cell–micropeg adhesion facilitates the generation of contractile forces, which in turn activates a broader gene program that influences morphology, cytoskeletal architecture, and ultimately cell fate (Figure 7). Our findings add additional support to the broadly emerging notion that mechanical inputs to cells can profoundly influence canonical cell behaviors through actomyosin-based signaling events.[29–31]

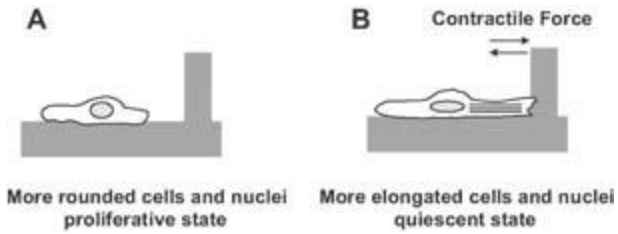

Figure 7. A model for micropeg-induced changes in cell morphology and contractility. A) A cell is depicted not to be in contact with a micropeg. This situation results in a lower CSI, NSI, and normal proliferation from the cell. B) A cell is shown in contact with a micropeg. The contact yields a quiescent cell with a lower CSI and NSI.

It is important to note that we found adhesion-dependent suppression of proliferation in two physiologically distinct cell lines: NIH 3T3 fibroblasts and C2C12 skeletal myoblasts. Even in the undifferentiated (i.e., nonsyncytiated) state, C2C12 myoblasts display highly developed and aligned contractile myofibrils on completely flat substrates;[32] moreover, C2C12 myoblasts proliferate at a much higher basal rate than NIH 3T3 fibroblasts.[33–35] Thus, it is remarkable that

micropeg adhesion alone is capable of stunting C2C12 proliferation to such a significant degree. This finding also suggests that micropegs may be incorporated into tissue engineering scaffolds as a generalizable strategy for controlling proliferation, even in cell types that proliferate at prodigious rates or do not require topographical cues to develop an oriented cytoskeleton or exert significant contractile forces. In exploring the mechanism of the micropegs' ability to curb proliferation, we inhibited cellular contractility through two nominally independent mechanisms: ROCK and MLCK. Intriguingly, both ROCK and MLCK inhibition reduced the ability of micropeg adhesion to suppress proliferation, even though each enzyme activates a distinct pool of cellular myosins.[36, 37] We also observed that inhibition of either ROCK or MLCK increased micropeg adhesion; it is unclear why this is the case, but to a first approximation one can envision two alternative possibilities: first, inhibition of contractility could cause the cells to "seek out" micropegs, possibly for mechanical support; second, inhibition of contractility could render the cells unable to fully dissociate from the micropegs once adhesions are formed. High-resolution time-lapse imaging of cells migrating on these scaffolds would help distinguish between these two hypotheses.

While our studies provide a clear phenomenological link between cell contractility and proliferation, the precise mechanism remains unclear. Indeed, our results raise the question of whether adhesive contacts formed against the vertically oriented micropegs are fundamentally different from adhesive contacts formed on flat portions of the substrate, and if so, how these differences give rise to the observed changes in physiology. The finding that suppression of proliferation is independent of micropeg height suggests that these effects are not due strictly to altered numbers of integrin–ECM contacts. One possibility is that the micropegs alter the distribution or mean area of cell–ECM focal adhesions, consistent with previous studies that demonstrate that focal adhesion size correlates with generation of cell–ECM traction and traction-dependent behaviors.[38–40] Another possibility is that attachment to a vertically oriented surface provides a geometry that favors optimal anchoring of cellular contractile elements, such as stress fibers.[41] This notion is supported by earlier studies, which demonstrated significant increases in myofibrillar mass in cardiomyocytes attached to micropegs.[22] Direct comparison of the contractility of cells attached to micropegs with that of cells cultured on flat substrates would help to explore this hypothesis more fully. Another possibility is that micropeg-bound adhesions contain different panels of adhesive proteins than their counterparts on flat substrates. Although we find that both populations of adhesions are vinculin-positive, this does not rule out the possibility that the distributions of other adhesive proteins may differ, particularly those that participate in the sensing of mechanical inputs from the ECM.[42]

Micropeg adhesion gives rise to a pronounced elongation of cell and nuclear morphology. Changes in both of these parameters have been associated with altered cell fate decisions in many systems in which cells are cultured on engineered scaffolds. For example, endothelial cells proliferate when allowed to spread onto large ECMs but apoptose when restricted to comparatively small ECMs.[1] Cell shape has also been shown to guide developmental trajectories in mesenchymal stem cells in a manner that is largely independent of soluble factors.[43] Similarly, nuclear shape has been correlated in several cell types with cell proliferation and differentiation[44, 45] and secretion of ECM components.[46] Nuclear shape has also been shown to influence the rate of transport through to the nucleus and affect the size and confirmation of nuclear pores and the genetic material inside the nucleus.[47] In considering the mechanistic link between micropeg adhesion and proliferation, many studies have revealed direct physical connections between cell-surface integrins and cell and nuclear architecture,[48–51] which suggests

strongly that the cytoskeleton is the physical actuator that translates forces applied at the cell surface into shape-dependent physiology. This is manifested in our experiments by the finding that cell–micropeg adhesion and adhesion-dependent suppression are profoundly affected when cell contractility is pharmacologically inhibited. Given this likely connection of integrin engagement to the cytoskeleton, it would be interesting to determine if the phenomena we observe depend on ligation of specific integrin subtypes or on the integrity of other cytoskeletal networks (microtubules, intermediate filaments).

Returning to the broader question of achieving microscale and spatially variable control of cell function in tissue engineering systems, our studies illustrate how relatively simple microscale topographical cues can be exploited to control proliferation rates from region to region in a single culture. It is conceivable that the adhesion-dependent proliferation observed here holds to varying degrees in different cell types, and in some cases may even follow an inverse relationship in which micropeg attachment promotes cell division. If this is the case, scaffolds like those used here could be designed with complex topographic patterns that selectively trigger changes in cell morphology, mechanics, and division at specific portions of the substrate, which could in turn provide the basis for guided assembly of complex, multicellular tissues. This prospect is particularly exciting given the recent explosion of work demonstrating that microscale, biophysical cues can direct stem cells down different developmental lineages.[13, 43, 52, 53] Additionally, it would be interesting to determine whether and to what extent these microtopographical cues can be combined with more traditional biochemical signals that are either immobilized on the scaffold (e.g., ECM-mimetic peptides) or released from the scaffold (e.g., eluted growth factors). Finally, there may even be an opportunity to combine scaffolds like these with active imposition of mechanical force on the microscale,[54] thus offering a route to control cell–scaffold mechanobiological crosstalk in the context of microscale actuators and devices.

Conclusions

We have shown that adhesion of cultured fibroblasts and myoblasts to microscale topographical cues leads to decreased cell proliferation, which is in turn dependent on the cells' ability to generate contractile force. Our finding adds new support to the notion that adhesion, contractility, and proliferation are intimately connected, and suggests that these connections can be exploited to control cell behavior in microengineered scaffolds for tissue engineering and regenerative medicine. In the next chapter the biophysical effects of micropeg adhesion on cells will be further explored.

Materials and Methods

Fabrication of micropeg arrays

Micropeg arrays were fabricated as reported previously.[21, 22, 55] To construct a photoresist (PR) mold, SU-8 2010 negative PR (Microchem, Newton, MA, USA) was spin-coated onto a single-crystal silicon wafer to a thickness of either 5 or 15 μm and baked at 95 °C for 3 min. Microscale holes were introduced by placing a patterned photomask over the coated wafer and exposing it to UV light for 25–30 s at an intensity of 5 mW cm^{-2}. The uncrosslinked PR was then removed by washing the wafer in SU-8 developer (Microchem) for 30 s, and then the SU-8 molds were baked at 95 °C for 3 min. The dimensions of the resulting microscale holes were then

verified by light microscopy and surface profilometry. To create polymeric micropeg arrays for cell culture, PDMS and curing agent were prepared and mixed as directed by the manufacturer (Sylgard 184, Dow Corning, MI), degassed under vacuum, poured onto the SU-8 mold, and spin-coated at 200 rpm for 1 min followed by 250 rpm for 30 s to achieve a thickness of 5 or 15 μm. The PDMS–wafer composite was then baked for >2 h at 70 °C. After the PDMS had cured, the micropatterned PDMS membranes were peeled from the SU-8 masters. Unpatterned PDMS membranes were fabricated in an identical manner, except for the use of unpatterned, non-PR-coated silicon wafers as masters. Prior to use in cell culture experiments, the PDMS was rendered hydrophilic by exposure to oxygen plasma and then incubated with mouse laminin (Invitrogen, Carlsbad, CA) at a concentration of 0.05 mg mL^{-1} in phosphate-buffered saline (pH 7.4) for 60 min at 4 °C.

Cell culture

NIH 3T3 mouse fibroblasts and C2C12 mouse myoblasts (ATCC, Manassas, VA) were cultured on tissue culture plastic in a complete medium consisting of Dulbecco's Modified Eagle's Medium (DMEM) with 10% fetal bovine serum and 1% penicillin/streptomycin (Gibco-BRL, Grand Island, NY). Cell cultures were maintained in a humidity-controlled 5% CO2 incubator at 37 °C. Prior to seeding on fabricated substrates, cells were allowed to grow to about 90% confluence, trypsinized, resuspended in complete medium, plated on the fabricated surfaces at a density of 10 000 cells cm^{-2}, and washed after 10–20 min to remove nonadherent cells. Longer incubation times led to an overly confluent substrate, and lower seeding densities at higher incubation times failed to produce a sufficient density of cells on the micropeg-bearing portion of the substrate for statistical analysis.

SEM

Cells were fixed in a 3% glutaraldehyde (Sigma–Aldrich, St. Louis, MO) in 0.1 M sucrose-cacodylate (Sigma–Aldrich, St. Louis, MO) buffer for 72 h at room temperature. Following fixation, samples were rinsed three times in 0.1 M sucrose-cacodylate buffer for 5 min. Samples were then dehydrated by removing the buffer and adding and replacing a series of ethanol solutions in a graded series as follows: 35, 50, 70, 95, and 100% (twice). Each ethanol solution was applied for 10 min. The final 100% ethanol solution was replaced with hexamethyldisilazane (HMDS; PolySciences, Inc., Warrington, PA) for 10 min and removed promptly. Samples were allowed to air dry for 30 min and then sputter-coated with a gold–palladium alloy.

Immunofluorescence staining

Cells were fixed in 4% paraformaldehyde (Fisher Scientific, Pittsburgh, PA) for 15 min, permeabilized with 0.5% Triton X-100 (Sigma, St. Louis, MO) for 15 min, and blocked with 1% bovine serum albumin (BSA; Sigma, St. Louis, MO) for 30 min. F-actin was stained using Alexa Fluor 488 phalloidin (Molecular Probes, Eugene, OR) for 30 min. To stain for vinculin, following the blocking step, cells were incubated with mouse anti-vinculin IgG (Sigma, St. Louis, MO) for 1.5 h at room temperature, and incubated with Alexa 563-conjugated donkey anti-mouse IgG (Molecular Probes, Eugene, OR) for 1 h at room temperature. Nuclei were stained with Hoechst 33258 (Molecular Probes, Eugene, OR). All images were acquired on a Nikon TE3000U epifluorescence microscope.

Measurement of cell proliferation

Cell proliferation was measured by incorporation of 5-bromo-2′-deoxyuridine (BrdU). Cells were cultured in complete medium for 24 h, incubated with 10 μM BrdU (Amersham, Piscataway, NJ) for 1 h, and then fixed with paraformaldehyde. To determine the incorporation of BrdU, cells were pretreated with 50% methanol, permeabilized with 0.5% Triton X-100, and then treated with 2N HCl. BrdU was stained by treating the cells with a mouse anti-BrdU primary antibody (BD Biosciences, San Jose, CA) and a fluorescein isothiocyanate-tagged goat-anti-mouse secondary antibody (Jackson ImmunoResearch). Cell nuclei were stained with 1 μg mL^{-1} propidium iodide (PI; Molecular Probes) for 5 min. The percentage of BrdU-positive nuclei was determined by dividing the number of BrdU-positive nuclei (defined by co-incorporation of BrdU and PI) by the total number of nuclei (defined by incorporation of PI).

Contractility inhibitors

To abrogate cellular contractility, Y-27632 was used to inhibit ROCK and ML-7 was used to inhibit MLCK (Calbiochem, San Diego, CA). Both drugs were diluted to 25 μM in complete medium prior to addition to the cultures. In all cases, cells were seeded and allowed to attach and spread for 2 h before application of the drug, and the drug was left in the culture for 24 h prior to analysis.

Morphometric analysis

CSI was defined here as the dimensionless ratio $4\pi(\text{cell area})(\text{cell perimeter})^{-2}$. CSI is a measure of the circularity of a cell; circular-shaped cells have CSI values approaching 1, and elongated cells have CSI values approaching 0. Similarly, the NSI was defined as $4\pi(\text{nuclear area})(\text{nuclear perimeter})^{-2}$. Both CSI and NSI were determined directly from phase-contrast images.

Statistical analysis

Statistically significant differences in multicondition data sets were detected by performing analysis of variance (ANOVA). Sequential Holm *t*-tests were then performed to identify differences between specific pairs of conditions.

References

1. C.S. Chen, M. Mrksich, S. Huang, G.M. Whitesides, D.E. Ingber, Geometric control of cell life and death. Science, 1997, 276, 1425–1428.
2. Y. C. Wang and C. C. Ho, Micropatterning of proteins and mammalian cells on biomaterials, FASEB J., 2004, 18, 525–527.
3. R. S. Kane, S. Takayama, E. Ostuni, D. E. Ingber, G. M. Whitesides, Patterning proteins and cells using soft lithography, Biomaterials, 1999, 20, 2363–2376.
4. C. J. Lee, M. S. Blumenkranz, H. A. Fishman and S. F. Bent, Controlling cell adhesion on human tissue by soft lithography, Langmuir, 2004, 20, 4155–4161.
5. H. Huang, R. D. Kamm, R. T. Lee, Cell mechanics and mechanotransduction: pathways, probes, and physiology, Am. J. Physiol. Cell Physiol, 2004, 287, C1–C11.
6. K. R. Milner, C. A. Siedlecki, Submicron poly(L-lactic acid) pillars affect fibroblast adhesion and proliferation, J. Biomed. Mater. Res. A, 2007, 82, 80–91.
7. J. A. Pedersen, M. A. Swartz, Mechanobiology in the third dimension, Ann. Biomed. Eng.,

2005, 33, 1469–1490.
8. A.J. Engler, S. Sen, H.L. Sweeney, D.E. Discher, Matrix elasticity directs stem cell lineage specification, Cell, 2006, 126, 677–689
9. A. Saez, M. Ghibaudo, A. Buguin, P. Silberzan, B. Ladoux, Rigidity-driven growth and migration of epithelial cells on microstructured anisotropic substrates, Proc. Natl. Acad. Sci. USA, 2007, 104, 8281–8286.
10. C. S. Wallace, S. A. Strike, G. A. Truskey, Smooth muscle cell rigidity and extracellular matrix organization influence endothelial cell spreading and adhesion formation in coculture, Am. J. Physiol. Heart Circ. Physiol., 2007, 3, 1978–1986.
11. J. Salber, S. Grater, M. Harwardt, M. Hofmann, D. Klee, J. Dujic, H. Jinghuan, J. Ding, S. Kippenberger, A. Bernd, J. Groll, J. P. Spatz, M. Moller, Influence of Different ECM Mimetic Peptide Sequences Embedded in a Nonfouling Environment on the Specific Adhesion of Human-Skin Keratinocytes and Fibroblasts on Deformable Substrates, Small, 2007, 3, 1023–1031.
12. R. G. Thakar, F. Ho, N. F. Huang, D. Liepmann, S. Li, Regulation of vascular smooth muscle cells by micropatterning, Biochem. Biophys. Res. Commun., 2003, 307, 883–890.
13. K. Kurpinski, J. Chu, C. Hashi, and S. Li, Anisotropic mechanosensing by mesenchymal stem cells, Proceedings of the National Academy of Sciences of the United States of America., 2006, 103, 16095–16100.
14. R. K. Birla, G. H. Borschel, R. G. Dennis, In vivo conditioning of tissue-engineered heart muscle improves contractile performance, Artif. Organs, 2005, 29, 866–875.
15. J. Leor, S. Aboulafia-Etzion, A. Dar, L. Shapiro, I. M. Barbash, A. Battler, Y. Granot, S. Cohen, Bioengineered cardiac grafts: A new approach to repair the infarcted myocardium?, Circulation, 2000, 102, III56–III61.
16. G. M. Puddu, E. Cravero, G. Arnone, A. Muscari, P. Puddu, Molecular aspects of atherogenesis: new insights and unsolved questions, J. Biomed. Sci., 2005, 12, 839–853.
17. A. B. Reiss, A. D. Glass, Atherosclerosis: Immune and inflammatory aspects, J. Investig. Med., 2006, 54, 123–131.
18. G. Ren, O. Dewald, N. G. Frangogiannis, Inflammatory mechanisms in myocardial infarction, Curr. Drug Targets Inflamm. Allergy, 2003, 2, 242–256.
19. Y. Sun, M. F. Kiani, A. E. Postlethwaite, K. T. Weber, Infarct scar as living tissue, Basic Res. Cardiol., 2002, 97, 343–347.
20. H. Takahashi, D. Letourneur, D. W. Grainger, Delivery of Large Biopharmaceuticals from Cardiovascular Stents: A Review, Biomacromolecules, 2007, 8, 3281–3293.
21. D. Motlagh, S. E. Senyo, T. A. Desai, B. Russell, Microtextured substrata alter gene expression, protein localization and the shape of cardiac myocytes, Biomaterials, 2003, 24, 2463–2476.
22. S. Y. Boateng, T. J. Hartman, N. Ahluwalia, H. Vidula, T. A. Desai, B. Russell, Inhibition of fibroblast proliferation in cardiac myocyte cultures by surface microtopography, Am. J. Physiol. Cell Physiol., 2003, 285, C171–C182.
23. G. M. Whitesides, E. Ostuni, S. Takayama, X. Jiang, D. E. Ingber, Soft lithography in biology and biochemistry, Annu. Rev. Biomed. Eng., 2001, 3, 335–373.
24. A. Lang, D. A. Brenner, Gene regulation in hepatic stellate cell, Ital. J. Gastroenterol. Hepatol., 1999, 31, 173–179.
25. S. Pelletier, C. Julien, M. R. Popoff, N. Lamarche-Vane, S. Meloche, Cyclic AMP induces morphological changes of vascular smooth muscle cells by inhibiting a rac-dependent signaling pathway, J. Cell Physiol., 2005, 204, 412–422.

26. G. Totsukawa, Y. Yamakita, S. Yamashiro, D. J. Hartshorne, Y. Sasaki, F. Matsumura, Distinct roles of rock (Rho-Kinase) and MLCK in spatial regulation of MLC phosphorylation for assembly of stress fibers and focal adhesions in 3t3 fibroblasts, J. Cell Biol., 2000, 150, 797–806.
27. F. Matsumura, Regulation of myosin II during cytokinesis in higher eukaryotes, Trends Cell Biol., 2005, 15, 371–377.
28. J. A. McKenzie, A. J. Ridley, Roles of Rho/ROCK and MLCK in TNF-α-induced changes in endothelial morphology and permeability, J. Cell Physiol., 2007, 213, 221–228.
29. K. Clark, M. Langeslag, C. G. Figdor, F. N. van Leeuwen, Myosin II and mechanotransduction: a balancing act, Trends Cell Biol., 2007, 17, 178–186.
30. K. Katoh, Y. Kano, M. Amano, H. Onishi, K. Kaibuchi, K. Fujiwara, Rho-Kinase–Mediated Contraction of Isolated Stress Fibers, J. Cell Biol., 2001, 153, 569–584.
31. M. Yanase, H. Ikeda, I. Ogata, A. Matsui, E. Noiri, T. Tomiya, M. Arai, Y. Inoue, K. Tejima, K. Nagashima, T. Nishikawa, M. Shibata, M. Ikebe, M. Rojkind, K. Fujiwara, Functional diversity between Rho-kinase- and MLCK-mediated cytoskeletal actions in a myofibroblast-like hepatic stellate cell line, Biochem. Biophys. Res. Commun., 2003, 305, 223–228.
32. D. K. McMahon, P. A. Anderson, R. Nassar, J. B. Bunting, Z. Saba, A. E. Oakeley, N. N. Malouf, C2C12 cells: biophysical, biochemical, and immunocytochemical properties, Am. J. Physiol., 1994, 266, C1795–C1802.
33. G. Biswas, H. K. Anandatheerthavarada, N. G. Avadhani, Mechanism of mitochondrial stress-induced resistance to apoptosis in mitochondrial DNA-depleted C2C12 myocytes, Cell Death Differ., 2005, 12, 266–278.
34. R. G. Dennis, P. E. Kosnik, II, M. E. Gilbert, J. A. Faulkner, Excitability and contractility of skeletal muscle engineered from primary cultures and cell lines, Am. J. Physiol. Cell Physiol., 2001, 280, C288–C295.
35. P. E. Kosnik, J. A. Faulkner, R. G. Dennis, Functional Development of Engineered Skeletal Muscle from Adult and Neonatal Rats, Tissue Eng., 2001, 7, 573– 584.
36. K. Katoh, Y. Kano, S. Ookawara, Rho-kinase dependent organization of stress fibers and focal adhesions in cultured fibroblasts, Genes Cells, 2007, 12, 623–638.
37. G. Totsukawa, Y. Wu, Y. Sasaki, D. J. Hartshorne, Y. Yamakita, S. Yamashiro, F. Matsumura, Distinct roles of MLCK and ROCK in the regulation of membrane protrusions and focal adhesion dynamics during cell migration of fibroblasts, J. Cell Biol., 2004, 164, 427–439.
38. J. L. Tan, J. Tien, D. M. Pirone, D. S. Gray, K. Bhadriraju, C. S. Chen, Cells lying on a bed of microneedles: An approach to isolate mechanical force, Proc. Natl. Acad. Sci. USA, 2003, 100, 1484–1489.
39. N. Q. Balaban, U. S. Schwarz, D. Riveline, P. Goichberg, G. Tzur, I. Sabanay, D. Mahalu, S. Safran, A. Bershadsky, L. Addadi, B. Geiger, Force and focal adhesion assembly: a close relationship studied using elastic micropatterned substrates, Nat. Cell Biol., 2001, 3, 466–472.
40. J. M. Goffin, P. Pittet, G. Csucs, J. W. Lussi, J. J. Meister, B. Hinz, Focal adhesion size controls tension-dependent recruitment of α-smooth muscle actin to stress fibers, J. Cell Biol., 2006, 172, 259–268.
41. S. Kumar, I. Z. Maxwell, A. Heisterkamp, T. R. Polte, T. P. Lele, M. Salanga, E. Mazur, D. E. Ingber, Viscoelastic Retraction of Single Living Stress Fibers and Its Impact on Cell Shape, Cytoskeletal Organization, and Extracellular Matrix Mechanics, Biophys. J., 2006, 90, 3762–3773.
42. T. P. Lele, J. Pendse, S. Kumar, M. Salanga, J. Karavitis, D. E. Ingber, Mechanical forces alter zyxin unbinding kinetics within focal adhesions of living cells, J. Cell Physiol., 2006, 207,

187–194.
43. R. McBeath, D. M. Pirone, C. M. Nelson, K. Bhadriraju, C. S. Chen, Cell Shape, Cytoskeletal Tension, and RhoA Regulate Stem Cell Lineage Commitment, Dev. Cell 2004, 6, 483–495.
44. D. E. Ingber, D. Prusty, Z. Sun, H. Betensky, N. Wang, Cell shape, cytoskeletal mechanics, and cell cycle control in angiogenesis, J. Biomech., 1995, 28, 1471–1484.
45. S. A. Lelievre, M. J. Bissell, P. Pujuguet, Cell nucleus in context, Crit. Rev. Eukaryot. Gene Expr., 2000, 10, 13–20.
46. C. H. Thomas, J. H. Collier, C. S. Sfeir, K. E. Healy, Engineering gene expression and protein synthesis by modulation of nuclear shape, Proc. Natl. Acad. Sci. USA, 2002, 99, 1972–1977.
47. C. M. Feldherr, D. Akin, The permeability of the nuclear envelope in dividing and nondividing cell cultures, J. Cell Biol., 1990, 111, 1–8.
48. A. J. Maniotis, C. S. Chen, D. E. Ingber, Demonstration of mechanical connections between integrins, cytoskeletal filaments, and nucleoplasm that stabilize nuclear structure, Proc. Natl. Acad. Sci. USA, 1997, 94, 849–854.
49. A. S. Belmont, F. M. Kendall, C. A. Nicolini, Coupling of nuclear morphometry to cell geometry and growth in human fibroblasts, Cell Biophys. 1980, 2, 165–175.
50. M. J. Dalby, M. O. Riehle, D. S. Sutherland, H. Agheli, A. S. Curtis, Use of nanotopography to study mechanotransduction in fibroblasts – methods and perspectives, Eur. J. Cell Biol., 2004, 83, 159–169.
51. S. Hu, J. Chen, N. Wang, Cell spreading controls balance of prestress by microtubules and extracellular matrix, Front. Biosci. 2004, 9, 2177–2182.
52. A. Chaubey, K. J. Ross, R. M. Leadbetter, K. J. Burg, Surface patterning: tool to modulate stem cell differentiation in an adipose system, J. Biomed. Mater. Res. B. Appl. Biomater., 2008, 84, 70–78.
53. R. Peerani, B. M. Rao, C. Bauwens, T. Yin, G. A. Wood, A. Nagy, E. Kumacheva, P. W. Zandstra, Niche-mediated control of human embryonic stem cell self-renewal and differentiation, EMBO J., 2007, 26, 4744–4755.
54. N. J. Sniadecki, A. Anguelouch, M. T. Yang, C. M. Lamb, Z. Liu, S. B. Kirschner, Y. Liu, D. H. Reich, C. S. Chen, Magnetic microposts as an approach to apply forces to living cells, Proc. Natl. Acad. Sci. USA, 2007, 104, 14553–14558.
55. J. Deutsch, D. Motlagh, B. Russell, T. A. Desai, Fabrication of microtextured membranes for cardiac myocyte attachment and orientation, J. Biomed. Mater. Res., 2000, 53, 267–275.

Chapter 3 - Biophysical mechanisms of single-cell interactions with microtopographical cues

Originally published by Springer: http://www.springerlink.com/content/kq53170601550614/

Abstract

In the previous chapter we studied the effects of adhesion to a micropeg on cell proliferation and shape, and hypothesized that these changes were due to changes in the cellular adhesion and contractility. We now directly investigate this possibility at the microscale through a combination of live-cell imaging, single-cell mechanics methods, and analysis of gene expression. Using time-lapse imaging, we show that when cells break adhesive contacts with micropegs, they form F-actin-filled tethers that extend and then rupture at a maximum, critical length that is greater than trailing-edge tethers observed on topographically flat substrates. This critical tether length depends on myosin activation, with inhibition of Rho-associated kinase abolishing topography-dependent differences in tether length. Using cellular de-adhesion and atomic force microscopy indentation measurements, we show that the micropegs enhance cell-scaffold adhesive interactions without changing whole-cell elasticity. Moreover, micropeg adhesion increases expression of specific mechanotransductive genes, including RhoA GTPase and myosin heavy chain II, and, in myoblasts, the functional marker connexin 43. Together, our data support a model in which microtopographical cues alter the local mechanical microenvironment of cells by modulating adhesion and adhesion-dependent mechanotransductive signaling.

Introduction

One of the most important emerging themes in the field of bio-interfacial design is that biophysical signals encoded in biomaterial scaffolds may be used to control cell behavior independently of signals in the soluble milieu. For example, dictation of cell geometry by micropatterning the extracellular matrix (ECM) has been demonstrated to regulate cell proliferation and death[1,2] and stem cell differentiation.[3,4] Similarly, manipulation of ECM elasticity may be used to control a wide range of cellular functions, including adhesion and migration,[5,6] lineage commitment and differentiation,[7,8] and contractile and beating properties.[9] Both shape- and rigidity-encoded cues are believed to be processed through mechanotransductive pathways that include activation and clustering of integrins, assembly and recruitment of focal adhesion proteins and cytoskeletal networks, and alterations in cellular mechanics and contractility.[10-12] In this sense, cells and the ECM participate in a reciprocal mechanical relationship in which cells adapt their intrinsic mechanical properties to ECM-encoded biophysical cues, as evidenced by the observations that changes in ECM stiffness and geometry can induce dramatic changes in cellular indentational elasticity.[13,14]

While considerable attention has been paid to the role of ECM geometry and elasticity, much less is known about the contributions of scaffold topography. A variety of previous studies have shown that culturing cells on scaffolds containing 10–100 μm-sized ridges and grooves promotes cell elongation and orientation,[14-18] and this topographically-induced alignment has been used in combination with substrate stretch to promote vascular differentiation of mesenchymal stem cells.[19] Even scaffolds patterned with features much smaller than the size of

the cell (100 nm - 1 μm) can strongly influence cell adhesion, assembly, and migration.[20-23] Recent studies with corneal fibroblasts suggest that this effect may be due to altered nanoscale clustering of integrins, which in turn leads to altered focal adhesion assembly and cytoskeletal organization.[20] Similarly, culturing cells on scaffolds containing arrays of microscale protrusions (micropegs) promotes cell attachment and has the surprising effect of reducing cell proliferation.[24-27] Even when micropegs are freed from their substrate and embedded in isotropic three-dimensional gels, the structures serve as contact guidance cues for cells and support cell adhesion and elongation and cytoskeletal orientation, while still suppressing cell proliferation.[28]

Seeking to understand mechanistic connections between ECM microtopography, cell proliferation, and mechanotransductive signaling, we recently cultured living fibroblasts and myoblasts on microfabricated scaffolds featuring arrays of micropegs.[29] Consistent with earlier observations, we found that adhesion to a micropeg substantially reduced the propensity of a cell to proliferate; this was accompanied by cell and nuclear elongation. Suspecting that micropeg adhesion might suppress proliferation through a contractility-dependent mechanism, we repeated these experiments in the setting of pharmacologic inhibition of Rho-associated kinase (ROCK) and myosin light-chain kinase (MLCK), indirect inhibitors of myosin, which strongly reduced the antiproliferative effects of micropeg adhesion. These results led us to speculate that micropeg adhesion might alter the mechanobiological properties of cells, including adhesive and migratory dynamics, mechanics, and expression of genes associated with mechanotransductive signaling. However, we did not directly test any of these hypotheses in our earlier report, leaving the micro- and nanoscale basis of cell-micropeg interactions an open question. Exploring these issues would lend mechanistic insight into the role of micropegs in controlling cellular assembly and proliferation in our system and, more generally, into the growing number of biomaterial and tissue engineering systems that seek to control cell behavior by encoding micro- and nanoscale topographical cues in the scaffold.

To address these challenges, we now directly demonstrate that micropeg adhesion alters the mechanobiological properties of living cells at the microscale. Through a combination of time-lapse phase and fluorescence imaging, cellular de-adhesion and atomic force microscopy (AFM) indentation measurements, and analysis of mechanotransductive gene expression, we show that adhesion to micropegs alters the local mechanical microenvironment by offering enhanced adhesive support to cells, which in turn enhances cell-scaffold mechanochemical feedback and amplifies expression of mechanotransductive genes.

Results

Migrating cells form adhesive tethers on flat and micropeg-textured scaffolds

In our previous study, we cultured 3T3 fibroblasts and C2C12 myoblasts on micropeg-textured, laminin-functionalized PDMS scaffolds and showed that adhesion of either cell type to a micropeg produced a suite of phenotypic changes that included cell and nuclear elongation and reduced proliferation rate. These effects could be partially blocked by inhibiting ROCK or MLCK, which led us to postulate that the micropegs acted in part by altering cellular mechanobiological properties.[29] To gain additional insight into adhesive interactions between an individual cell and a micropeg, we began here by using phase-contrast imaging to obtain time-lapse movies of 3T3 fibroblasts randomly migrating on the same flat and micropeg-textured PDMS scaffolds we had used previously (Fig. 1). Cells migrating on flat substrates developed well-defined leading and trailing edges, with the trailing edge forming “tethers” that thinned,

extended, and eventually ruptured as the cell body translocated forward (Fig. 1(A)). We continued to observe these tethers when we pharmacologically inhibited either MLCK (Fig. 1(B)) or ROCK (Fig. 1(C)) under conditions we had shown earlier were capable of blocking the effects of micropegs on proliferation. When we repeated these experiments on micropeg-textured substrates (Figs. 1(D-F)), we noticed that fibroblasts migrating away from micropegs formed similar adhesive tethers with the micropegs as they broke adhesive contact, with the tethers also persisting in the setting of either MLCK or ROCK inhibition.

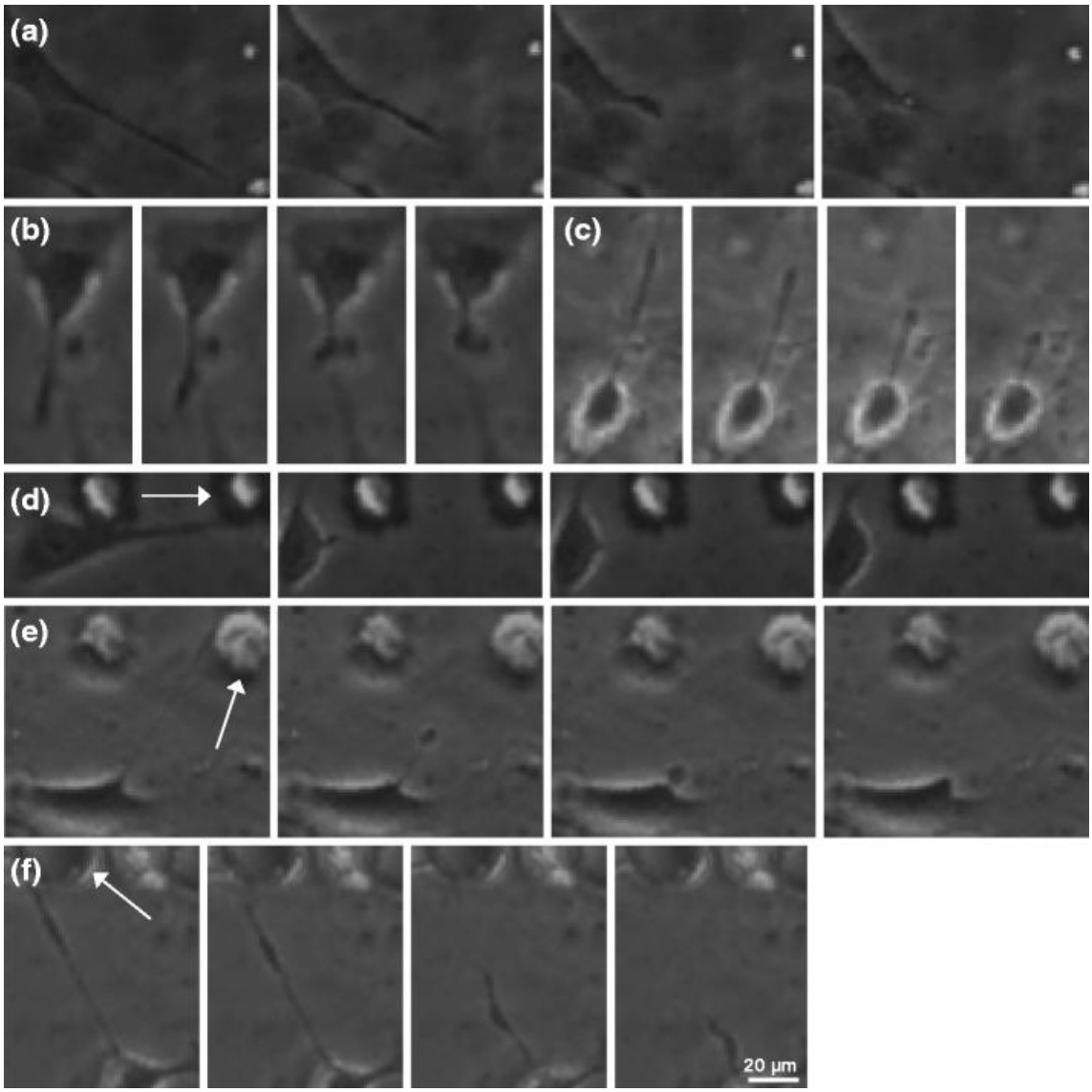

Fig. 1 Adhesive tether rupture and retraction on flat and micropeg-textured scaffolds. 3T3 fibroblasts were cultured on flat (**A–C**) or micropeg-textured (**D–F**, note white arrows) laminin-coated PDMS scaffolds and followed by phase-contrast time-lapse imaging in the presence of no drug (A, D), ML-7 (B, E), or Y-27632 (C, F). In all cases, the elapsed time between adjacent frames is 1 min. Scale bar = 20 µm

Tether length is modulated by scaffold microtopography and cell contractility

Retraction of the trailing edge of cells during migration reflects a mechanical balance between cell-generated contractile forces and cell-scaffold adhesive contacts.[30] Thus, we

reasoned that the length at which these tethers rupture (i.e., the maximum tether length) might reflect the relative strength of cellular contractility and cell-scaffold adhesion and therefore change with scaffold microtopography and the activation of myosin-based contractility. To verify that the tethers observed in our system contain contractile elements and are not empty membrane tethers, we transfected fibroblasts with green fluorescent protein-tagged actin (GFP-actin) and used time-lapse epifluorescence imaging to image actin cytoskeletal dynamics during tether retraction (Fig. 2(A)). Indeed, we found that the tethers contained actin-positive bundles that were contiguous with the cell's peripheral stress fiber network.

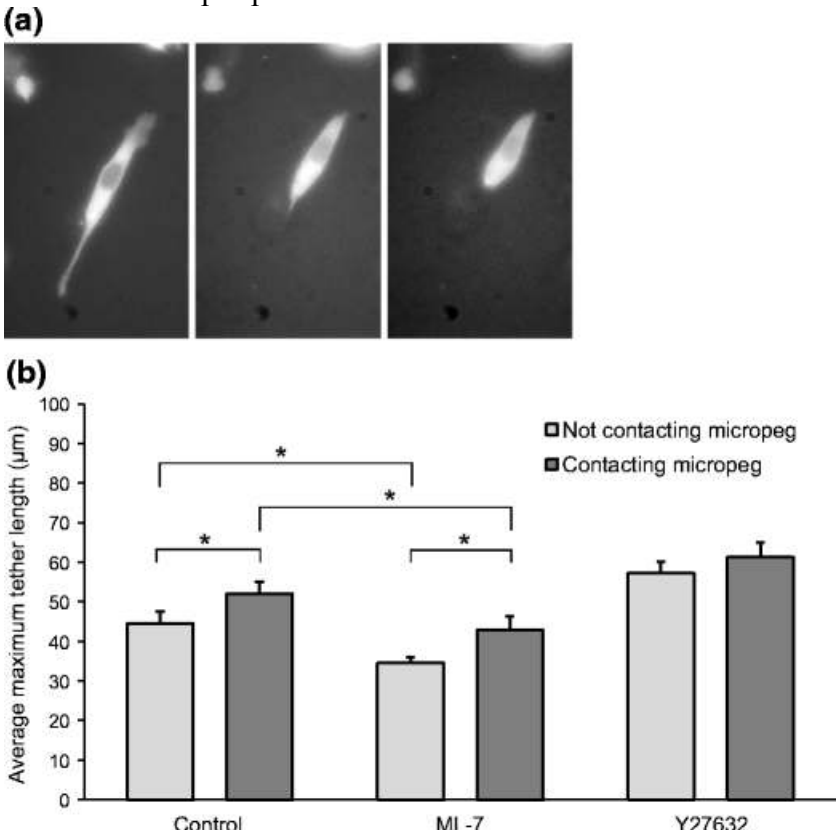

Fig. 2 Adhesive tethers contain F-actin bundles and change with MLCK and ROCK inhibition. (**A**) Time-lapse imaging of GFP-actin. 3T3 fibroblasts were transfected with GFP-actin and imaged for 5 h to capture adhesive interactions with the scaffold. 3T3 fibroblast tether retraction is shown at initial tether, tether immediately before rupture, and immediately after retraction. Cells were transfected with GFP-actin and imaged for 5 h. Tethers feature prominent F-actin-based bundles that appear contiguous with the cellular stress fiber network and retract into the cell body over time. (**B**) Maximum tether lengths in the presence and absence of topographical cues and the contractility inhibitors ML-7 and Y-27632 (*$p < 0.05$ by ANOVA followed by t-test). Error bars represent standard errors of the mean

We next performed quantitative morphometric analysis to extract average maximum tether lengths in for cells cultured on flat and micropeg-textured scaffolds, and in the presence and absence of MLCK and ROCK inhibition (Fig. 2B). We observed that in the absence of inhibitor, cells cultured on micropeg-textured scaffolds exhibited greater mean tether lengths than cells cultured on flat scaffolds, suggesting that the micropegs alter cell-micropeg adhesive interactions, contractile interactions, or both. This difference persisted in the setting of MLCK inhibition; remarkably, the average maximum tether length on micropeg-textured scaffolds under MLCK inhibition was comparable to that observed on flat scaffolds without drug, suggesting that

adhesion to a micropeg might rescue the effects of MLCK inhibition. Interestingly, ROCK inhibition abolished tether length differences between flat and micropeg-textured scaffolds and increased tether lengths overall, consistent with previous studies with other cell types[31] and reflecting reduced contractile forces at the trailing edge.

Cell de-adhesion is slowed by attachment to a micropeg

To gain additional quantitative insight into how micropeg engagement might regulate cell-scaffold adhesion and mechanics, we applied a modified version of a trypsin de-adhesion assay we recently developed, in which we enzymatically detach adherent cells and quantify the rate at which the cells round, expressed as the change in normalized projected cell area as a function of time (see Methods).[32] When we conducted this assay for cells cultured on flat and micropeg-textured scaffolds (Fig. 3), we observed that cells in contact with a micropeg detached from the surface more slowly than cells on a flat scaffold, indicating that the micropegs either decrease cell contractility or increase adhesion strength. The notion that the micropegs might enhance scaffold adhesion is further supported by the observation that on micropeg-textured scaffolds, which contain both micropegs and intervening flat regions, cells associated with a micropeg remained attached to the scaffold much longer than their counterparts on flat regions of the scaffold during enzymatic digestion (data not shown).

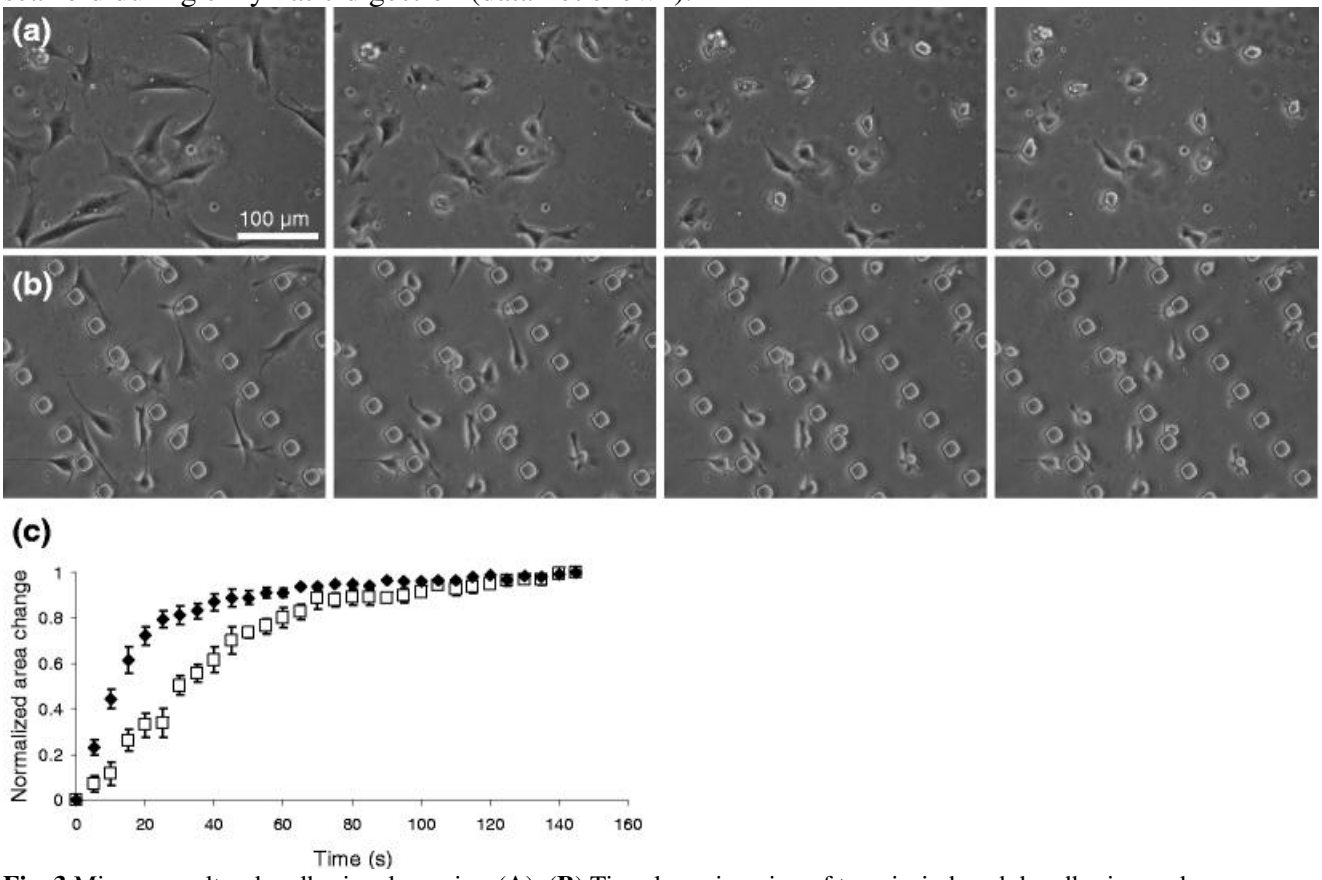

Fig. 3 Micropegs alter de-adhesive dynamics. (**A**)–(**B**) Time-lapse imaging of trypsin-induced de-adhesion and retraction of C2C12 skeletal myoblasts on (A) flat and (B) micropeg-textured scaffolds. Cells were plated on each surface, allowed to spread for 24 h, and then detached with trypsin as previously described [29]. The time elapsed between each panel is 1 min. (**C**) Normalized area change vs. time on flat (diamonds) and micropeg-textured (squares) scaffolds. Normalized area change is defined as $[A_i - A(t)]/[A_i - A_f]$ where A_i is the initial area, $A(t)$ is the area at time t, and A_f is the final area. Error bars represent standard errors of the mean.

Micropeg adhesion does not significantly alter whole-cell elasticity

Taken together, our tether length analysis and de-adhesion assays indicate that micropeg attachment alters either cellular adhesion, contractile mechanics, or both. To measure contributions of micropeg adhesion to whole-cell contractile mechanics in a more isolated fashion, we used AFM indentation to measure the cortical elasticity of cells on flat and micropeg-textured surfaces (Fig. 4). Cells cultured on flat and micropeg-textured substrates had mean elasticities of 3.92 and 3.05 kPa, respectively, a range consistent with our and others' previous measurements across multiple cell types.[14,32] Although cells cultured on flat substrates "trend" toward higher stiffnesses than those attached to micropegs, the difference is both statistically insignificant and small compared to the >5-fold differences in cell stiffnesses reported to be induced by pharmacologic dissipation of actomyosin contractility.[33] Thus, micropeg adhesion at best minimally alters global cellular contractile mechanics, which strongly suggests that the changes in tether and de-adhesion dynamics are primarily due to changes in cell-scaffold adhesion.

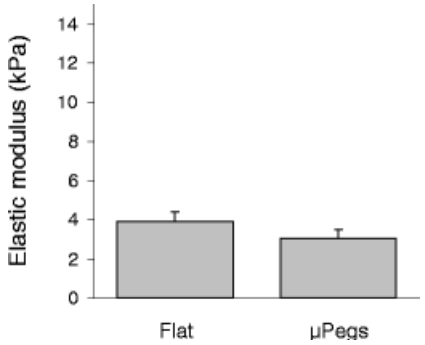

Fig. 4 Micropegs do not significantly alter cell stiffness. AFM indentation of cells indicates that the elastic modulus between cells attached to micropegs and cells on flat surface are not significantly different. Cells were seeded on surfaces and allowed to attach for 24 h before taking measurements. Measurements of cells attached to micropegs are taken as close to the micropeg as possible. Each condition represents 30–40 cells being indented with $p > 0.1$ by standard t-Test. Error bars indicate SEM

Micropeg adhesion alters expression of Myosin Heavy Chain, RhoA GTPase, and Connexin 43

While our AFM measurements failed to demonstrate significant regulation by micropegs of whole-cell contractile mechanics, it occurred to us that micropeg adhesion might still alter the expression of genes relevant to cell-scaffold mechanobiology, including elements of the myosin contractility pathway. To explore this possibility, we used Western blotting to compare the expression of selected proteins on flat versus micropeg-textured scaffolds (Fig. 5). C2C12 cells attached to micropegs exhibited increased expression of both RhoA GTPase and myosin heavy chain II (MYH2), which are critical to the assembly and activity of contractile stress fiber bundles. Importantly, because protein lysates obtained from micropeg-textured scaffolds are partially "diluted" by the contributions of cells adherent to flat regions that lie between the micropegs, any observed differences in protein expression between flat and micropeg-textured scaffolds provide a conservative underestimate of micropeg-induced effects. Interestingly, myoblasts on micropeg-textured scaffolds also displayed enhanced expression of Connexin43 (Cxn43), which plays a critical role in the fusion and differentiation of individual myoblasts into multicellular myotubes,[34,35] hinting that micropeg adhesion may promote myoblast maturation.

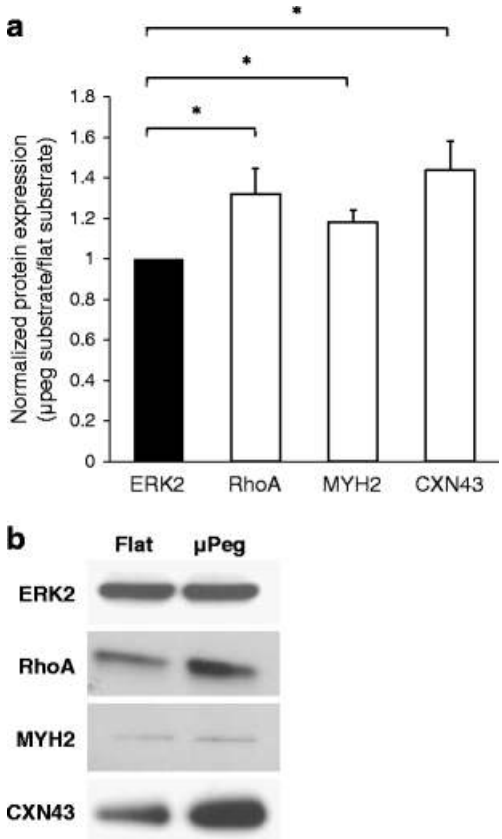

Fig. 5 Effect of micropegs on expression of selected mechanobiological genes. (**A**) Calculation of ratio of protein expression on micropeg-textured scaffolds to flat scaffolds, as measured by Western Blot. Both expression levels were normalized to expression of the loading control ERK2 on each scaffold. Expression of RhoA GTPase (RhoA), myosin heavy chain II (MYH2), and connexin 43 (CXN43) was statistically significantly higher on micropeg-textured scaffolds than on flat scaffolds ($*p < 0.05$ by log-transformed one-sample t-test). Error bars indicate SEM over at least 3 independent experiments. (**B**) Representative raw Western blot data for ERK2, RhoA, MYH2, and CXN43

Discussion

In this study, we have used live-cell time-lapse imaging, AFM, and analysis of protein expression to investigate the role played by microtopographical cues on the adhesion and mechanics of single cells. Our data support a model in which these cues alter the local physical microenvironment of cultured cells by enhancing adhesive interactions and expression of proteins that participate in cell-scaffold mechanochemical feedback. This also builds directly on our previous study, which showed that adhesion to a micropeg suppresses proliferation in a manner that can be blocked by inhibiting the ability of the cell to generate force against the scaffold, suggesting that the micropegs control cell behavior in part by altering cell-scaffold biomechanical feedback. Our current results provide the first direct evidentiary support for that hypothesis by directly demonstrating that the micropegs alter these biophysical interactions; to our knowledge, this is also the first detailed microscale analysis of mechanical and adhesive interactions between cells and microtopographical features.

Our initial hint that engagement of a micropeg might alter cell-scaffold adhesion came from observations of tethers formed by the trailing edges of cells as they migrate away and break adhesive contact from micropegs. Extrusion and characterization of membrane tethers has been

used on many previous occasions to quantify local membrane and cytoskeletal mechanics, typically in the context of optical or magnetic tweezer studies.[36-39] In these studies, membrane tethers are much smaller (<1 μm) than those observed here and devoid of cytoskeletal components. However, even under those circumstances, critical tether lengths are highly sensitive to both the state of the cytoskeleton and particle-tether adhesivity. For example, Titushkin and Cho found 2.5-fold increases in maximum tether length following cytochalasin-mediated disruption of the actin cytoskeleton in osteoblasts, corresponding to a 47% reduction in cortical elasticity by AFM.[39]

In migrating cells, retraction of the trailing edge has been widely described as reflecting a balance between cell-generated contractile forces and cell-scaffold adhesion, with enhanced adhesion to the substrate and reduced cytoskeletal contractility promoting greater tether lengths.[30,31,40,41] Indeed, maximum process length has been used previously as a semi-quantitative metric of this force balance; for example, Iwanicki and colleagues recently reported that serum-starved fibroblasts form trailing-edge tethers that are approximately fourfold longer than those observed in serum-cultured controls and that this difference can be eliminated by lysophosphatidic acid-mediated stimulation of RhoA GTPase, which would be expected to potentiate contractility. Conversely, Palecek and colleagues observed that highly adhesive scaffolds slow cell migration by limiting the rate of trailing-edge detachment, which is in turn accompanied by production of broad and highly stable lamellipodia.[42] Placing our findings in the context of this paradigm, we hypothesize that the micropegs provide an enhanced adhesive environment that supports greater tether lengths than flat scaffolds; whether this results from the provision of additional integrin ligation sites, a locally three-dimensional environment, or some combination of the two remains unclear.

While we do not find substantial micropeg-induced changes in cortical mechanics (Fig. 4), we do observe significant upregulation of expression of several elements of the myosin contractility pathway, including Rho GTPase and myosin II heavy chain (Fig. 5). An interesting explanation for these data is that micropeg adhesion induces only *local* changes in cellular mechanobiology, without altering the mechanics of the entire cell. Under this scenario, micropeg adhesion might enhance adhesion-dependent signaling and assembly of contractile structures only in the immediate vicinity of the micropeg without altering global cell mechanics. Here, contractility proteins or their mRNA precursors might be preferentially trafficked towards these new adhesive/contractile structures, analogous to previous observations of ribosomal recruitment to newly-formed focal adhesions.[43]

Our study adds new intracellular, microscale insight into a rich body of evidence that illustrates how powerfully micro- and nanoscale topographical cues can regulate cell adhesion and adhesion-dependent signaling in a manner that is largely independent of soluble biochemical cues.[17,19,26] Intriguingly, these cues can profoundly influence cell behavior even when the textured structures are orders of magnitude smaller than the cells themselves. For example, culturing smooth muscle cells on substrates nanopatterned with grooves of only 350 nm in width causes alignment along the grooves and suppression of cell proliferation.[21] Similarly, the proliferation of corneal fibroblasts can be modulated over a wide range through incorporation of nanoscale ridges and grooves into the scaffold, with smaller pitch sizes suppressing proliferation the most.[23] Even non-oriented micro- and nanoscale topographical features can strongly regulate cell behavior; for example, nonspecific decoration of planar scaffolds with metal oxide-based nanorods restricts cell spreading, and deposition of these nanorods into spatially-defined positions on the scaffold can be used as the basis of cell patterning.[44,45] In virtually all of these

cases, the nanotextured structures have been proposed to act by regulating integrin clustering and focal adhesion at the nanoscale, thereby influencing all downstream adhesion-dependent signaling. In our case, the microtextured structures are on the order of micrometers, i.e., larger than the features considered in these studies but on the same size scale as a single focal adhesion. We speculate that the enhanced adhesion and altered adhesion-dependent signaling that we observe may be derived from altered assembly of adhesive structures at the cell-micropeg interface, and we anticipate that by labeling and imaging adhesive structures at very high spatial and temporal resolution, we may be able to explore this possibility in greater detail.

Conclusions

We have explored biophysical interactions between single cells and microtopographical protrusions ("micropegs"). Using live-cell phase-contrast and fluorescence imaging, single-cell de-adhesion measurements, and AFM, we have shown that micropeg adhesion enhances cell-scaffold adhesion without altering global cell mechanics. Comparative analysis of gene expression reveals that micropeg adhesion also amplifies expression of the mechanotransductive proteins RhoA GTPase and myosin heavy chain II. We hypothesize that micropeg engagement locally reinforces cell-scaffold adhesive contacts, which in turn modulates adhesion-dependent signaling and may account for the ability of the micropegs to suppress cell proliferation.

In the next chapter we shift our focus from the behavior of fibroblasts and skeletal muscle cells to cardiomyocytes. Specifically, we will focus on how micropegs can be used to control cardiomyocyte adhesion and organization.

Materials and methods

Fabrication of PDMS micropegs

PDMS micropeg arrays were fabricated as previously described.[29] Briefly, SU-8 2010 negative photoresist (PR) (Microchem, Newton, MA) was spin-coated onto a single-crystal silicon wafer and baked at 95°C for 3 min. Microscale holes were introduced by placing a patterned photomask over the coated wafer and exposing it to UV light for 25–30 s at an intensity of 5 mW cm^{-2}, washing in SU-8 developer (Microchem) for 30 s to remove uncrosslinked PR, then baking at 95°C for 3 min. To create PDMS micropeg arrays , PDMS and curing agent were prepared and mixed as directed by the manufacturer (Sylgard 184, Dow Corning, MI), degassed under vacuum, and spin-coated onto SU-8 mold. The PDMS was baked for >2 h at 70°C, then peeled from the SU-8 masters. Unpatterned PDMS membranes were fabricated in an identical manner, except for the use of non-PR-coated silicon wafers as masters. Prior to use in cell culture experiments, the PDMS was rendered hydrophilic by exposure to air or oxygen plasma and then incubated with mouse laminin (Invitrogen, Carlsbad, CA) at a concentration of 0.02 mg mL^{-1} in phosphate-buffered saline (pH 7.4) for 60 min at 4°C. For all studies, we used rectangular micropeg arrays featuring micropegs of 15 μm height and 25 μm diameter, and with nearest-neigbor array spacings of 50 μm and 125 μm center to center.

Cell culture

NIH 3T3 mouse fibroblasts and C2C12 mouse myoblasts (ATCC, Manassas, VA) were cultured on tissue culture plastic in complete medium consisting of Dulbecco's Modified Eagle's Medium (DMEM) (Gibco, Carlsbad, CA) with 10% calf serum (JR Scientific, Woodland, CA)

and 1% penicillin/streptomycin (Gibco) for fibroblasts, and 10% fetal bovine serum (JR Scientific), 1% sodium pyruvate (Gibco), and 1% penicillin/streptomycin for myoblasts. Cell cultures were stored in a humidity-controlled 5% CO2 incubator at 37°C. For experiments, cells were allowed to grow to confluence, trypsinized, resuspended in complete medium, and plated on PDMS surfaces.

Analysis of tether length

To measure tether lengths, cells were plated on both flat and patterned PDMS substrates, allowed to spread for 4 h, and then imaged for 20 h. Tethers on each surface were measured at their maximum length before detaching or breaking. Approximately 50–60 tethers were measured per condition, and in cases in which a single cell sequentially formed and broke single tethers with one or more micropegs during timelapse imaging, each tether was measured and analyzed as a separate event. Where indicated, the MLCK inhibitor ML-7 or the ROCK inhibitor Y-27632 (Calbiochem, San Diego, CA) were diluted to 25 μM in complete medium prior to addition to cultures. Cells were plated and allowed to spread for 4 h before addition of ML-7, then imaged for 20 h.

Live-cell fluorescence imaging

Cells were plated on PDMS substrates and grown to 20–40% confluence in a 35 mm dish before transfection. The medium was then removed and replaced with 1 mL serum-free medium containing 10 μg of Lipofectamine (Invitrogen) and 1.5 μg of GFP-actin plasmid. Cells were incubated at 37°C for 24 h, after which the medium was removed and replaced with complete medium. Images were taken with a Nikon TE2000E2 epifluorescence microscope.

De-adhesion assay

Trypsin de-adhesion was performed and analyzed as previously described.[32] Briefly, cells plated on scaffolds were allowed to attach and spread for 24 h. To assess de-adhesion, media was completely removed and replaced with warm 0.5% trypsin (Gibco). Images of cells were taken every 5 s until cells were rounded and no change in area could be observed. To quantify de-adhesion, cell area was measured by tracing the outline of the cell at various time points using ImageJ (NIH). The normalized area change over time was quantified by dividing the difference between the cell area at time t and the initial spread area ($A\,i - A(t)$) by the difference in area between the first and last time points ($A\,i - A\,f$).

Atomic force microscopy (AFM)

Cells were cultured on PDMS as described above. Substrates were placed on a glass slide and mounted onto the stage of an Asylum MFP3D AFM (Asylum Research, CA) coupled to a Nikon TE2000E2 epifluorescence microscope. Cells were indented using a pyramid-tipped probe (Veeco Instruments, Santa Barbara, CA). Spring constants were determined using the thermal calibration method. Force curves were obtained for 30–35 cells for each condition. Each profile was fit with a modified Hertzian model of a cone indenting a semi-infinite elastic material to extract a set of elastic moduli.

Western blotting

Cells were allowed to adhere and spread on either flat or micropeg-patterned PDMS as above, followed by trypsinization and harvest of lysate. Protein levels were determined by

Western blot, with detection by HRP-conjugated secondary antibodies (Santa Cruz Biotechnology, Inc.) and development using Novex ECL chemiluminescent substrate (Invitrogen). ImageJ was used to determine band intensity levels from the developed blots. All intensity levels were internally normalized to the loading control ERK2 prior to calculating ratios of protein levels on micropeg-textured versus flat scaffolds. Note that lysate collected from flat scaffolds contains protein contributions only from cells adhered to a flat substrate, whereas lysate collected from micropeg-textured scaffolds contains the combined protein contributions of cells adhered to micropegs and cells adhered to the intervening flat regions. Thus, comparative analysis of lysates obtained from these two scaffold types yields a conservative underestimate of the effects of the micropegs on protein expression.

Statistics

Results are presented as mean ± standard error of the mean (SEM). Data are analyzed by Student's t-test for significance, except for Western blot analysis, which utilized a Log-transformed One-sample t-test due to the use of normalized values.

References

1. C.S. Chen, M. Mrksich, S. Huang, G.M. Whitesides, D.E. Ingber, Geometric control of cell life and death, Science, 1997, 276, 1425–1428.
2. C.M. Nelson, R.P. Jean, J.L. Tan, W.F. Liu, N.J. Sniadecki, A.A. Spector, and C.S. Chen, Emergent patterns of growth controlled by multicellular form and mechanics, Proceedings of the National Academy of Sciences of the United States of America, 2005, 102, 11594–11599.
3. R. McBeath, D.M. Pirone, C.M. Nelson, K. Bhadriraju, C.S. Chen, Cell shape, cytoskeletal tension, and RhoA regulate stem cell lineage commitment, Developmental Cell, 2004, 6, 483–495.
4. S.A. Ruiz, C.S. Chen, Emergence of patterned stem cell differentiation within multicellular structures, Stem Cells, 2008, 26, 2921–2927.
5. X.Q. Brown, J.Y. Wong, Substrate stiffness enhances the stimulatory effect of PDGF on VSMC, Mol. Biol. Cell, 2004, 15, 301A.
6. S.R. Peyton, A.J. Putnam, Extracellular matrix rigidity governs smooth muscle cell motility in a biphasic fashion. J. Cell Physiol., 2005, 204, 198–209.
7. A.J. Engler, S. Sen, H.L. Sweeney, D.E. Discher, Matrix elasticity directs stem cell lineage specification, Cell, 2006, 126, 677–689.
8. K. Saha, A.J. Keung, E.F. Irwin, Y. Li, L. Little, D.V. Schaffer, K.E. Healy, Substrate modulus directs neural stem cell behavior, Biophys. J., 2008, 95, 4426–4438.
9. A.J. Engler, C. Carag-Krieger, C.P. Johnson, M. Raab, H.Y. Tang, D.W. Speicher, J.W. Sanger, J.M. Sanger, D.E. Discher, Embryonic cardiomyocytes beat best on a matrix with heart-like elasticity: scar-like rigidity inhibits beating, J. Cell Sci., 2008, 121, 3794–3802.
10. M.G. Chown, S. Kumar, Imaging and manipulating the structural machinery of living cells on the micro- and nanoscale, Int. J. Nanomedicine, 2007, 2, 333–344.
11. S. Kumar, V. Weaver, Mechanics, malignancy, and metastasis: the force journey of a tumor cell, Cancer Metastasis Rev, 2009, 28, 113–127.
12. T.P. Lele, S. Kumar, Brushes, cables, and anchors: recent insights into multiscale assembly and mechanics of cellular structural networks, Cell Biochem, Biophys., 2007, 47, 348–360.
13. S. Sen, M. Dong, S. Kumar, Isoform-specfic contributions of a-actinin to glioma cell

mechanobiology, PLoS ONE, 2009, 4, e8427.
14. J. Solon, I. Levental, K. Sengupta, P.C. Georges, P.A. Janmey, Fibroblast adaptation and stiffness matching to soft elastic substrates, Biophys. J, 2007, 93, 4453–4461.
15. P. Clark, P. Connolly, G.R. Moores, Cell guidance by micropatterned adhesiveness invitro, J. Cell Sci, 1992, 103, 287–292.
16. C. Miller, H. Shanks, A. Witt, G. Rutkowski, S. Mallapragada, Oriented Schwann cell growth on micropatterned biodegradable polymer substrates, Biomaterials, 2001, 22, 1263–1269.
17. J.B. Recknor, J.C. Recknor, D.S. Sakaguchi, S.K. Mallapragadaa, Oriented astroglial cell growth on micropatterned polystyrene substrates, Biomaterials, 2004, 25, 2753–2767.
18. R.G. Thakar, Q. Cheng, S. Patel, J. Chu, M. Nasir, D. Liepmann, K. Komvopoulos, S. Li, Cell-shape regulation of smooth muscle cell proliferation, Biophys. J., 2009, 96, 3423–3432.
19. K. Kurpinski, J. Chu, C. Hashi, and S. Li, Anisotropic mechanosensing by mesenchymal stem cells, Proceedings of the National Academy of Sciences of the United States of America, 2006, 103, 16095–16100.
20. N.W. Karuri, P.F. Nealey, C.J. Murphy, R.M. Albrecht, Structural organization of the cytoskeleton in SV40 human corneal epithelial cells cultured on nano- and microscale grooves, Scanning, 2008, 30, 405–413.
21. S.J. Liliensiek, S. Campbell, P.F. Nealey, C.J. Murphy, The scale of substratum topographic features modulates proliferation of corneal epithelial cells and corneal fibroblasts, J. Biomed. Mater. Res. A, 79A, 185–192.
22. K.R. Milner, C.A. Siedlecki, Fibroblast response is enhanced by poly(L-lactic acid) nanotopography edge density and proximity, Int. J. Nanomedicine, 2007, 2, 201–211.
23. E.K.F. Yim, R.M. Reano, S.W. Pang, A.F. Yee, C.S. Chen, K.W. Leong, Nanopattern-induced changes in morphology and motility of smooth muscle cells, Biomaterials, 2005, 26, 5405–5413.
24. S.Y. Boateng, T.J. Hartman, N. Ahluwalia, H. Vidula, T.A. Desai, B. Russell, Inhibition of fibroblast proliferation in cardiac myocyte cultures by surface microtopography, Am. J. Physiol. Cell Physiol., 2003, 285, C171–C182.
25. J. Deutsch, D. Motlagh, B. Russell, T.A. Desai, Fabrication of microtextured membranes for cardiac myocyte attachment and orientation, J. Biomed. Mater Res., 2000, 53, 267–275.
26. D. Motlagh, T.J. Hartman, T.A. Desai, B. Russell, Microfabricated grooves recapitulate neonatal myocyte connexin43 and N-cadherin expression and localization, J. Biomed. Mater. Res. A, 2003, 67, 148–157.
27. D. Motlagh, S.E. Senyo, T.A. Desai, B. Russell, Microtextured substrata alter gene expression, protein localization and the shape of cardiac myocytes, Biomaterials, 2003b, 24, 2463–2476.
28. J.J. Norman, J.M. Collins, S. Sharma, B. Russell, T.A. Desai, Microstructures in 3D biological gels affect cell proliferation, Tissue Engineering Part A, 2008, 14, 379–390.
29. R.G. Thakar, M.G. Chown, A. Patel, L. Peng, S. Kumar, T.A. Desai, Contractility-dependent modulation of cell proliferation and adhesion by microscale topographical cues, Small, 2008, 4, 1416–1424.
30. S.P. Palecek, A. Huttenlocher, A.F. Horwitz, D.A. Lauffenburger, Physical and biochemical regulation of integrin release during rear detachment of migrating cells, J. Cell Sci., 1998, 111, 929–940.
31. T.A. Ulrich, E.M. de Juan Pardo, S. Kumar, The mechanical rigidity of the extracellular matrix regulates the structure, motility, and proliferation of glioma cells, Cancer Res., 2009, 69, 4167–4174.

32. S. Sen, S. Kumar, Cell-matrix de-adhesion dynamics reflect contractile mechanics, Cell Mol. Bioeng., 2009, 2, 218–230.
33. C. Rotsch, F. Braet, E. Wisse, M. Radmacher, AFM imaging and elasticity measurements on living rat liver macrophages, Cell Biol. Int., 1997, 21, 685–696.
34. R. Araya, D. Eckardt, M.A. Riquelme, K. Willecke, J.C. Saez, Presence and importance of connexin43 during myogenesis, Cell Commun. Adhes., 2003, 10, 451–456.
35. R. Squecco, C. Sassoli, F. Nuti, M. Martinesi, F. Chellini, D. Nosi, S. Zecchi-Orlandini, F. Francini, L. Formigli, E. Meacci, Sphingosine 1-phosphate induces myoblast differentiation through Cx43 protein expression: a role for a gap junction-dependent and -independent function, Mol. Biol. Cell, 2006, 17, 4896–4910.
36. G. Girdhar, J.Y. Shao, Simultaneous tether extraction from endothelial cells and leukocytes: observation, mechanics, and significance, Biophys. J., 2007, 93, 4041–4052.
37. E. Tabdanov, N. Borghi, F. Brochard-Wyart, S. Dufour, J.P. Thiery, Role of e-cadherin in membrane-cortex interaction probed by nanotube extrusion, Biophys. J., 2009, 96, 2457–2465.
38. I. Titushkin, M. Cho, Distinct membrane mechanical properties of human mesenchymal stem cells determined using laser optical tweezers, Biophys. J., 90, 2582–2591.
39. I. Titushkin, M. Cho, Modulation of cellular mechanics during osteogenic differentiation of human mesenchymal stem cells, Biophys. J., 2007, 93, 3693–3702.
40. S.P. Palecek, C.E. Schmidt, D.A. Lauffenburger, A.F. Horwitz, Integrin dynamics on the tail region of migrating fibroblasts, J. Cell Sci., 1996, 109, 941–952.
41. R. Rid, N. Schiefermeier, I. Grigoriev, J.V. Small, I. Kaverina, The last but not the least: the origin and significance of trailing adhesions in fibroblastic cells, Cell Motil. Cytoskelet., 2005, 61, 161–171.
42. S.P. Palecek, J.C. Loftus, M.H. Ginsberg, D.A. Lauffenburger, A.F. Horwitz, Integrin-ligand binding properties govern cell migration speed through cell-substratum adhesiveness, Nature, 1997, 385, 537–540.
43. M.E. Chicurel, R.H. Singer, C.J. Meyer, D.E. Ingber, Integrin binding and mechanical tension induce movement of mRNA and ribosomes to focal adhesions, Nature, 1998, 392, 730–733.
44. J. Lee, B.H. Chu, K.-H. Chen, F. Ren, T.P. Lele, Randomly oriented, upright SiO2 coated nanorods for reduced adhesion of mammalian cells, Biomaterials, 2009, 30, 4488–4493.
45. J.Y. Lee, B.S. Kang, B. Hicks, T.F. Chancellor, B.H. Chu, H.T. Wang, B.G. Keselowsky, F. Ren, T.P. Lele, The control of cell adhesion and viability by zinc oxide nanorods, Biomaterials, 2008, 29, 3743–3749.

Chapter 4 – Microtopographical assembly of cardiomyocytes

Abstract

Having explored the mechanisms through which fibroblast proliferation is reduced in the presence of micropegs, we shift our attention to the control of cardiomyocyte behavior. One of the central challenges in cardiac tissue engineering is the control of the assembly and organization of functional cardiac tissue. Maintenance of a three-dimensional tissue architecture is key to myocardial function in vivo, and a variety of studies hint that provision of topological cues within scaffolds can facilitate the engineering of functional myocardial tissue by promoting this architecture. To explore this possibility in an isolated and well-defined fashion, we have designed scaffolds of polydimethylsiloxane (PDMS) with microtopographic pillars ("micropegs") to provide cells with defined structures with which to interact in three dimensions. We show that these surfaces permit HL-1 cardiomyocytes to grow, form myofibrillar structures and cell–cell adhesions, and beat spontaneously. Additionally, the cells and their nuclei interact with the full length of the micropegs, indicating that the micropegs promote a three-dimensional cytoarchitecture in the context of a two-dimensional scaffold. We also show that the number of cells interacting with a micropeg can be controlled by manipulating incubation time, micropeg spatial arrangement, or micropeg diameter. Western blots reveal that the expression of the junctional markers N-cadherin and connexin 43 is upregulated in the presence of specific arrangements of micropegs, suggesting that micropegs can enhance cardiomyocyte function. Together, these data show that microtopography can be used to provide three-dimensional adhesion and control the assembly of functional cardiac tissue on a two-dimensional surface.

Introduction

The incorporation of material-encoded biophysical signals has emerged as a powerful tool for controlling cellular assembly and function in the design of tissue engineering scaffolds. At the single-cell level, control of cell shape *via* extracellular matrix (ECM) geometry has been shown to regulate cell growth and death, adhesion, and stem cell differentiation.[1–4] Modulation of the elasticity of the ECM has also been shown to regulate adhesion and migration, lineage commitment and differentiation, and contractile properties.[5–9] These ideas have also been extended to the organization of whole tissues. For example, decellularized matrices that retain three-dimensional ECM structure but completely lack cells have been successfully used as a scaffold for engineering a variety of functional tissues and organs.[10,11] Moreover, geometric patterns that promote mechanical gradients can produce spatially-ordered stem cell differentiation in the context of both two- and three-dimensional scaffolds.[12]

Whereas the majority of the field's attention has focused on the influence of substrate geometry and elasticity, scaffold microtopography has been relatively underexplored and remains poorly understood, despite the fact that it too has been shown to strongly influence cell behavior. For example, microgrooved substrates have been used to support the adhesion, alignment, and proliferation of various cell types,[13,14] and cyclic stretching of mesenchymal stem cells on these substrates enhances differentiation into vascular cells.[15] We recently showed that provision of micron-sized protrusions ("micropegs") on a two-dimensional scaffold can strongly regulate the

proliferation of fibroblasts and skeletal myoblasts through a mechanism that depends on the cell's ability to generate contractile force against these protrusions.[16] Consistent with this notion, we later showed that attachment to micropegs can regulate adhesion strength, motility, and expression of contractile markers.[17]

Microtopography bears particular promise for the engineering of myocardial tissue, in which well-defined, three-dimensional lateral and transmural architectures are key to the coordinated conduction of electrical signals and efficient generation of mechanical force. For example, it has been shown that changes in intracellular levels of Ca^{2+} and increased pacemaking activity in cardiomyocytes can be controlled by the use of microgrooved scaffolds that support a three-dimensional cytoarchitecture.[18] Furthermore, microcantilever displacement measurements have shown that cardiomyocytes grown on microgrooved surfaces generate higher contractile forces than those on flat surfaces.[19] Provision of tissue-like topographic cues has also been shown to reduce cell proliferation within mixed embryonic stem cell-derived cardiomyocyte cultures prior to terminal differentiation.[20]

While these studies have helped to establish the potential relevance of microtopographical features in the design of myocardial tissue engineering scaffolds, they leave several open questions: can these design concepts, which have largely been established with either heterogeneous progenitor populations or fully differentiated primary cardiomyocytes, be translated to immortalized cardiomyocyte culture models, which are relatively homogeneous and bear interest for high-throughput screening and toxicology applications? Can microtopographical cues be spatially patterned, thereby concurrently promoting both a three-dimensional cytoarchitecture and ordered lateral assembly? Finally, does the presence of topographical cues influence the expression of markers of cardiomyocyte function and maturation? In this study, we address all of these questions through the use of newly-designed PDMS scaffolds containing microtopographical features patterned in a variety of two-dimensional configurations. We culture HL-1 cardiomyocytes[21] on these scaffolds and show that the micropatterned surfaces support growth, beating, and expression of functional cardiomyocyte markers. Confocal imaging reveals that the cardiomyocytes interact with the full vertical dimension of the micropegs, thereby adopting a three-dimensional architecture, and time lapse imaging demonstrates that the micropegs serve as preferential adhesion sites for cells, suggesting that these structures might be exploited as physical organizing centers that could facilitate the assembly of cultured cardiomyocytes into multicellular units.

Results

Geometrical arrangements of micropegs

In our previous work, we showed that inclusion of microtopographical protrusions ("micropegs") into two-dimensional scaffolds can regulate the adhesion, polarity, and migration of a variety of cultured cell types, including fibroblasts and differentiated neonatal cardiomyocytes.[16,17,22–24] In those previous studies, the micropegs were presented as simple rows, with 50 μm spacing between adjacent micropegs and 125 μm between rows, where the spacings indicate the center-to-center distance between micropegs. This arrangement was chosen to present cells enough flat space to adhere and migrate as well as to interact with one or more micropegs. In the current study, we began by asking whether this approach could be extended to micropegs arranged in more complex geometries, which in turn might enable us to better understand the relationship between micropeg spacing and cell behavior and potentially allow us

to spatially pattern the cells themselves. To test the effects of the geometry of surface topography on cardiomyocyte assembly and function, we recreated the rows and also developed three other arrangements of micropegs: densely packed (50 μm × 50 μm spacing), sparsely packed (125 μm × 125 μm spacing), and clustered (50 μm between adjacent micropegs, 200 μm between clusters) (Fig. 1). The dense and sparse arrangements were chosen to further elucidate the effects of micropeg spacing on cardiomyocyte arrangement, and the clustered arrangement was chosen to determine regulatory effects of locally concentrating the micropegs. In all subsequent studies, we compared results obtained on each of these substrates to one another and to a flat PDMS surface used as a control.

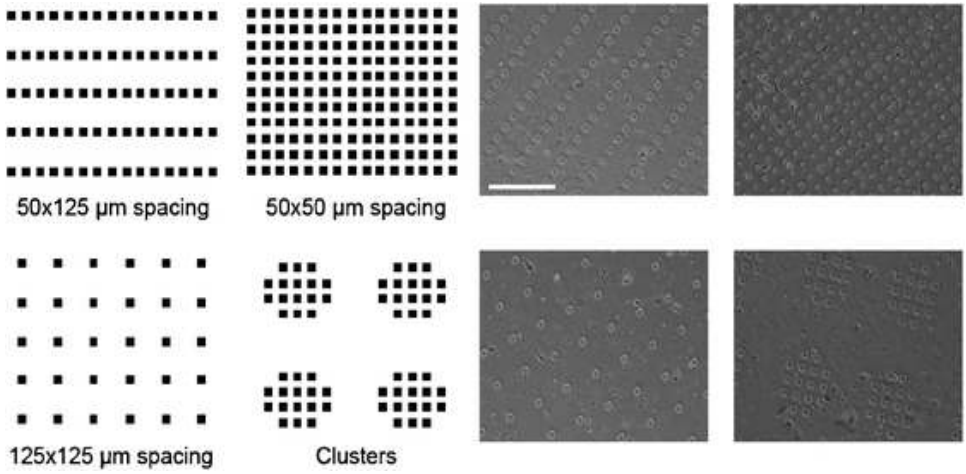

Fig. 1 Spatial arrangements of micropegs. Schematic illustrations of the four different arrangements of micropegs (left) with phase-contrast images of HL-1 cells adherent to each scaffold (right). The numbers beneath the first three arrangements represent center-to-center spacings between adjacent micropegs along each axis of the array. In the "clusters" arrangement, the center-to-center spacing between micropegs within a cluster is 50 μm and the center-to-center distance between adjacent clusters is 350 μm. Micropegs are 25 μm wide and 15 μm tall. All experiments were performed on each of these substrates as well as flat PDMS. Scale bar = 250 μm.

Micropatterned surfaces permit growth of HL-1 cells

An important limitation of our previous studies was the use of fully differentiated neonatal cardiomyocytes, which must be freshly isolated from tissue, suffer from batch-to-batch variation, and cannot be propagated in culture. Moreover, these cells lack the throughput and self-renewal properties of cardiomyocyte progenitors desired in toxicology, drug screening, and tissue engineering and regenerative medicine applications. While defined culture systems for generating cardiomyocytes from multipotent and pluripotent stem and progenitor cells have recently begun to emerge, their use remains technically demanding, with isolation of stable cardiomyocyte progenitors proving particularly challenging.[25,26] As an alternative, a continuous culture model known as the HL-1 line was recently developed from immortalized mouse atrial cardiomyocytes that is capable of self-renewal, synchronous beating, and expresses cardiac-specific functional markers, including many proteins relevant to formation of gap junctions and other cell–cell junctional complexes. While these cells differ somewhat from primary cardiomyocytes in their electrophysiological and contractile properties, they are nonetheless finding increasing use in the modeling of myocardial disease and in pharmacological testing.[27–32] HL-1 cells are traditionally grown on glass or tissue culture plastic functionalized with gelatin and fibronectin. Thus, we first asked whether PDMS with a similar coating could support adhesion and growth of HL-1 cells by culturing cells on each scaffold and counting the number of adherent cells at early and late time points after seeding, as measured by DAPI-positive nuclei

(Fig. 2). All scaffolds supported attachment of HL-1 cells within 6 hours of plating, with the number of attached cells increasing at 3 days, demonstrating that cells can proliferate on all scaffolds. Exclusion of the collagen/fibronectin coating nearly completely abolished HL-1 adhesion (data not shown), indicating that the biochemical information encoded in these matrix proteins is necessary for attachment.

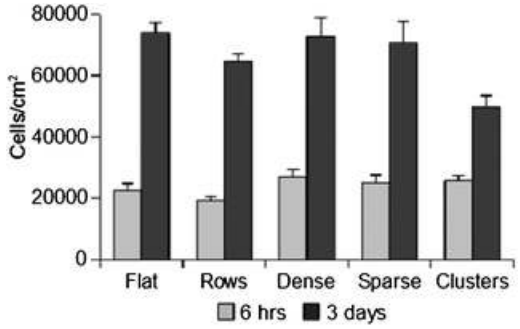

Fig. 2 Flat and patterned PDMS surfaces support the adhesion and growth of HL-1 cardiomyocytes. Cells were cultured for either 6 hours or 3 days on a specified PDMS scaffold, then fixed and fluorescently stained with DAPI, and counted using a fluorescence microscope. Cell counts were then normalized to the flat surface area available for adhesion on a given scaffold. Each condition shows significant growth from 6 hours to 3 days as measured by the Student *t*-test ($p < 0.01$). However, the differences in growth rate between conditions have not been shown to be significant. Error bars represent SEM.

HL-1 cardiomyocytes spontaneously beat on PDMS surfaces

The ability to spontaneously beat in culture is a signature property of differentiated cardiomyocytes, and HL-1 cardiomyocytes have previously been shown to beat spontaneously on gelatin/fibronectin-coated glass in culture medium that contains norepinephrine. Thus, we used phase-contrast time-lapse imaging to capture beating on our scaffolds and to quantify the beating rate (Fig. 3). Because cells were only observed to beat after reaching confluence, we performed our imaging once cultures had reached that point, which typically occurred three days after seeding (although the exact time depended on initial cell density). All scaffolds supported beating with rates in the range of 90–120 beats per minute, similar to previously-reported HL-1 beating rates.[33,34] In all cases, beating was only observed in the context of multicellular foci, implying that all scaffolds are capable of supporting mechanical and electrophysiological coupling between cells.

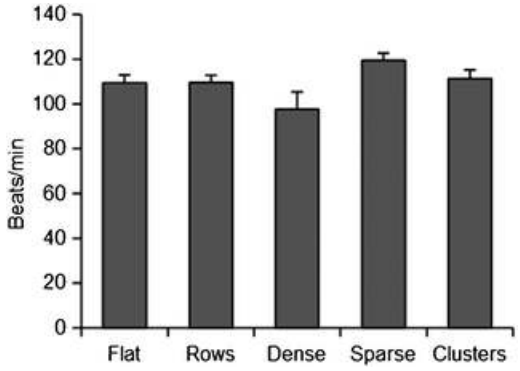

Fig. 3 HL-1 beating rates remain consistent across different patterned surfaces. HL-1 beating was visualized using time-lapse phase-contrast imaging and measured by counting the number of beats in a 60 second period. Measurements were taken once cells reached confluence, which occurred three days after seeding. Error bars represent SEM, and $p > 0.05$ across all conditions by the Student *t*-test.

Ratio of cells in contact with micropegs depends upon time and the arrangement and width of micropegs

The above data establish that micropegs facilitate cardiomyocyte attachment and do not preclude the ability to form cell–cell contacts needed for beating. In order to better understand the dynamics of this process, we measured the ratio of cells in contact with micropegs on each surface at both 24 hours and 48 hours after seeding (Fig. 4). The ratio of cells in contact with micropegs is quantified by counting the number of cells touching micropegs and dividing by the total number of cells per field of view. In both the clustered and sparse arrangements, this ratio increases with time, as opposed to the rows arrangement where this ratio remains constant (Fig. 4A). For the dense arrangement of micropegs, these contact ratios were, as expected, typically very close to 1, *i.e.*, all cells were in contact with a micropeg (not shown). To more closely examine the effect of differences in micropeg density available for cell adhesion, we normalized the number of micropeg-attached cells by the number of micropegs for each field of view (Fig. 4B). This revealed consistent values across all scaffolds at 24 h post-seeding, with an increase for the sparse and clustered arrangements at 48 h (Fig. 4C).

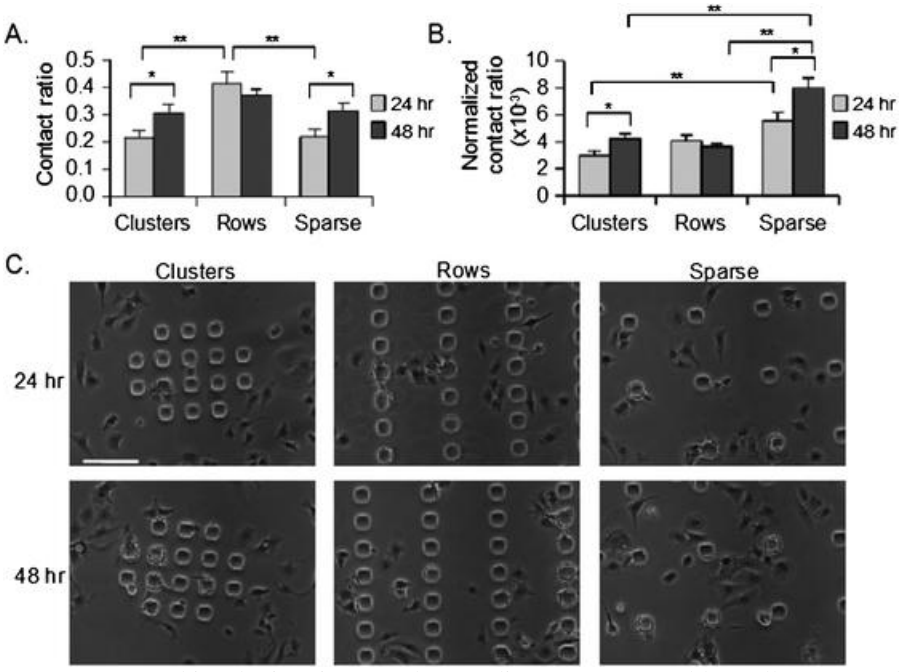

Fig. 4 Micropeg arrangement and incubation time regulate cardiomyocyte assembly. Cells were seeded on patterned substrates and analyzed after 24 or 48 hours. (A) Micropeg contact ratio on each surface at 24 and 48 hours post seeding, as defined by the ratio of cells in contact with a micropeg to the total number of cells in a field of view. Error bars represent SEM. Asterisk indicates significant difference ($p < 0.05$) and double asterisk indicates a very significant difference ($p < 0.01$). (B) Micropeg contact ratio normalized by the number of micropegs in a given field of view. Error bars represent SEM. Asterisk indicates significant difference ($p < 0.05$) and double asterisk indicates a very significant difference ($p < 0.01$). (C) Representative phase-contrast images for each condition. Scale bar = 100 μm.

We further investigated the ability of the micropegs to control cell organization by varying the height and width of individual micropegs while keeping the arrangement of the micropegs constant. Using the sparse arrangement of micropegs, we varied the height of micropegs between 5, 15, and 50 μm, and the width of micropegs between 15, 25, and 50 μm (Fig. 5). We observed that the contact ratio did not vary significantly with micropeg height but

did rise with increasing micropeg width, as expected, given that wider micropegs provide additional surface area for attachment (Fig. 5A). Consistent with our observations with standard-sized micropegs (Fig. 4) contact ratios in all cases increased from 24 to 48 hours. When these values were normalized to the width of the micropegs, we found that some of the effects of the increasing width on the contact ratio were washed out, but that the normalized ratio for the narrower micropegs was slightly higher for each height (Fig. 5B).

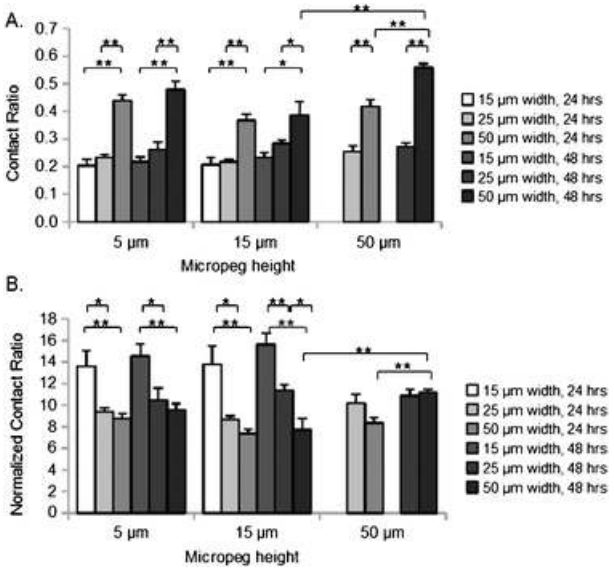

Fig. 5 Cardiomyocyte assembly depends on micropeg width but not height. Cells were seeded on "sparse" patterned substrates with micropegs of varying height and width and analyzed after 24 and 48 hours. (A) Micropeg contact ratio on each surface at 24 and 48 hours post-seeding, as defined by the ratio of cells in contact with a micropeg to the total number of cells in a field of view. Error bars represent SEM. Asterisk indicates significant difference ($p < 0.05$) and double asterisk indicates a very significant difference ($p < 0.01$). (B) Micropeg contact ratio normalized by the width of the micropegs. Note that data for the tallest and thinnest micropegs (15 µm width, 50 µm height) are absent because the high fragility of these structures precluded their robust fabrication and manipulation in culture.

Taken together, these data are consistent with a kinetic model in which cells initially adhere to flat portions of the scaffold, encounter micropegs as they migrate, and preferentially adhere to these structures over time. In other words, even for scaffolds in which a small minority of the available adhesive area is occupied by micropegs, these micropegs eventually retain and sequester a disproportionate number of cardiomyocytes.

HL-1 cells exhibit myofibrillar structures and cell–cell adhesions and interact with the full length of the micropegs

As described earlier, a key design advantage of micropeg-based scaffolds is that they are expected to promote a three-dimensional cytoarchitecture that is more representative of cellular morphology in tissue and is critically tied to coordination of function. To assess the degree to which our scaffolds promote three-dimensional topologies, we used confocal microscopy to visualize the expression and subcellular localization of the cardiac-specific myosin heavy chain, which also serves as a secondary marker of cardiomyocyte function (Fig. 6). For all scaffolds, cardiomyocytes expressed cardiac-specific myosin robustly, with localization reflecting myofibril assembly. Cells frequently wrapped themselves around the micropegs, with cell nuclei flattened against the micropeg walls. For dense scaffolds and scaffolds arrayed as rows and

clusters, cells were sometimes observed to bridge adjacent micropegs. Optical sectioning revealed that the cardiomyocytes also interacted with the full height of the micropegs, consistent with adoption of a three-dimensional architecture. To investigate scaffold effects on cell–cell adhesion, we immunostained and performed confocal imaging against N-cadherin (Fig. 7). Clear localization of this marker to cell–cell interfaces was observed across all scaffolds. Curiously, N-cadherin was also observed at the cell–micropeg interface, although it is unclear whether this represents ectopic localization to cell-matrix contacts or merely reflects the projection of nonspecific N-cadherin staining across multiple horizontal planes. As with myosin, N-cadherin staining was observed along the entire length of the micropeg, supporting the notion that the cells engage the full vertical aspect of these structures and thereby maintain a three-dimensional architecture.

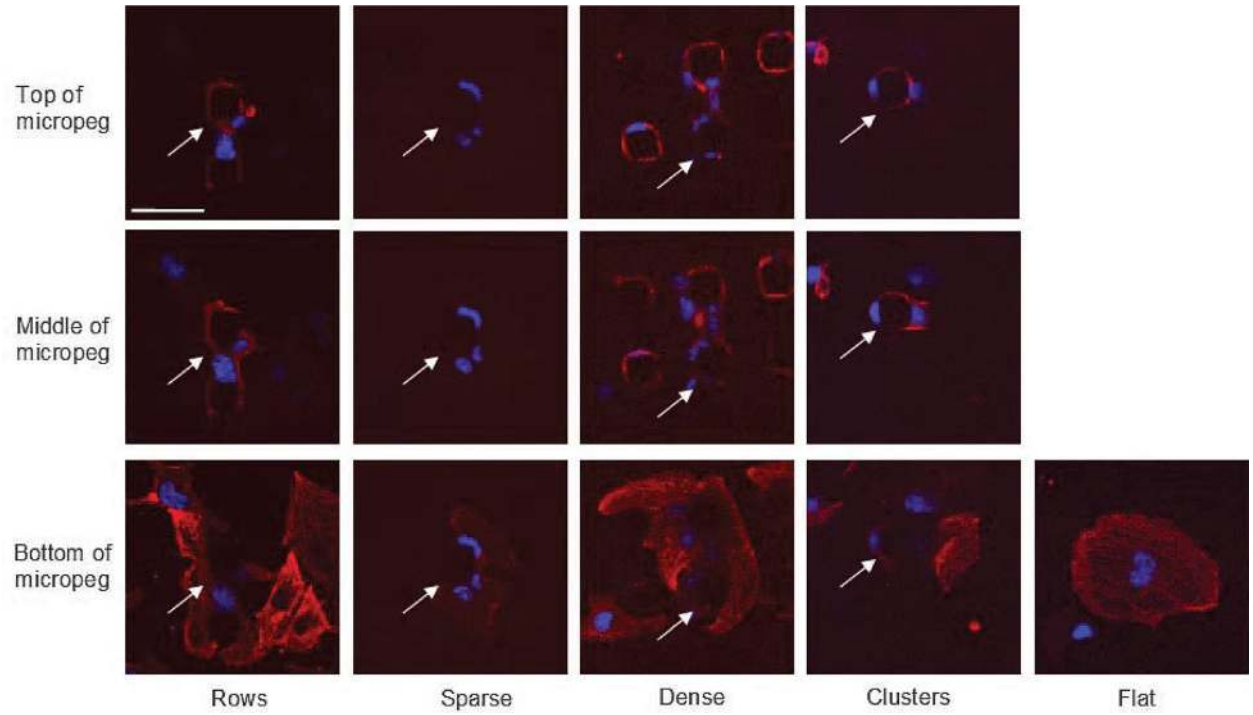

Fig. 6 Myosin heavy chain is expressed along the full length of the micropegs and incorporates into myofibrils. HL-1 cells were cultured for 3 days, fixed and immunostained for the myosin heavy chain (red) and DAPI (blue) and imaged with a confocal microscope. Images were taken at three positions for each condition: the flat surface of the PDMS, the vertical midpoint of the micropeg, and the top of the micropeg. For completely flat PDMS, images were taken at the surface. White arrows indicate the location of one micropeg within the field of view. Scale bar = 50 μm.

N-cadherin and connexin 43 expression can be controlled by micropeg arrangement

Having shown that the micropeg surfaces can regulate the cytoarchitecture of the cardiomyocytes without compromising beating, we next sought to quantify the extent to which micropegs could be used to quantitatively regulate expression of functional markers. We focused on the cell–cell adhesion proteins N-cadherin and connexin 43, the former serving as an early marker of cell–cell structural/mechanical coupling and the latter serving as a later marker of cell–cell electrical coupling (Fig. 8).[35] Western blots revealed comparable expression levels of both markers across all scaffolds, with modest (10–30%) but statistically significant increases in N-cadherin expression on dense and clustered substrates and in connexin-43 expression on row and

dense substrates. Importantly, inclusion of micropegs did not reduce expression of either marker, consistent with the notion that the presence of these structures does not compromise cardiomyocyte function.

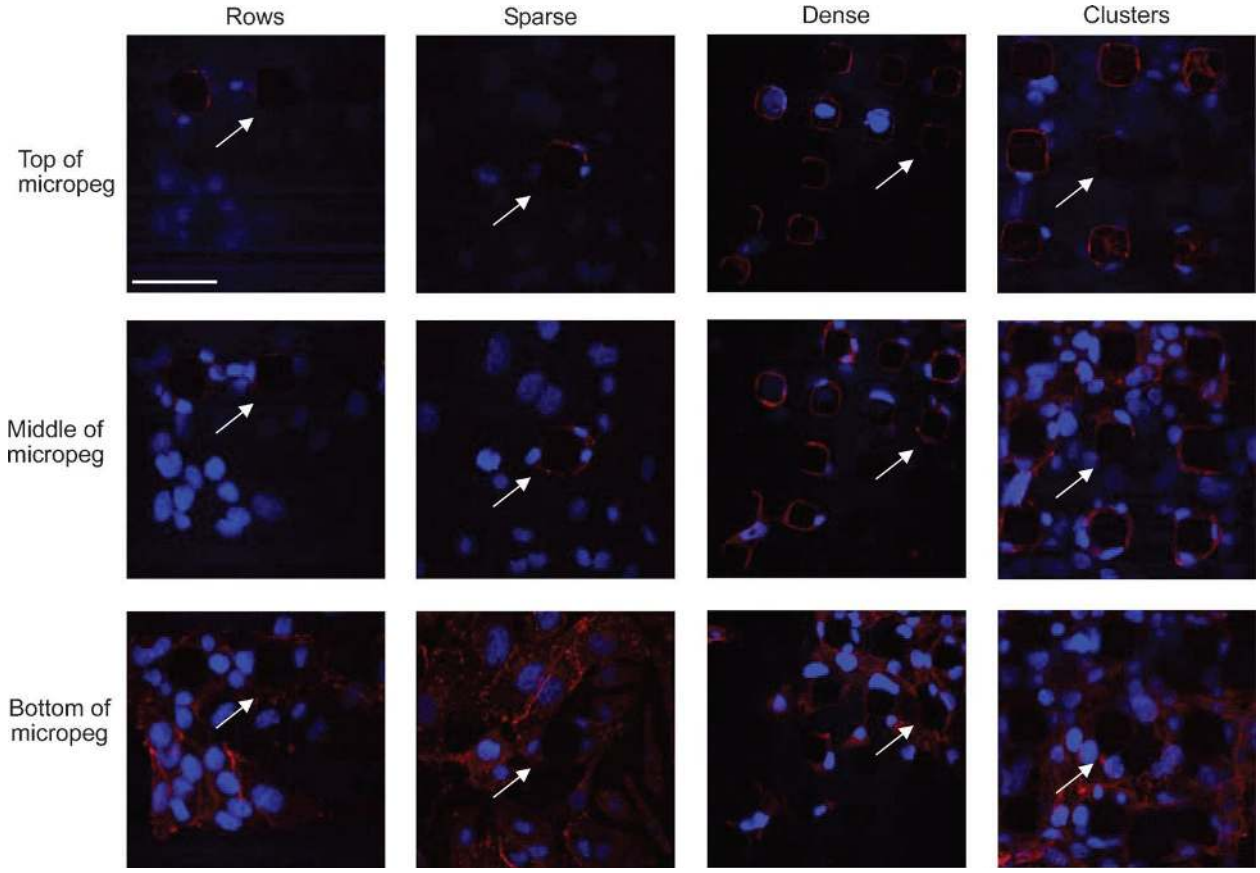

Fig. 7 Scaffold microtopography affects N-cadherin expression. HL-1 cells were cultured for 3 days, fixed and immunostained for N-cadherin (red) and DAPI (blue) and imaged with a confocal microscope. Images were taken at three positions for each condition: the flat surface of the PDMS, the vertical midpoint of the micropeg, and the top of the micropeg. White arrows indicate the location of one micropeg within the field of view. Scale bar = 50 μm.

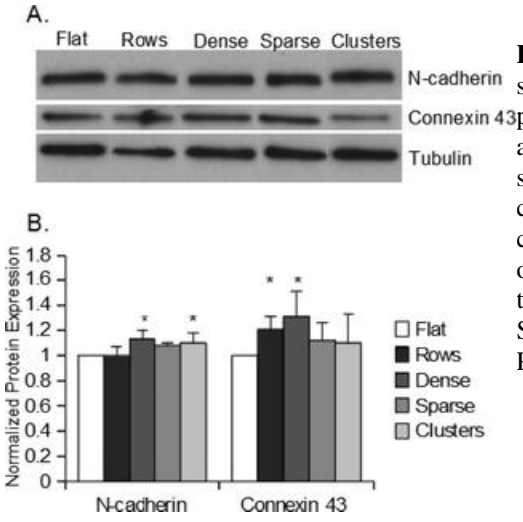

Fig. 8 Expression of cell–cell junctional proteins depends on the spatial arrangement of micropegs. (A) Representative Western blot of protein expression of cell–cell adhesion junction proteins N-cadherin and connexin 43 and loading control tubulin on each patterned PDMS substrate. Cells were seeded onto each substrate and lysates were collected after 72 hours. (B) Ratio of protein expression of N-cadherin and connexin 43 on each patterned PDMS substrate to that on a flat substrate after 72 hours. Expression levels were normalized to the expression of tubulin on each surface. Errors bars represent SEM. Asterisk indicates significant difference from expression on flat PDMS ($p < 0.05$).

Discussion

We have used live cell time lapse imaging, confocal fluorescence microscopy, and analysis of protein expression to investigate the role played by microtopographical cues in controlling the adhesion, organization, and function of cardiomyocytes. We find that these micropegs can be patterned in specific geometric arrangements that can in turn promote sequestration of cardiomyocytes into specific macro-architectures on the scaffold. Inclusion of these microtopographical features does not compromise cardiomyocyte function as measured by beating rate and expression and localization of specific functional markers. Attachment to a micropeg also promotes adoption of a three-dimensional morphology in which cardiomyocytes associate with the lateral walls of the micropeg. Combined with our previous work detailing increased cell adhesion strength to micropegs compared to flat surfaces, these results support a model in which micropegs serve as organizing centers that recruit and retain cardiomyocytes over time and could potentially serve as nucleating sites for the assembly of functional clusters of cardiac tissue.

A significant new finding of this study is that the arrangement of the micropegs determines how likely the cardiomyocytes are to attach to them. For all the patterns, the ratio of cells in contact with micropegs is greater than one would expect to occur through random distribution of cells on the surface. This is most pointedly illustrated by the fact that the pattern with the lowest global density of micropegs was the one with the highest ratio of cells contacting micropegs. The preferential attachment of cardiomyocytes to micropegs leads to increased clustering, three-dimensional cellular organization, and changes in the localization and orientation of the nucleus. These changes suggest that cellular organization can be controlled by modulating the arrangement of the microtopographical features. While the degree of cell patterning observed here is relatively modest, one could envision enhancing this effect by creating haptotactic or durotactic cues on the scaffold that promote migration to the topographical features. Moreover, the micropegs themselves conceivably could be chemically functionalized with specific adhesive ligands or even used as depots for the controlled release of differentiation factors. Future efforts will focus on incorporating these functionalities.

Our studies reveal that incorporation of micropegs into scaffolds does not compromise, and in some cases may modestly enhance, expression of N-cadherin and connexin-43, two markers of cardiac maturation. These two proteins cooperate to propagate mechanical and electrical signals that underlie synchronous beating of cardiac tissue.[35] Developmentally, N-cadherin expression precedes connexin 43 expression in the fetal heart and is a prerequisite for the formation of gap junctions in the intercalated disk.[36,37] N-cadherin is also important for the anchoring of myofibrils and the transmission of force from cell to cell, and N-cadherin dependent mechanosensing has been shown to be a regulator of cardiomyocyte shape, myofibrillar organization, and cortical stiffness.[38,39] Loss of N-cadherin expression has been linked to the development of myocardial arrhythmia due to slowed conduction velocity and gap junction remodeling.[40] Similarly, connexin 43 is the primary component of gap junctions and allows for the conduction of the electrical signal among neighboring cardiac cells.[35] Loss of connexin 43 expression and changes in its spatial distribution in the intercalated disc can lead to fatal cardiac arrhythmia and dysfunction.[41,42] Further study should help to determine whether scaffold geometry can be used to manipulate myocardial function *per se*, including the magnitude of force generation and the speed with which electrical signals are conducted across the scaffold surface.

These results add to a growing body of evidence supporting a role for the mechanical and topographical environments in the design of cardiac tissue engineering applications. Scaffold stiffness has previously been shown to regulate stem cell differentiation, cardiac organization, beating rate, and contractility.[6,8,43–45] Recently, a parallel set of studies has shown that the introduction of microrods into 3D cardiac tissue engineering scaffolds can be used to modulate cardiac function, scar tissue formation, and stem cell differentiation, implying that microtopographical cues can be incorporated into three-dimensional hydrogel scaffolds.[46–48] In each of these cases, the microrods are embedded in a gel scaffold oriented randomly. Based on our results, we speculate that the functionality and organization of the cardiomyocytes in these scaffolds could be further manipulated by controlling the spatial arrangement of the microrods.

Conclusions

We have demonstrated that we can promote both the three-dimensional architecture and lateral organization of cardiomyocytes through the use of microtopographical patterning. These micropatterned substrates are capable of supporting cardiomyocyte growth, beating, myofibril assembly, and expression of functional markers. These results suggest that topographical patterning may be used to control the assembly of cardiac tissue in cell culture and tissue engineering applications.

To more directly test how the presence of topography on a surface controls cardiomyocyte adhesion, in the next chapter we will explore the use of microwells to present cells with the option of adhering to either a flat surface or to three-dimesional architecture.

Materials and Methods

Cell culture

HL-1 mouse cardiomyocytes were generously provided by Dr William C. Claycomb, Louisiana State University. Following established HL-1 culture protocols,[21] tissue culture flasks were prepared by precoating with a solution containing 0.02% gelatin (Fisher Scientific, Pittsburgh, PA) and 5 μg ml^{-1} fibronectin (Sigma-Aldrich, St Louis, MO) and incubating overnight at 37 °C. Cultures were maintained in these flasks in complete medium consisting of Claycomb Medium (Sigma-Aldrich) supplemented with 10% fetal bovine serum (Sigma-Aldrich), 0.1 mM norepinephrine (Sigma-Aldrich), 1× L-glutamine (Sigma-Aldrich), and 1% penicillin/streptomycin (Gibco, Carlsbad, CA). Cell cultures were stored in a humidity-controlled 5% CO_2 incubator at 37 °C. For experiments, cells were allowed to grow to confluence, trypsinized, resuspended in complete medium, and plated on PDMS scaffolds.

Fabrication of PDMS micropegs

PDMS micropeg arrays were fabricated as previously described.[16] Briefly, an SU-8 negative photoresist (PR) (Microchem, Newton, MA) was spin-coated onto a single-crystal silicon wafer and baked at 95 °C for 3 min. SU-8 2005, 2010, and 2035 were used to make thicknesses of 5, 15, and 50 μm, respectively. Microscale holes were introduced by placing a patterned photomask over the coated wafer and exposing it to UV light for 25–30 s at an intensity of 5 mW cm^{-2}, washing in an SU-8 developer (Microchem) for 30 s to remove uncrosslinked PR, then baking at 95 °C for 3 min. Different patterns were created by changing the pattern of the photomask. To create PDMS micropeg arrays, PDMS and the curing agent

were prepared and mixed as directed by the manufacturer (Sylgard 184, Dow Corning, MI), degassed under vacuum, and spin-coated onto an SU-8 mold. The PDMS was baked for 1 h at 80 °C, then peeled from the SU-8 masters. Unpatterned PDMS membranes were fabricated in an identical manner. Prior to use in cell culture experiments, the PDMS was rendered hydrophilic by exposure to air plasma and then incubated with the gelatin/fibronectin mix mentioned above for 2 h at 37 °C. For experiments on PDMS surfaces with no ECM, the same procedure was followed but the gelatin/fibronectin was replaced by phosphate-buffered saline. For studies with fixed micropeg height and width, we used arrays featuring micropegs of 15 μm height and 25 μm diameter.

Growth and micropeg contact ratio measurements

Cells were plated on either glass or PDMS at a concentration of 10^4 cells ml^{-1} and were fixed with 4% paraformaldehyde (PFA) at appropriate time points. Cells were then incubated with 4′,6-diamidino-2-phenylindole (DAPI) (Invitrogen, Carlsbad, CA) for 25 min at room temperature to visualize nuclei. Cells were then visualized with a Nikon TE2000E2 epifluorescence microscope. For growth studies, the number of nuclei at each time point was quantified using ImageJ (NIH). For contact ratio studies, the numbers of nuclei were counted manually and then compared to phase images to determine whether cells were in contact with micropegs or completely in flat space.

Beating measurements

Cells were plated on PDMS and allowed to grow to confluence. Beating cells were localized and recorded using time-lapse phase contrast imaging (Nikon TE2000E2). To quantify beating rates, individual beating foci were recorded for 30 s and the number of beats was divided by the time elapsed.

Immunostaining and confocal imaging

Cells grown on PDMS surfaces were fixed with 4% PFA at room temperature for 10 min, or with 19:1 ethanol:acetone at 4 °C for 15 min for the myosin heavy chain. Cells were then permeabilized, blocked with 5% normal goat serum, then incubated in mouse primary antibodies directed against either N-cadherin (BD Biosciences, San Jose, CA) diluted 1:100 or the sarcomeric myosin heavy chain (Developmental Studies Hybridoma Bank, Iowa City, IA) diluted 1:20 for 1 h, followed by incubation with DAPI and a goat anti-mouse secondary antibody conjugated to an Alexa Fluor dye (Invitrogen) for 45 min at 1:500 for N-cadherin and 1:750 for the myosin heavy chain. Confocal images were acquired with a Zeiss LSM 510 Meta Confocal Laser Scanning Microscope.

Western blotting

Cells were allowed to adhere and spread on either flat or micropeg-patterned PDMS as above, followed by trypsinization and harvest of lysate. Protein levels were determined by a Western blot using mouse primary antibodies against N-cadherin (BD Biosciences) and tubulin (Sigma-Aldrich) and a rabbit antibody against connexin 43 (Cell Signaling Technology, Danvers, MA), all diluted at 1:50000 and incubated overnight at 4 °C. Bands were then detected using HRP-conjugated goat–anti-mouse and goat–anti-rabbit secondary antibodies (Invitrogen) diluted 1:100000 and incubated for 45 min at room temperature, followed by development using the Novex ECL chemiluminescent substrate (Invitrogen). ImageJ was used to determine band

intensity levels from the developed blots. All intensity levels were internally normalized to the tubulin loading control prior to calculating ratios of protein levels on micropeg-textured *versus* flat scaffolds. It is important to note that lysates obtained from micropeg-textured scaffolds contain protein contributions both from cells adhered to micropegs and cells adhered to the intervening flat regions. Thus, immunoblots obtained with these scaffolds necessarily *underestimate* the effects of the micropegs on protein expression relative to completely flat scaffolds.

Statistics

Results are presented as mean with error bars representing the standard error of the mean (SEM). Data were analyzed by Student's *t*-test for significance.

References

1. C. S. Chen, M. Mrksich, S. Huang, G. M. Whitesides and D. E. Ingber, Geometric control of cell life and death, Science, 1997, 276, 1425–1428.
2. C. J. Lee, M. S. Blumenkranz, H. A. Fishman and S. F. Bent, Controlling cell adhesion on human tissue by soft lithography, Langmuir, 2004, 20, 4155–4161.
3. R. McBeath, D. M. Pirone, C. M. Nelson, K. Bhadriraju and C. S. Chen, Cell shape, cytoskeletal tension, and RhoA regulate stem cell lineage commitment, Dev. Cell, 2004, 6, 483–495.
4. K. A. Kilian, B. Bugarija, B. T. Lahn and M. Mrksich, Geometric cues for directing the differentiation of mesenchymal stem cells, Proc. Natl. Acad. Sci. U. S. A., 2010, 107, 4872–4877.
5. T. A. Ulrich, E. M. de Juan Pardo and S. Kumar, The mechanical rigidity of the extracellular matrix regulates the structure, motility, and proliferation of glioma cells, Cancer Res., 2009, 69, 4167–4174.
6. A. J. Engler, S. Sen, H. L. Sweeney and D. E. Discher, Matrix elasticity directs stem cell lineage specification, Cell, 2006, 126, 677–689.
7. K. Saha, A. J. Keung, E. F. Irwin, Y. Li, L. Little, D. V. Schaffer and K. E. Healy, Substrate modulus directs neural stem cell behavior, Biophys. J., 2008, 95, 4426–4438.
8. A. J. Engler, C. Carag-Krieger, C. P. Johnson, M. Raab, H. Y. Tang, D. W. Speicher, J. W. Sanger, J. M. Sanger and D. E. Discher, Embryonic cardiomyocytes beat best on a matrix with heart-like elasticity: scar-like rigidity inhibits beating, J. Cell Sci., 2008, 121, 3794–3802.
9. W. A. Lam, L. Cao, V. Umesh, A. J. Keung, S. Sen and S. Kumar, Extracellular matrix rigidity modulates neuroblastoma cell differentiation and N-myc expression, Mol. Cancer, 2010, 9, 35, e8427.
10. H. C. Ott, T. S. Matthiesen, S. K. Goh, L. D. Black, S. M. Kren, T. I. Netoff and D. A. Taylor, Perfusion-decellularized matrix: using nature's platform to engineer a bioartificial heart, Nat. Med., 2008, 14, 213–221.
11. T. H. Petersen, E. A. Calle, L. Zhao, E. J. Lee, L. Gui, M. B. Raredon, K. Gavrilov, T. Yi, Z. W. Zhuang, C. Breuer, E. Herzog and L. E. Niklason, Tissue-engineered lungs for in vivo implantation, Science, 2010, 329, 538–541.
12. S. A. Ruiz and C. S. Chen, Emergence of patterned stem cell differentiation within multicellular structures, Stem Cells, 2008, 26, 2921–2927.
13. Y. C. Wang and C. C. Ho, Micropatterning of proteins and mammalian cells on biomaterials,

FASEB J., 2004, 18, 525–527.
14. R. B. Vernon, M. D. Gooden, S. L. Lara and T. N. Wight, Microgrooved fibrillar collagen membranes as scaffolds for cell support and alignment, Biomaterials, 2005, 26, 3131–3140.
15. K. Kurpinski, J. Chu, C. Hashi and S. Li, Anisotropic mechanosensing by mesenchymal stem cells, Proc. Natl. Acad. Sci. U. S. A., 2006, 103, 16095–16100.
16. R. G. Thakar, M. G. Chown, A. Patel, L. Peng, S. Kumar and T. A. Desai, Contractility-dependent modulation of cell proliferation and adhesionby microscale topographical cues, Small, 2008, 4, 1416–1424.
17. A. A. Patel, R. G. Thakar, M. Chown, P. Ayala, T. A. Desai and S. Kumar, Biophysical mechanisms of single-cell interactions with microtopographical cues, Biomed. Microdevices, 2010, 12, 287–296.
18. L. Yin, H. Bien and E. Entcheva, Scaffold topography alters intracellular calcium dynamics in cultured cardiomyocyte networks, Am. J. Physiol.: Heart Circ. Physiol., 2004, 287, H1276–H1285.
19. J. Kim, J. Park, K. Na, S. Yang, J. Baek, E. Yoon, S. Choi, S. Lee, K. Chun and S. Park, Quantitative evaluation of cardiomyocyte contractility in a 3D microenvironment, J. Biomech., 2008, 41, 2396–2401.
20. J. K. Biehl, S. Yamanaka, T. A. Desai, K. R. Boheler and B. Russell, Proliferation of mouse embryonic stem cell progeny and the spontaneous contractile activity of cardiomyocytes are affected by microtopography, Dev. Dyn., 2009, 238, 1964–1973.
21. W. C. Claycomb, N. A. Lanson, Jr, B. S. Stallworth, D. B. Egeland, J. B. Delcarpio, A. Bahinski and N. J. Izzo, Jr, HL-1 cells: a cardiac muscle cell line that contracts and retains phenotypic characteristics of the adult cardiomyocyte,Proc.Natl. Acad. Sci. U. S.A., 1998, 95, 2979–2984.
22. S. Y. Boateng, T. J. Hartman, N. Ahluwalia, H. Vidula, T. A. Desai and B. Russell, Inhibition of fibroblast proliferation in cardiac myocyte cultures by surface microtopography, Am. J. Physiol. Cell Physiol., 2003, 285, C171–C182.
23. J. Deutsch, D. Motlagh, B. Russell and T. A. Desai, Fabrication of microtextured membranes for cardiac myocyte attachment and orientation, J. Biomed. Mater. Res., 2000, 53, 267–275.
24. D. Motlagh, S. E. Senyo, T. A. Desai and B. Russell, Microtextured substrata alter gene expression, protein localization and the shape of cardiac myocytes, Biomaterials, 2003, 24, 2463–2476.
25. Z.Melkoumian, J. L.Weber, D. M.Weber, A. G. Fadeev, Y. Zhou, P. Dolley-Sonneville, J. Yang, L. Qiu, C. A. Priest, C. Shogbon, A. W. Martin, J. Nelson, P. West, J. P. Beltzer, S. Pal and R. Brandenberger, Synthetic peptide–acrylate surfaces for long-term self-renewal and cardiomyocyte differentiation of human embryonic stem cells, Nat. Biotechnol., 2010, 28, 606–610.
26. S. T. Wall, C. C. Yeh, R. Y. Tu, M. J. Mann and K. E. Healy, Biomimetic matrices for myocardial stabilization and stem cell transplantation, J. Biomed. Mater. Res., Part A, 2010, 95, 1055–1066.
27. D. B. Sanders, D. F. Larson, K. Hunter, M. Gorman and B. Yang, Comparison of tumor necrosis factor-alpha effect on the expression of iNOS in macrophage and cardiac myocytes, Perfusion, 2001, 16, 67–74.
28. B. J. Brundel, H. H. Kampinga and R. H. Henning, Calpain inhibition prevents pacing-induced cellular remodeling in a HL-1 myocyte model for atrial fibrillation, Cardiovasc. Res., 2004, 62, 521–528.

29. M. E. Hensler, S. Miyamoto and V. Nizet, Group B streptococcal beta-hemolysin/cytolysin directly impairs cardiomyocyte viability and function, PLoS One, 2008, 3, e2446.
30. U. Hellman, L. Malm, L. P. Ma, G. Larsson, S. Morner, M. Fu, A. Engstrom-Laurent and A. Waldenstrom, Growth factor PDGF-BB stimulatescultured cardiomyocytes to synthesize the extracellular matrix component hyaluronan, PLoS One, 2010, 5, e14393.
31. T. Budde, J. Haney, S. Bien, M. Schwebe, A. Riad, C. Tschope, A. Staudt, G. Jedlitschky, S. B. Felix, H. K. Kroemer and M. Grube, Acute exposure to doxorubicin results in increased cardiac P-glycoprotein expression, J. Pharm. Sci., 2011, 100, 3951–3958.
32. M. Poteser, H. Schleifer, M. Lichtenegger, M. Schernthaner, T. Stockner, C. O. Kappe, T. N. Glasnov, C. Romanin and K. Groschner, PKC-dependent coupling of calcium permeation through transient receptor potential canonical 3 (TRPC3) to calcineurin signaling in HL-1 myocytes, Proc. Natl. Acad. Sci. U. S. A., 2011, 108, 10556–10561.
33. Z. Yang and K. T. Murray, Ionic mechanisms of pacemaker activity in spontaneously contracting atrial HL-1 cells, J. Cardiovasc. Pharmacol., 2011, 57, 28–36.
34. C. H. George, G. V. Higgs and F. A. Lai, Ryanodine receptor mutations associated with stress-induced ventricular tachycardia mediate increased calcium release in stimulated cardiomyocytes,
Circ. Res., 2003, 93, 531–540.
35. M. Noorman, M. A. van der Heyden, T. A. van Veen, M. G. Cox, R. N. Hauer, J. M. de Bakker and H. V. van Rijen, Cardiac cell–cell junctions in health and disease: Electrical versus mechanical coupling, J. Mol. Cell. Cardiol., 2009, 47, 23–31.
36. H. Reinecke, M. Zhang, T. Bartosek and C. E. Murry, Survival, integration, and differentiation of cardiomyocyte grafts: a study in normal and injured rat hearts, Circulation, 1999, 100, 193–202.
37. S. Kostin, S. Hein, E. P. Bauer and J. Schaper, Spatiotemporal development and distribution of intercellular junctions in adult rat cardiomyocytes in culture, Circ. Res., 1999, 85, 154–167.
38. Y. Luo and G. L. Radice, Cadherin-mediated adhesion is essential for myofibril continuity across the plasma membrane but not for assembly of the contractile apparatus, J. Cell Sci., 2003, 116, 1471–1479.
39. A. Chopra, E. Tabdanov, H. Patel, P. A. Janmey and J. Y. Kresh, Cardiac myocyte remodeling mediated by N-cadherin-dependent mechanosensing, Am. J. Physiol.: Heart Circ. Physiol., 2011, 300, H1252–H1266.
40. J. Li, V. V. Patel, I. Kostetskii, Y. Xiong, A. F. Chu, J. T. Jacobson, C. Yu, G. E. Morley, J. D. Molkentin and G. L. Radice, Cardiac specific loss of N-cadherin leads to alteration in connexins with conduction slowing and arrhythmogenesis, Circ. Res., 2005, 97, 474–481.
41. M. S. Spach, J. F. Heidlage, P. C. Dolber and R. C. Barr, Electrophysiological effects of remodeling cardiac gap junctions and cell size: experimental and model studies of normal cardiac growth, Circ. Res., 2000, 86, 302–311.
42. M. R. Abraham, C. A. Henrikson, L. Tung, M. G. Chang, M. Aon, T. Xue, R. A. Li, B. O' Rourke and E. Marban, Antiarrhythmic engineering of skeletal myoblasts for cardiac transplantation, Circ. Res., 2005, 97, 159–167.
43. K. Shapira-Schweitzer and D. Seliktar, Matrix stiffness affects spontaneous contraction of cardiomyocytes cultured within a PEGylated fibrinogen biomaterial, Acta Biomater., 2007, 3, 33–41.
44. B. Bhana, R. K. Iyer, W. L. Chen, R. Zhao, K. L. Sider, M. Likhitpanichkul, C. A. Simmons and M. Radisic, Influence of substrate stiffness on the phenotype of heart cells, Biotechnol.

Bioeng., 2010, 105, 1148–1160.
45. A.Marsano, R. Maidhof, L. Q. Wan, Y.Wang, J. Gao, N. Tandon and G. Vunjak-Novakovic, Scaffold stiffness affects the contractile function of three-dimensional engineered cardiac constructs, Biotechnol. Prog., 2010, 26, 1382–1390.
46. M. W. Curtis, S. Sharma, T. A. Desai and B. Russell, Hypertrophy, gene expression, and beating of neonatal cardiac myocytes are affected by microdomain heterogeneity in 3D, Biomed. Microdevices, 2010, 12, 1073–1085.
47. P. Ayala, J. I. Lopez and T. A. Desai, Microtopographical cues in 3D attenuate fibrotic phenotype and extracellular matrix deposition: implications for tissue regeneration, Tissue Eng. A, 2010, 16, 2519–2527.
48. J. M. Collins, P. Ayala, T. A. Desai and B. Russell, Three dimensional culture with stiff microstructures increases proliferation and slows osteogenic differentiation of human mesenchymal stem cells, Small, 2010, 6, 355–360.

Chapter 5 – Isolation of cells in microwells to measure 2D vs. 3D attachment

Abstract

One of the central challenges of cardiac tissue engineering is the control of the assembly of functional cardiac tissue. In the previous chapter we showed that microtopographical cues can provide cells with the ability to attach to a surface in three-dimensions. Here we aim to test the hypothesis that individual cells, when given the choice between two- and three-dimensional architecture, are more likely to adhere to a surface in three-dimensions. Using scaffolds of polydimethylsiloxane (PDMS) patterned with microwells, we isolated cells in microwells of varying dimensions to determine whether cells were more often attached to flat space or vertical walls. We see that though cell adhesion to vertical walls is slightly dependent on microwell geometry, significantly more cells attach to side walls than to flat spaces, in all conditions regardless of the width or depth of the microwell. Cells also tend to attach to corners of the microwells. Myosin inhibition via blebbistatin reduces these effects, pushing cells away from corners and into flat space. Proliferation of cells attached to the walls of microwells is moderately decreased compared to cells on flat surfaces. Interestingly, addition of blebbistatin increases proliferation rate of cells in microwells, presumably due to the increased ability of cells to detach from the sides of microwells. Taken together, these data indicate a mechanism in which the attachments to vertical walls are stronger than those to flat surfaces.

Introduction

Precise control over the biophysical cues within a tissue engineering scaffold can be a powerful tool to regulate cellular assembly and function. For example, cell shape can be manipulated by the controlling the geometry of the adhesive domains of the ECM, directly impacting cell growth and death,[1] adhesion,[2] and differentiation.[3,4] Similarly, the elasticity of the underlying ECM has been shown to be an important determinant of cell migration,[5] lineage commitment,[6,7] and contractility.[8] The importance of mechanical architecture has recently been highlighted by the successful use of decellularized matrices, which retain the three-dimensional architecture of the ECM but completely lack cells, in the engineering of a variety of tissues, such as lung and heart.[9,10]

While manipulation of substrate elasticity and geometry are commonly explored methods of controlling cell behavior, the influence of microtopography is relatively poorly understood. Several studies have shown, however, that this can also be just as important a factor for regulating functional cellular assembly. Microgrooves patterned into a surface with defined geometry have been shown to control cell adhesion, alignment, and proliferation for several cell types,[11,12] while cyclical stretching of these grooves can be used to regulate lineage commitment of mesenchymal stem cells.[13] We have previously shown that micron-sized protrusions from a surface, or micropegs, can be used to control proliferation and cell shape of fibroblasts and skeletal myoblasts through stress-fiber based adhesion.[14] We later further demonstrated this through changes in the adhesion and and expression of stress-fiber associated proteins.[15]

We also recently demonstrated that microtopographical cues can be used to control the assembly and organization of functional cardiac tissue.[16] By patterning a polydimethylsiloxane (PDMS) surface with micropegs of defined diameter and spacing, we demonstrated that these

cues could be used to enhance functionality of tissue by promoting clustering around micropegs. Similar studies on the effects of microtopography on cardiac function have also shown the ability to regulate several markers of cardiac functionality, such as Ca^{2+} signaling,[17] contractility,[18] and beating rates.[19]

While our previous studies indicated that cells tend to cluster around the three-dimensional micropeg structures, the likelihood of a single cell attaching to a vertical structure as opposed to flat space was not directly tested, as cells almost always appeared in clusters. Thus the mechanism by which microtopography controls cellular organization is still unclear. Therfore, we used PDMS-based microwell arrays to isolate cells within microwells of varying geometry to allow single cells to interact with side walls. We cultured HL-1 cardiomyocytes[20] on these surfaces and measured the interactions of these cells the microwell surroundings. After using blocking solution to prevent attachment to the flat portions between wells, we used phase and epifluorescence imaging to determine the locations of cells, the fraction of cells adhered to walls, and the number of walls they are contacting. We see that even in large microwells a significant portion of cells is bound to side walls or wedged into corners. Addition of blebbistatin allows these to detach from the walls and return to flat space, indicating that the interaction between the cells and side walls is myosin-based. We then used BrdU incorporation to measure proliferation of the cells and see that addition of blebbistatin increases this rate of proliferation, indicating that topographical features can be used to provide cells with a preferred three-dimensional attachment configuration.

Results

Isolation of cells within microwells

To prevent the attachment of cells to the flat portion of the PDMS scaffold between the microwells, a strategy to selectively block this portion was developed. The procedure that was adapted to accomplish this purpose was similar to microcontact printing. Briefly, a non-treated polystyrene dish was incubated with a blocking solution of 0.2% Pluronic F-127 for 1 h at room temperature (RT). PDMS substrates that had been rendered hydrophilic using a plasma oxidizer were then stamped, pattern-side down, onto these surfaces for 1 min at RT, followed by incubation with ECM protein. Cell adhesion to flat portions of the substrate outside the microwells was significantly reduced on blocked surfaces (Fig. 1). Fig. 1A-B show phase and fluorescence images, respectively, of cells adhered to a surface where the flat regions have blocked, while Fig. 1C-D shows phase and fluorescence images of cells on an unblocked surface. Fig. 1E shows a closeup of an example how a cell climbs up the corner of a microwell, with actin filaments in green and the nucleus in blue. This procedure also helped reduce the number of cells entering or exiting a microwell, ensuring that measurements reflect effects of single-cell confinement.

Cells attach preferentially to the side walls of microwells instead of flat space

We then set out to measure the fraction of cells adhered to side walls of a microwell for each size and depth of well in order to determine whether cells were preferentially adhering to vertical walls (Fig. 2). For each condition, 70-100% of cells were observed to climb up the side walls. As expected, cells in 25 μm wide microwells were more likely to be adhered to a side wall than cells in 50 μm microwells, but for each width the number of cells adhered to side walls was significantly greater than the number of cells in flat space. Addition of 50 μM blebbistatin, an

inhibitor of non-muscle myosin II, to the culture reduced attachment of cells to the side walls. For each condition, the fraction of cells contacting a wall decreased in the presence of blebbistatin, consistent with a mechanism in which attachment to the walls occurs through myosin-based adhesion.

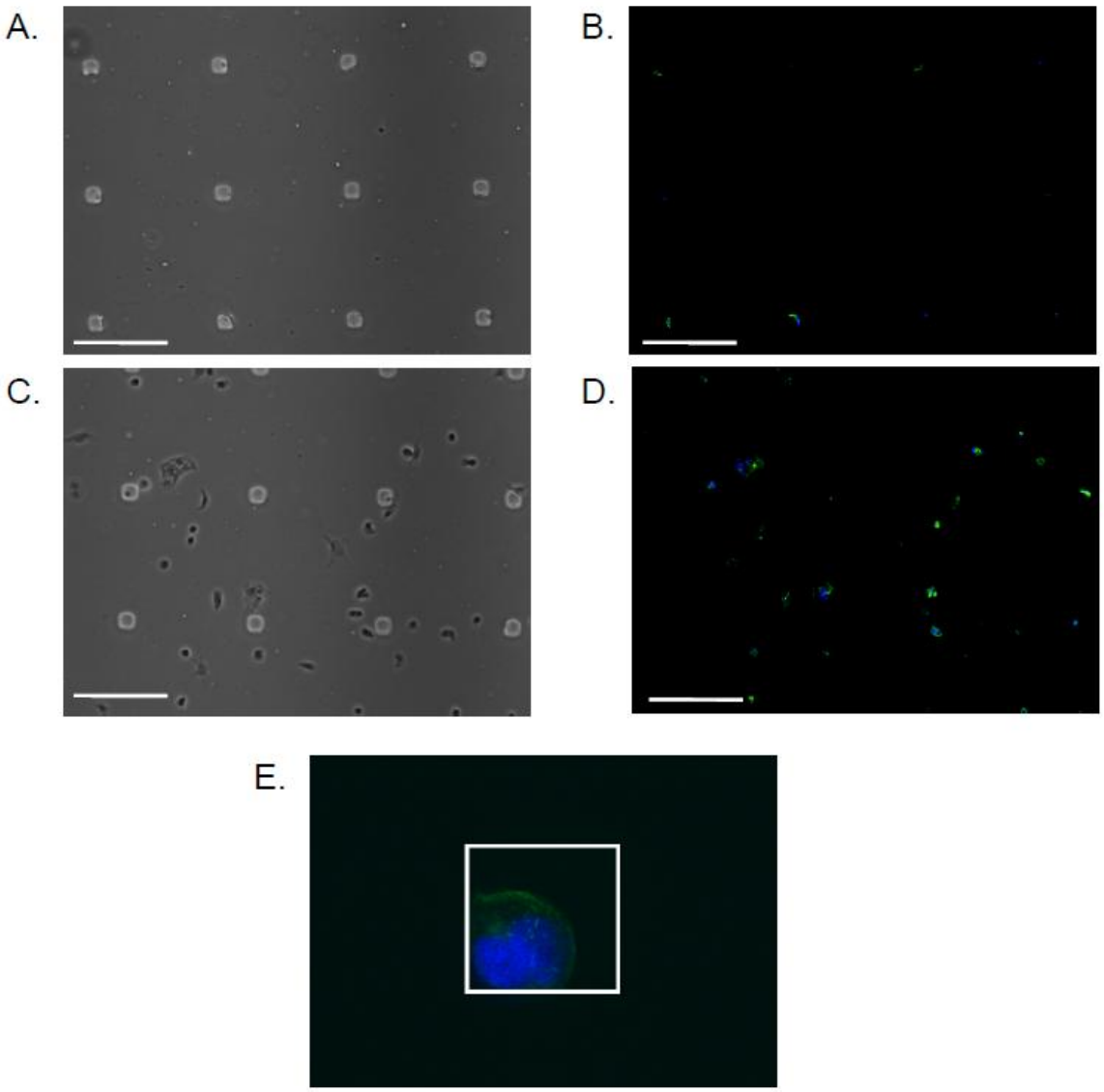

Fig. 1. Cells can be isolated into PDMS microwells by specifically blocking the regions of PDMS between microwells. (A)-(B) Phase and fluorescence images of cells on a surface that has been blocked. Green represents F-actin and blue represents the nuclear stain DAPI. Scale bar represents 100 µm. (C)-(D) Phase and fluorescence images of cells on a surface that has not been blocked. Green represents F-actin and blue represents the nuclear stain DAPI. Scale bar represents 100 µm. (E) High magnification image of a cell in the corner of a 25 µm microwell with the microwell outlined in white.

Cells in microwells tend to adhere to the corners

The tendency of cells to wedge into corners of microwells was measured by determining the average number of walls contacted by each cell (Fig. 3). For example, a cell in a corner is defined as contacting 2 walls. Fig. 3A shows the average number of walls contacted for cells in

each condition. It should be noted that cells adhered to zero side walls were omitted from this average so as to distinguish between wall and corner preferences with maximal sensitivity. A

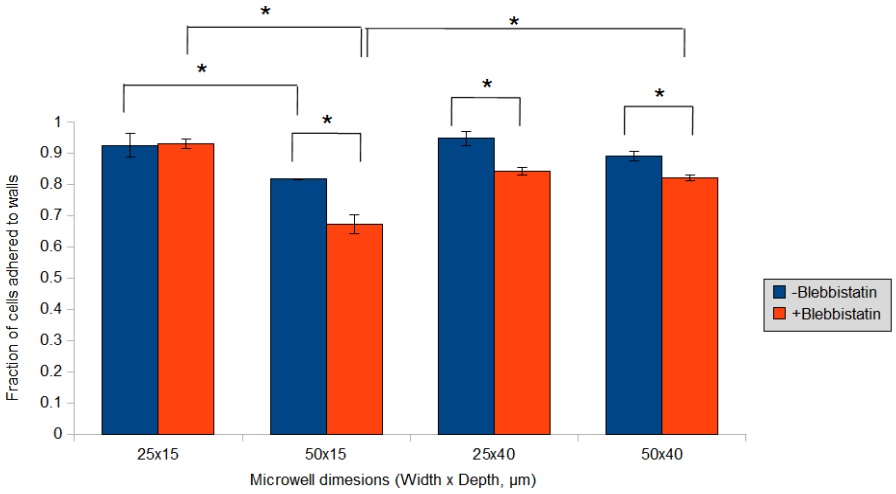

Fig. 2. Cells in microwells preferentially attach to vertical side walls via myosin-based adhesion. Cells were isolated in microwells of varying dimensions and the fraction of these cells in contact with side walls was calculated using epifluorescence imaging of DAPI to locate cells and phase imaging to determine if they were contacting side walls. -Blebbistatin and +blebbistatin indicate the absence or presence of 50 μM blebbistatin in the culture. Error bars represent SEM. Asterisk indicates significant difference with $p<0.05$.

value of 1.5 indicates that approximately 50% of cells that are adhered to a wall are wedged into a corner. Similar to the wall contact fraction data in Fig. 2, in each microwell geometry the addition of 50 μM blebbistatin decreased the number of walls that each cell was contacting,

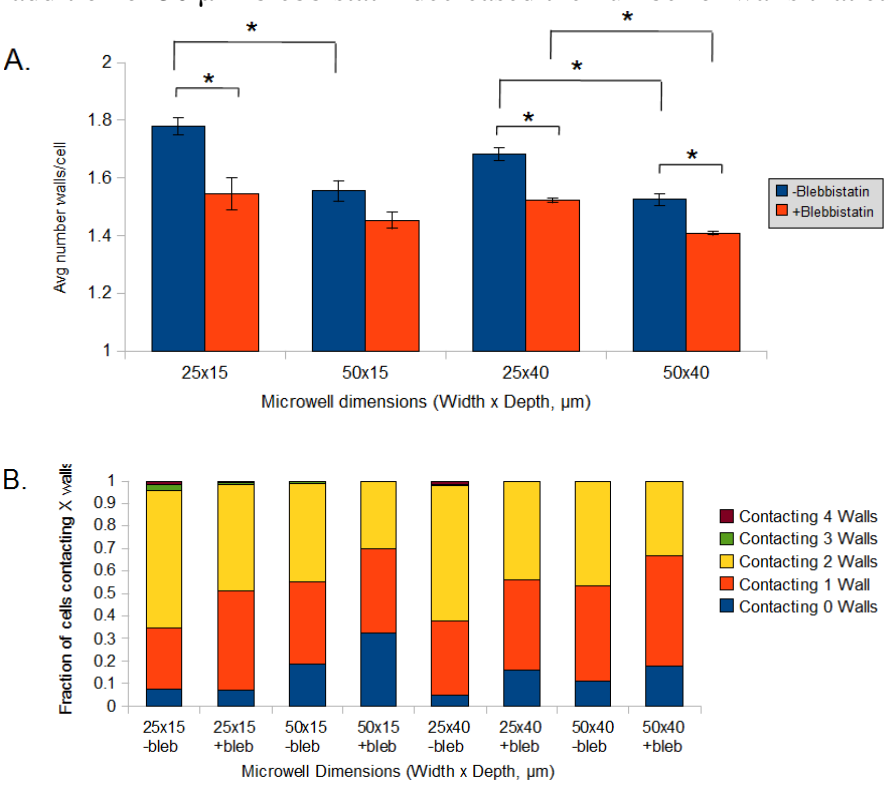

Fig. 3 Cells generally attach to multiple walls. (A) The tendency of cells to wedge into corners was measured by counting the average number of walls that each cell touched. Cells not touching any walls were excluded from set (A). The walls contacted was calculated using epifluorescence imaging of DAPI to locate cells and phase imaging to determine the number of walls contacted. -Blebbistatin and +blebbistatin indicate the absence or presence of 50 μM blebbistatin in the culture. Error bars represent SEM. Asterisk indicates significant difference with $p<0.05$. (B) Histogram representation of the data in (A), with cells in flat space included.

indicating that inhibition of myosin adhesion reduced cellular adhesive preferences for corners. Fig. 3B is histogram representation of this data, with cells in flat space of the microwells included. This data indicates which portion of the cells were solely attached to side walls as opposed to wedged into corners.

Attachment to a side wall reduces the proliferation of cells

To determine how attachment to a side wall might modulate cell function, proliferation was measured via incorporation of BrdU (Fig. 4). Cells were allowed to grow for 24 h before addition of BrdU to the culture medium for 90 mins. BrdU incorporation was visualized by incubation with appropriate primary and secondary antibodies. For each condition, addition of blebbistatin to the culture moderately increased the levels of proliferation.

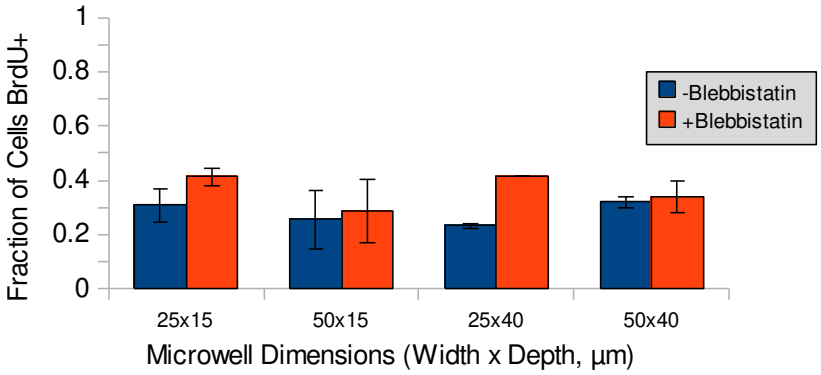

Fig.4. Addition of blebbistatin modestly increases cell proliferation within microwells. Proliferation was measured by BrdU incorporation followed by immunostaining with BrdU antibody and appropriate secondary. Fraction represents cells with BrdU colocalized with DAPI normalized by total number of cells. Error bars represent SEM.

Discussion

In this study we used PDMS patterned with arrays of microwells to directly test on a single-cell basis whether cells, when given the option to orient itself on a flat or a three-dimensional surface, will preferentially adhere to the vertical surface. These results directly build on our previous studies in which it was shown that cardiomyocytes tend to cluster around microtopographical features on a flat surface. We have also previously shown with fibroblasts and skeletal muscle cells that detachment of cells on a surface patterned with micropegs is slower than detachment from a flat surface. The results of these microwell studies further support a model in which microtopographical features allow for a three-dimensional adhesion that is stronger than adhesion on a two-dimensional surface.

The connection between attachment to side walls and a reduction in proliferation also corresponds with our previous work with micropegs, where it was shown that a cell attached to a micropeg is statistically less likely to proliferate than one on a flat surface. Interestingly, treatment with blebbistatin increased the proliferation of cells within microwells. Previous studies have shown that blebbistatin-induced myosin inhibition can prevent a cell from completing cytokinesis and therefore reduces proliferation rate.[21,22] Our hypothesis is that the cell's inability to detach from the lateral walls of the microwell stunts proliferation, but treatment with blebbistatin allows cells to more easily detach from side walls, thereby slightly increasing

proliferation rates.

These results allow us to gain greater insight into the mechanism by which topographical control is used to regulate cell behavior, both in 2D as well as 3D scaffolds used for tissue engineering. Manipulation of the mechanical microenvironment in 3D tissue engineering scaffolds has been shown to be an effective method of controlling the recruitment and adhesion of cells within the scaffold. Studies have shown that control of scaffold properties such as stiffness, roughness, fiber alignment, and spatial arrangement of adhesive domains can all be to control cell proliferation, adhesion, migration, and differentiation. In terms of cardiac tissue engineering, a recent set of studies has shown that introduction of microtopographical variances in the cardiac tissue scaffold microarchitecture by embedding microrods into them allows for greater control of cardiac function, scar tissue formation, and stem cell differentiation. Greater insight into the mechanism through which this occurs allows us to better control microtopographical features in future studies.

Conclusion

We have designed PDMS-based arrays of microwells in order to study the interaction of single cells with discrete microtopographical cues on a 2D surface. We have shown that cells are more likely to adhere to the vertical side walls of the microwell as opposed to the flat portion of the substrate, and that myosin-based adhesion pathways play a role in this interaction. Furthermore, by interrupting adhesion to vertical surfaces, we can increase the proliferation of these cells. These results suggest a mechanism by which topographical control of the microenvironment can be used to control cell adhesion in cardiac tissue engineering applications.

Materials and Methods

Cell culture

HL-1 mouse cardiomyocytes were generously provided by Dr. William C. Claycomb, Louisiana State University. Following established HL-1 culture protocols, tissue culture flasks were prepared by precoating with a solution containing 0.02% gelatin (Fisher Scientific, Pittsburgh, PA) and 5 μg ml^{-1} fibronectin (Sigma-Aldrich, St. Louis, MO) and incubating for at least 2 h at 37°C. Cultures were maintained in these flasks in complete medium consisting of Claycomb Medium (Sigma-Aldrich) supplemented with 10% fetal bovine serum (Sigma-Aldrich), 0.1 mM norepinephrine (Sigma-Aldrich), 1x L-glutamine (Sigma-Aldrich), and 1% penicillin/streptomycin (Gibco, Carlsbad, CA). Cell cultures were stored in a humidity-controlled 5% CO_2 incubator at 37°C. For experiments, cell were allowed to grow to confluence, trypsinized, resuspended in complete medium, and plated on PDMS scaffolds.

Fabrication of PDMS microwells

PDMS microwells were fabricated via soft lithography. An SU-8 negative photoresist (PR) (Microchem, Newton, MA) was spin-coated onto a single-crystal silicon wafer and baked at 95°C for 3 min. SU-8 2005, 2010, and 2035 were used to make thicknesses of 5, 15, and 40 μm, respectively. Microscale pegs were introduced by placing a patterned photomask over the coated wafer and exposing it to UV light for 25–30 s at an intensity of 5 mW cm^{-2}, washing in an SU-8 developer (Microchem) for 30 s to remove uncrosslinked PR, then baking at 95°C for 3-5 min. Different size pegs were created by changing the pattern of the photomask. To create PDMS

microwell arrays, PDMS and the curing agent were prepared and mixed as directed by the manufacturer (Sylgard 184, Dow Corning, MI), degassed under vacuum, and spin-coated onto an SU-8 mold patterned with microscale pegs. The PDMS was baked for 1 h at 80°C, then peeled from the SU-8 masters. Unpatterned PDMS membranes were fabricated in an identical manner with bare silicon wafers.

Preparation of experimental scaffolds

The following procedure was used to selectively coat the microwells with ECM protein while leaving flat portions blocked. Untreated polystyrene dishes were incubated with a blocking solution of 0.2% Pluronic F-127 (Sigma-Aldrich) for 1 h at room temperature (RT), after which the solution was aspirated out and the dishes were allowed to dry. PDMS patterned with microwells was rendered hydrophilic by exposure to air plasma for 3 min, then stamped, pattern-side down, onto the polystyrene dishes for 1 min. The scaffolds were then transferred to another dish pattern-side up and incubated with a gelatin/fibronectin mix mentioned above for at least 2 h at 37°C. Unblocked scaffolds were coated in ECM protein immediately after plasma oxidation. Cells were plated onto the surfaces and allowed to attach for 4 hours, at which point the medium was replaced with fresh medium either with or without 50 μM blebbistatin (Sigma-Aldrich).

Immunostaining

Cells grown on PDMS surfaces were fixed with 4% PFA at RT for 10 min, permeabilized with 0.1% Triton-X (EMD Chemicals, Philadelphia, PA) at RT for 5 min, then blocked with 5% normal goat serum for 1 h at RT. Actin filaments were labeled with AF 488 phalloidin (Invitrogen, Carlsbad, CA) diluted 1:200 for 45 mins at RT. Cell nuclei were labeled with 4′,6-diamidino-2-phenylindole (DAPI) (Invitrogen) diluted 1:2000 for at least 20 mins at RT. A Nikon TE2000E2 microscope was used to obtain epifluorescence images and a Zeiss LSM 510 Meta Confocal Laser Scanning Microscope was used to obtain confocal images.

Cell contact measurements

To determine whether cells were contacting walls, phase and epifluorescence images of PDMS scaffolds were obtained (Nikon TE2000E2). DAPI imaging was used to determine the location of cells, and phase imaging was used to determine whether cells were contacting walls. The number of cells contacting side walls was divided by the total number of cells within wells to determine wall contact ratios. The number of walls touched per cell was measured by counting this number for each cell in the phase image and obtaining the average across many cells.

BrdU analysis

Cell proliferation was measured by incorporation of 5-bromo-2′-deoxyuridine (BrdU). Cells were plated on surfaces, medium was replaced after 4 hours, then cells were allowed to grow for another 20 h. BrdU (Sigma-Aldrich) was then added to the medium at a 1:100 dilution and allowed to incubate for 90 min at 37°C, and then fixed with 4% PFA for 10 min at RT. To determine the incorporation of BrdU, cells were treated with 4 N HCl for 30 mins and permeabilized with 0.1% Triton X. BrdU was stained by treating the cells with a mouse anti-BrdU primary antibody (Sigma-Aldrich) diluted 1:100 for 1 h followed by incubation with AF 546-tagged goat-anti-mouse secondary antibody (Invitrogen) diluted 1:500 for 45 min. Cell nuclei were stained with DAPI diluted 1:200 for 20 min. The percentage of BrdU-positive nuclei of cells within microwells was determined by dividing the number of BrdU-positive nuclei

(defined by co-incorporation of BrdU and DAPI) by the total number of nuclei (defined by incorporation of DAPI).

Statistics

Results are presented as mean ± standard error of the mean (SEM). Data are analyzed by Student's t-test for significance.

REFERENCES

1. C. S. Chen, M. Mrksich, S. Huang, G. M. Whitesides, D. E. Ingber, Geometric control of cell life and death, Science, 1997, 276, 1425-1428.
2. C. J. Lee, M. S. Blumenkranz, H. A. Fishman, S. F. Bent, Controlling cell adhesion on human tissue by soft lithography, Langmuir : the ACS journal of surfaces and colloids, 2004, 20, 4155-4161.
3. R. McBeath, D. M. Pirone, C. M. Nelson, K. Bhadriraju, C. S. Chen, Cell shape, cytoskeletal tension, and RhoA regulate stem cell lineage commitment, Developmental cell, 2004, 6, 483-495.
4. K. A. Kilian, B. Bugarija, B. T. Lahn, M. Mrksich, Geometric cues for directing the differentiation of mesenchymal stem cells, Proceedings of the National Academy of Sciences of the United States of America, 2010, 107, 4872-4877.
5. T. A. Ulrich, E. M. de Juan Pardo, S. Kumar, The mechanical rigidity of the extracellular matrix regulates the structure, motility, and proliferation of glioma cells, Cancer research, 2009, 69, 4167-4174.
6. A. J. Engler, S. Sen, H. L. Sweeney, D. E. Discher, Matrix elasticity directs stem cell lineage specification, Cell, 2006, 126, 677-689.
7. K. Saha, A. J. Keung, E. F. Irwin, Y. Li, L. Little, D. V. Schaffer, K. E. Healy, Substrate modulus directs neural stem cell behavior, Biophysical journal, 2008, 95, 4426-4438.
8. A. J. Engler, C. Carag-Krieger, C. P. Johnson, M. Raab, H. Y. Tang, D. W. Speicher, J. W. Sanger, J. M. Sanger, D. E. Discher, Embryonic cardiomyocytes beat best on a matrix with heart-like elasticity: scar-like rigidity inhibits beating, Journal of cell science, 2008, 121, 3794-3802.
9. H. C. Ott, T. S. Matthiesen, S. K. Goh, L. D. Black, S. M. Kren, T. I. Netoff, D. A. Taylor, Perfusion-decellularized matrix: using nature's platform to engineer a bioartificial heart, Nature medicine, 2008, 14, 213-221.
10. T. H. Petersen, E. A. Calle, L. Zhao, E. J. Lee, L. Gui, M. B. Raredon, K. Gavrilov, T. Yi, Z. W. Zhuang, C. Breuer, E. Herzog, L. E. Niklason, Tissue-engineered lungs for in vivo implantation, Science, 2010, 329, 538-541.
11. R. B. Vernon, M. D. Gooden, S. L. Lara, T. N. Wight, Microgrooved fibrillar collagen membranes as scaffolds for cell support and alignment, Biomaterials, 2005, 26, 3131-3140.
12. Y. C. Wang, C. C. Ho, Micropatterning of proteins and mammalian cells on biomaterials, The FASEB journal : official publication of the Federation of American Societies for Experimental Biology, 2004, 18, 525-527.
13. K. Kurpinski, J. Chu, C. Hashi, S. Li, Anisotropic mechanosensing by mesenchymal stem cells, Proceedings of the National Academy of Sciences of the United States of America, 2006, 103, 16095-16100.
14. R. G. Thakar, M. G. Chown, A. Patel, L. Peng, S. Kumar, T. A. Desai, Contractility-dependent modulation of cell proliferation and adhesion by microscale topographical cues, Small, 2008, 4,

1416-1424.
15. A. A. Patel, R. G. Thakar, M. Chown, P. Ayala, T. A. Desai, S. Kumar, Biophysical mechanisms of single-cell interactions with microtopographical cues, Biomedical microdevices, 2010, 12, 287-296.
16. A. A. Patel, T. A. Desai, S. Kumar, Microtopographical assembly of cardiomyocytes, Integrative Biology, 2011, 3, 1011-1019.
17. L. Yin, H. Bien, E. Entcheva, Scaffold topography alters intracellular calcium dynamics in cultured cardiomyocyte networks, American journal of physiology. Heart and circulatory physiology, 2004, 287, H1276-1285.
18. J. Kim, J. Park, K. Na, S. Yang, J. Baek, E. Yoon, S. Choi, S. Lee, K. Chun, S. Park, Quantitative evaluation of cardiomyocyte contractility in a 3D microenvironment, Journal of biomechanics, 2008, 41, 2396-2401.
19. M. W. Curtis, S. Sharma, T. A. Desai, B. Russell, Hypertrophy, gene expression, and beating of neonatal cardiac myocytes are affected by microdomain heterogeneity in 3D, Biomedical microdevices, 2010, 12, 1073-1085.
20. W. C. Claycomb, N. A. Lanson, Jr., B. S. Stallworth, D. B. Egeland, J. B. Delcarpio, A. Bahinski, N. J. Izzo, Jr., HL-1 cells: a cardiac muscle cell line that contracts and retains phenotypic characteristics of the adult cardiomyocyte, Proceedings of the National Academy of Sciences of the United States of America, 1998, 95, 2979-2984.
21. T. Kondo, K. Hamao, K. Kamijo, H. Kimura, M. Morita, M. Takahashi, H. Hosoya, Enhancement of myosin II/actin turnover at the contractile ring induces slower furrowing in dividing HeLa cells, The Biochemical journal, 2011, 435, 569-576.
22. K. Murthy, P. Wadsworth, Myosin-II-dependent localization and dynamics of F-actin during cytokinesis, Curr Biol, 2005, 15, 724-731.

Chapter 6 – Conclusions and Future Directions

The field of tissue engineering provides a great deal of hope for the future of human health and medicine. The ability to regenerate tissue or even create whole organs will reduce our dependence on transplants to replace damaged tissues and organs, perhaps allowing us to treat patients faster or to tailor therapies to individual patients. While recent results have shown promise towards reaching this goal, the need to find ways to repair damage to vital organs continues to grow.

In this dissertation, we present one specific, yet very important, aspect in the design of tissue engineering scaffolds – the microtopographical environment that is presented to the cells. Specifically, we look at this in a cardiac tissue engineering scaffold. We begin by examining how microtopography might be able to reduce the scar tissue that forms as a result of a heart attack. We then study how these same microtopographical features might be used to control the adhesion and organization of cardiomyocytes. We then further explore the mechanisms that guide the specific interaction between a single cardiomyocyte and microtopographical features it may encounter. Together our data show the importance of considering the topography and architecture in tissue engineering scaffolds.

There are numerous ways in which the results from this data may be applied in the future. Work is already underway to translate these 2D experiments into 3D scaffolds by introducing microrods into gels in order to create structural heterogeneity. Our results show the potential to control cell behavior not only through the presence of microtopographical structures such as these but also through control of their geometric dimensions and spatial arrangement. One could possibly continue this work with stem cells or cardiac progenitor cells in order to study the effects of microtopography on a cell type that is more relevant to cardiac tissue engineering, as opposed to the cells in this dissertation which were all obtained from cell lines. Also, there is nothing to suggest that the incorporation of micropegs into scaffolds should be limited to cardiac tissue only – cellular organization is important to a wide variety of tissues, while scar tissue formation can occur at any site of damage within the body.

Future research in the design of scaffolds should take into consideration multiple parameters, whether it is substrate stiffness, topography, or biochemical pathways. Ideally, the knowledge gained from this work will be integrated into regeneration strategies combining both mechanical and biochemical cues in order to gain greater control over the assembly and function complex cellular structures and tissues.